ALMA MATER STUDIORUM - UNIVERSITÀ DI BOLOGNA

SCUOLA DI INGEGNERIA E ARCHITETTURA

Dipartimento di Ingegneria civile, chimica, ambientale e dei materiali (DICAM)

Master degree in

CHEMICAL AND PROCESS ENGINEERING

Sustainable Technologies of Energy and Material curriculum

MASTER THESIS

in

Bioreactors and downstream processes

Isolation of extracellular vesicles from *citrus limon* fruit through membrane-based techniques.

CANDIDATE

Sara Giancaterino

SUPERVISOR

Prof. Cristiana Boi

CO-SUPERVISOR

Prof. Serena Bandini

Academic year 2020/21

Summary

Introduction

Extracellular vesicles (EVs) are biological particles naturally released from cells that are delimited by a bi-layer phospholipidic membrane. EVs contain an incredibly rich bio-cargo of lipids, proteins and nucleic acids, all of which can be delivered in a functional way to recipient cells leading to a change in their phenotype. The key role EVs play in cell-to-cell communication and intracellular trafficking can be exploited in both physiological and pathological processes. This feature, together with their high biocompatibility, stability and low toxicity make them very attractive candidates as diagnostic biomarkers and in tissue regeneration, as well as drug delivery systems in the fields of medicine, cosmetics, and nutrition.

To date, most EVs have been produced from human cells cultured in T-flasks and purified by ultracentrifugation (UC)-based methods. From a manufacturing perspective UC has many limitations, thus it has seen a reduction in usage for alternative methods, such as filtration techniques, chromatographic separations as gel filtration, polymer precipitation, immunoaffinity capture and microfluidic technologies.

The most severe bottleneck of the progress in the field is the typical low yield. This severely limits the possibility to progress in research at clinical scales, as well as the realization of successful and cost‐effective EV‐based products. Besides the selection of a suitable and optimized purification technique, yields improvements can be achieved by changing the EV biological source.

The functions of EVs are strictly correlated to the cell phenotype. Consequently, different applications require EVs from different cells and, therefore, EVs production cannot rely on a single cell line, as for example in the field of monoclonal antibodies production that is uniquely based on CHO cells.

Most EVs are produced from different types of human cells, including stem cells, dendritic cells, mast cells, macrophages, epithelial cells, and cancer cells. However, the cultivation of human cells is challenging to upscale for several reasons, and researchers are motivated to explore alternative sources to mammalian EVs, looking for cheaper, scalable, and more flexible solutions.

In this context, the discovery that plants do release "exosome-like" extracellular vesicles opens the doors to many new possibilities in the field. Plant EVs are morphologically similar to the exosomes isolated from mammalian cell cultures, and the methods used for their isolation and characterization are also similar. To date, vesicles from ginger, grape, grapefruit, orange, lemons, broccoli, apple, kiwifruit, tomato, ginseng, coconut, blueberry, carrots etc. have been successfully isolated and observed by TEM microscopy.

Although their biogenesis mechanism is still not fully clarified, their role as cross-kingdom modulators, especially in animal-plant interactions, have been widely studied. In fact, it is now demonstrated that as we eat every day, plant and food miRNAs are absorbed by the digestive tract and can regulate our genes, contributing to the homeostasis of the whole body.

Since they are common components of our diet, plants are also considered inherently biocompatible and safe sources. Besides, plant vesicles have the main advantage of being easily accessible, cost-effective, scalable and, according to data from literature, they can be produced at higher yields. Interestingly, native plant derived extracellular vesicles (PDEVs) have been shown also to possess intrinsic therapeutic activities against diseases, as antitumor, anti-inflammatory, anti-aging, and anti-Alzheimer properties.

Due to their nature, food and plant-derived vesicles are regarded as excellent candidates as drug delivery systems (DDS). Compared with synthetic nanoparticles, endogenous DDS have recently shown promising results in enhancing drug delivery targeting and therapeutic efficacy because of their native biocompatibility and intrinsic safety. PDEVs can be loaded, both with passive or active techniques, with exogenous therapeutic drugs such as proteins, miRNAs, siRNAs and expression vectors, to achieve superior effects against diseases, but also in nutraceutics and cosmetics by enhancing the beneficial action of natural bioactive phyto-molecules.

The experimental work carried out in the current project is aimed at the development of a membrane-based protocol for the isolation of extracellular vesicles from lemon (*citrus limon*) fruit.

The advantages in the use of filtration techniques in EVs isolation are many. In particular, tangential flow filtration (TFF) allow to process large volumes of samples and when compared to UC and SEC, and it is reported to be less time-consuming, more efficient, reproducible, gentler method for EVs isolation. Lemon fruit is chosen as model-PDEVs source material due to its availability and cheapness together with its beneficial properties. Experimental findings demonstrate that lemon fruit possesses strong antioxidant, anti-microbial and anti-inflammatory properties and its assumption is associated to a reduction of the risk to develop cardiovascular diseases and some types of cancer.

The proposed protocol is based on the extraction of lemon juice, followed by centrifugation and microfiltration steps, with the purpose of cells and cellular debris removal. The pretreated juice is subsequently purified through a diafiltration process, using ultrafiltration membranes. Both discontinuous dead-end and continuous cross-flow diafiltration processes are explored and compared. Different membranes, both in terms of materials and cut-offs, are tested.

The major pitfall of filtration processes is membrane fouling. In this context, efforts are undertaken to minimize vesicles losses and their consequent aggregation on the membrane cake, through the optimization of the process operative conditions.

EVs isolated through different membrane-based protocols are compared, in terms of vesicle yield, size distribution and level of contamination of the preparations.

The enrichment in EVs is primarily verified though size exclusion chromatography, used as analytical technique, in both FPLC and HPLC systems. Besides, the EVs preparations are characterized by means of dynamic light scattering (DLS) measurements, z-potential measurements and total protein quantification through BCA assay.

Finally, the encapsulation ability of the isolated lemon-vesicles is tested. Curcumin is selected as model hydrophobic drug for encapsulation. Despite having numerous bioactive and therapeutic properties (anti-inflammatory, anti-cancer, antioxidant properties), the poor solubility of curcumin, due to its hydrophobicity and preferential interaction with lipid membranes, is responsible for its dramatically poor bioavailability. This, together with its low stability, remains a major barrier for its exploitation and clinical efficacy.

In this framework, the uptake capability of the EV-enriched fraction is tested by means of passive cargo loading techniques and verified through spectrophotometric readings.

CHAPTER 1

Extracellular vesicles

Extracellular vesicles (EVs) are a heterogeneous group of membrane-covered nanoparticles of diverse sizes and shapes naturally released by prokaryotic and eukaryotic cells. Their membrane is formed by a phospholipid bilayer with integrated proteins that enclose the cytosol derived from the secreting cell. Another definition, from ISEV (International Society of Extracellular Vesicles):

"Extracellular vesicle is the generic term for particles naturally released from the cell that are delimited by a lipid bilayer and cannot replicate, i.e. do not contain a functional nucleus."

As shown in the timeline (Figure 1), the first observation of multivesicular bodies (MVBs) and their intraluminar vesicles occurred in the 1950s. MVBs were first recognized in algae and mammalian cells. After being recognized, in the late 1950s, EVs have been found throughout all domains of life. They were initially underestimated as "trash cans", structures facilitating cells getting rid of garbage material. In 1996 Raposo et al. suggested that EVs could influence antigen presentation in vivo, marking a turning point in the thinking of EVs. Their ubiquity was confirmed in 2000 when EVs were found even in Archea[1]. Nowadays their functions in cellular communication processes are well recognized in all their significance, both in physiological and pathological processes.
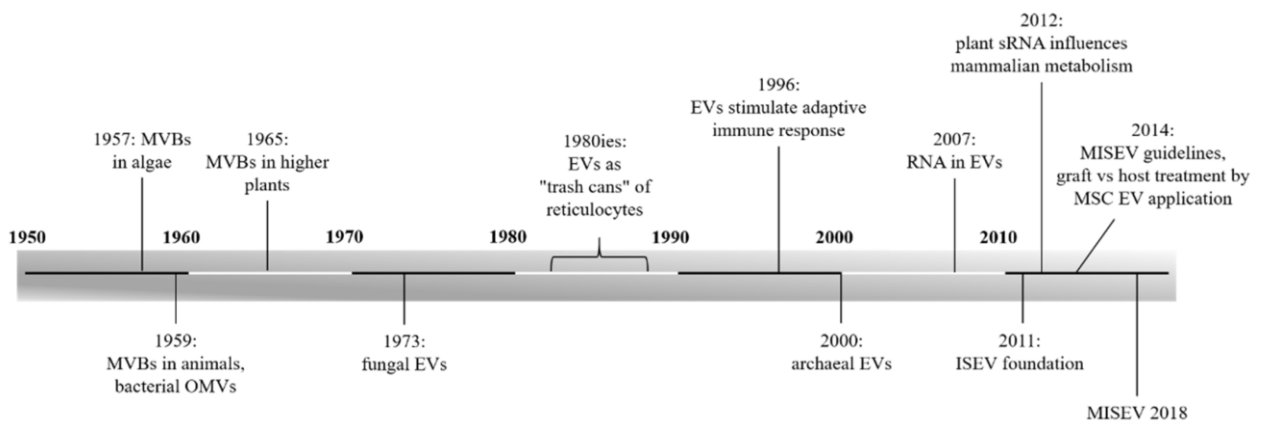

Figure 1: Timeline of EVs research by With et al. [1]

EVs contain surface receptors, membrane and soluble proteins, lipids, ribonucleic acids (mRNA, microRNA, tRNA, rRNA), and, according to some publications, genomic and mitochondrial DNAs[2] (Figure 2).
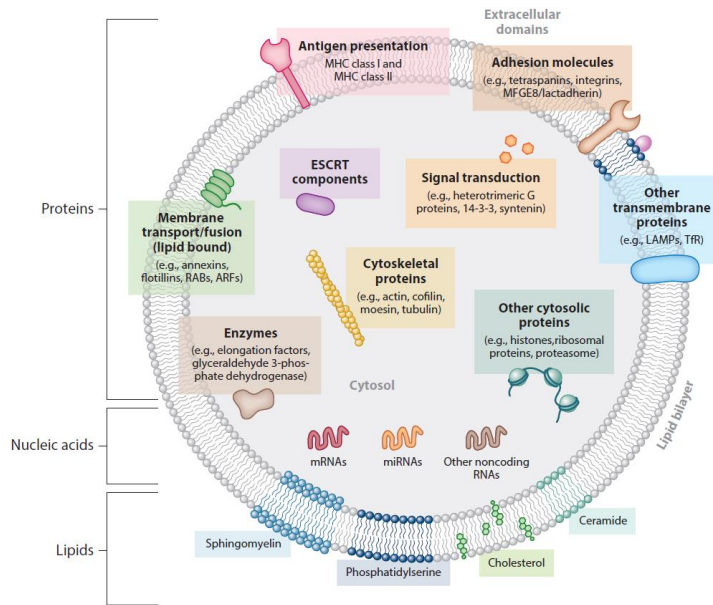
Figure 2: Composition of extracelluar vesicles by Colombo et al. [3]

EVs have been observed in all biological fluids of the human body: blood, urine, saliva, semen, bronchoalveolar lavage, bile, ascitic fluid, breast milk, cerebrospinal fluid, and so on. EVs are secreted by cells of all tissues and organs in both health and pathologies[2].

1.1 EVs classification and biogenesis

To date, extracellular vesicles have been classified on the basis of their cellular origin or biological function. However, the most popular way to classify EVs is based on their biogenesis pathway. Thus, most authors distinguish exosomes, microvesicles, and apoptotic bodies as the major types (Table 1, Figure 3).

Table 1; Classification on EVs based on their biogenesis pathways by Andaloussi et al. [5]

Vesicle types	Characteristics			
	Origin	Size	Markers	Contents
Exosomes	Endolysosomal pathway; intra-luminal budding of multivesicular bodies and fusion of multivesicular body with cell membrane	40–120 nm	Tetraspanins (such as TSPAN29 and TSPAN30), ESCRT components, PDCD6IP, TSG101, flotillin, MFGE8	mRNA, microRNA (miRNA) and other non-coding RNAs; cytoplasmic and membrane proteins including receptors and major histocompatibility complex (MHC) molecules
Microvesicles	Cell surface; outward budding of cell membrane	50–1,000 nm	Integrins, selectins, CD40 ligand	mRNA, miRNA, non-coding RNAs, cytoplasmic proteins and membrane proteins, including receptors
Apoptotic bodies	Cell surface; outward blebbing of apoptotic cell membrane	500–2,000 nm	Extensive amounts of phosphatidyl-serine	Nuclear fractions, cell organelles
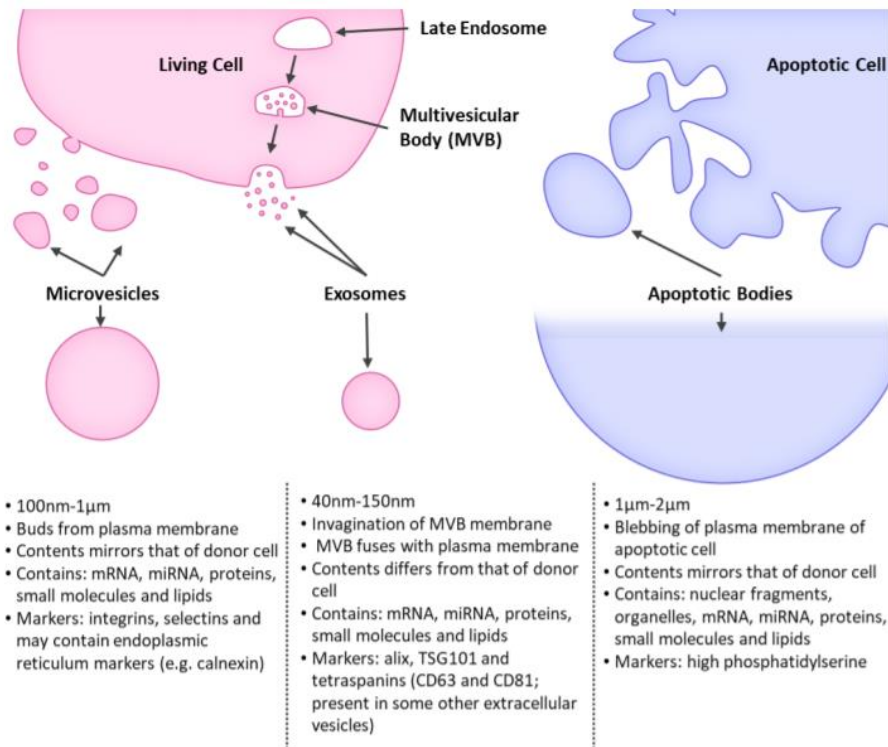
Figure 3: Schematic representation of the different EVs biogenesis pathways for eukaryotic cells, microvesicles, exosomes and apoptotic bodies biogenesis [6].

Exosomes (40-120 nm) are produced during formation of multivesicular bodies (MVB). These are generated through the invagination of the endosomal membranes. The MVB then fuses with the plasma membrane, releasing its luminal exosomes (Figure 4). Microvesicles (MVs) (50–1000 nm) are formed by direct outward budding of the plasma membrane, meaning that their content closely matches that of the donor cell. The largest EVs, apoptotic bodies (>1000 nm), form from membrane blebbing of apoptotic cells. They contain nuclear fragments and organelles.
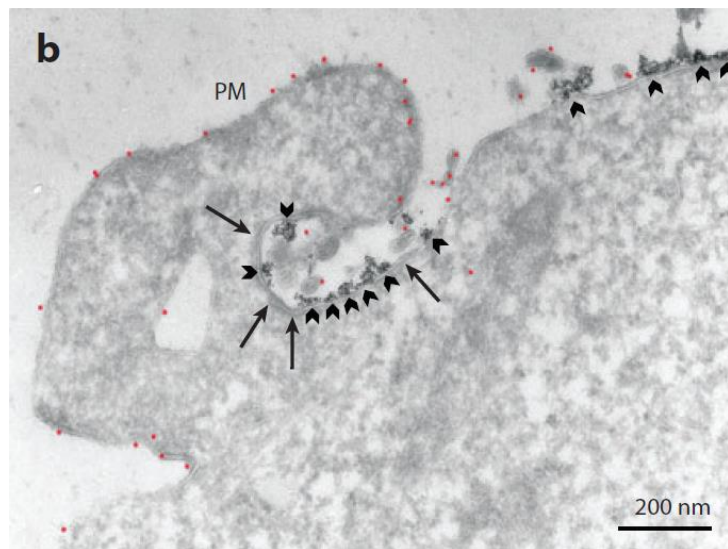
Figure 4: TEM image of fusion of a MVB with the plasma membrane in an Epstein-Barr virus–transformed B cell with BSA-gold (in red) internalized into MVB (arrowheads). Images by Columbo et al. [3]

Remarkably, a clear distinction between the single categories does not exist; there are multiple and simultaneous pathways of EV formation, which leads to the release of a heterogeneous population that may vary widely in size, composition, and function. Thus, it is difficult to assign a particular pathway based on the subpopulation of isolated vesicles. Accordingly, unless the EV release is caught by live-imaging techniques, ISEV recommends the use of 'EV' as an umbrella term for these types of vesicles[7]. Overall, EVs science is an ongoing process: there is a need for a better understanding of the factors that differentiate the biogenesis, sorting, and release of EVs.

1.2 EVs biological functions

Gandham et a. defined EVs as "*signalosomes, multifunctional signalling complexes for controlling fundamental cellular and biological functions*"[4]. ISEV recently referred to them as "*the cells' secret messangers*". EVs role in cell-to-cell communication, and in general in signaling processes, is undoubtedly the most intriguing.

EVs have been shown to transfer biomolecules such as lipids, proteins, and RNAs to other cells, distal organs, and even to other organisms. Once EVs are released into the extracellular space, they undergo internalization by recipient cells through many different mechanisms. They can directly activate recipient cell surface receptors via protein and lipid ligands, directly merge their contents into the recipient cell plasma membrane and deliver effectors as transcription factors, oncogenes, microRNAs, mRNAs and infectious particles (Figure 5).
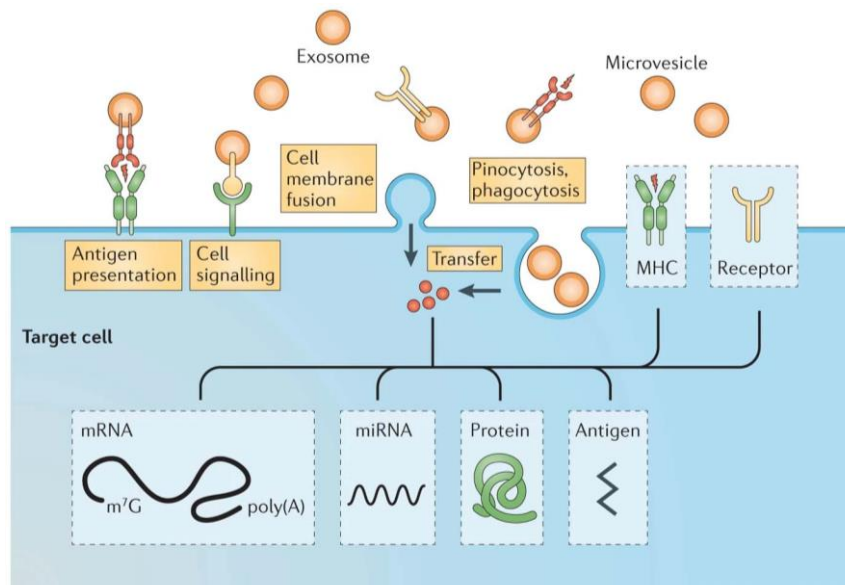
Figure 5: Mechanisms of uptake of EVs on eukaryotic cells [5]

The internalization mechanism determines the subcellular destination of their contents and their participation in different physiological processes as, for example, stem cell maintenance, tissue repair, immune surveillance and blood coagulation (Figure 6)[5].

For example, in the regulation of immune responses, EV cargo is used to deliver messages between immune cells (dendritic cells, B cells, T cells), leading to either immunosuppressive or immune-activating effects on the immune response[8].

In the brain, in addition to classical synaptic neurotransmission, neurons communicate via the secretion of extracellular vesicles that can contribute to a range of neurobiological functions. For example, in response to an enhanced glutamatergic activity, the cortical neurons react through an increased release of EVs containing neurotransmitter receptors[9]. EVs are also involved in cell

phenotype modulation, for example in converting stem cells into organ cells, and they are also implicated in stem cell maintenance and plasticity[5].

Their eclectic cellular and biological functions indicate that extracellular vesicles have innate therapeutic potential, for example, in the fields of regenerative medicine and immunotherapy.
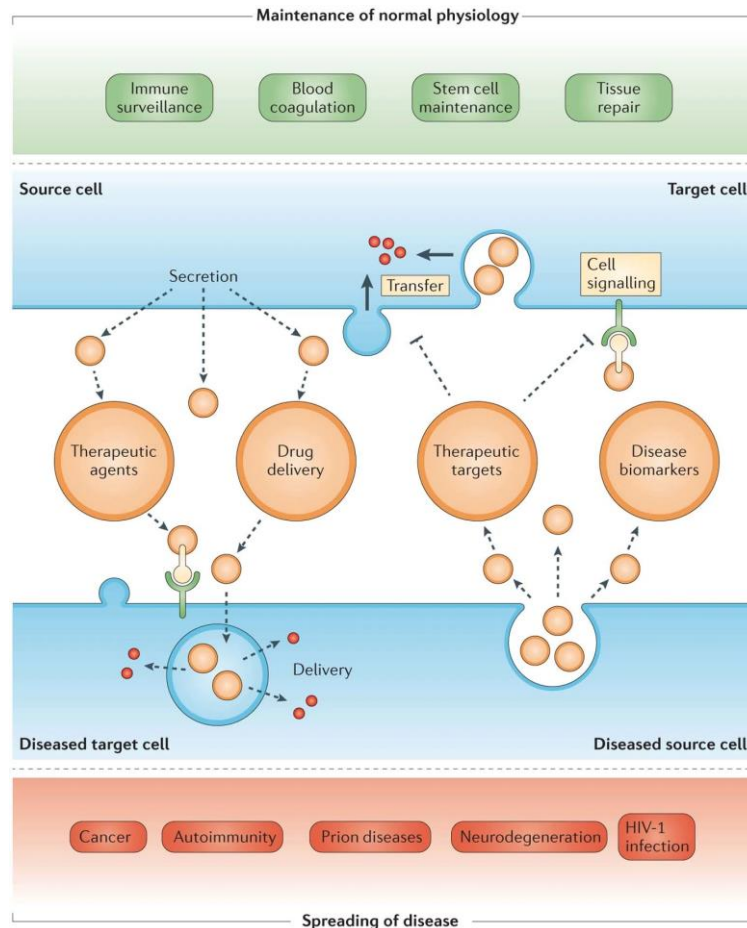
Figure 6: Roles of extracellular vesicles in normal physiology and disease pathogenesis by Andaloussi et al. [5]

Extracellular vesicles have an important role also in disease pathogenesis. They are proved to trigger tumour growth by stimulating the proliferation of cancer cells by inducing unwanted immune tolerance, spreading oncogenes and promoting metastases. Beyond cancer, extracellular vesicles have been implicated in the spread of numerous pathogens, including: HIV-1, Epstein–Barr virus (EBV) and prions, via the transfer viral material bound to the vesicles[5]. In the case of the development of autoimmune disease, extracellular vesicles can induce immune responses toward self-antigens[5].

Extracellular vesicles are also thought to contribute to the local propagation of neurodegenerative disease. Since neurons can communicate also through the secretion of EVs, they allow longer-range communication within the central nervous system and enhance the transfer of prion proteins and toxic protein aggregates to modulate the progression of the diseases[5]. For example, this mechanism was elucidated in the context of Alzheimer's and Parkinson's diseases, in which the two toxic protein species responsible for these diseases, have been shown to be released in association with exosomes, contributing their transport in other parts of the brain[10].

Overall, EVs displays an innate therapeutic potential that can be exploited using EVs as drug delivery vectors, in immunomodulatory or regenerative therapies, and antitumor and vaccines.

Chapter 1 references

1. Woith, E., Fuhrmann, G. & Melzig, M. F. Extracellular vesicles—connecting kingdoms. *International Journal of Molecular Sciences* vol. 20 (2019).

2. Konoshenko, M. Y., Lekchnov, E. A., Vlassov, A. V. & Laktionov, P. P. Isolation of Extracellular Vesicles: General Methodologies and Latest Trends. *BioMed Research International* vol. 2018 (2018).

3. Colombo, M., Raposo, G. & Théry, C. Biogenesis, secretion, and intercellular interactions of exosomes and other extracellular vesicles. *Annual review of cell and developmental biology* vol. 30 (2014).

4. Gandham, S. *et al.* Technologies and Standardization in Research on Extracellular Vesicles. *Trends in Biotechnology* vol. 38 (2020).

5. El Andaloussi, S., Mäger, I., Breakefield, X. O. & Wood, M. J. A. Extracellular vesicles: Biology and emerging therapeutic opportunities. *Nature Reviews Drug Discovery* vol. 12 (2013).

6. Timms, K. Investigating the effect of plant-derived extracellular vesicles on human placental function. 289 (2018).

7. Thery, C. *et al.* Minimal information for studies of extracellular vesicles 2018 (MISEV2018): a position statement of the International Society for Extracellular Vesicles and update of the MISEV2014 guidelines. *J. Extracell. vesicles* **7**, (2018).

8. Théry, C., Ostrowski, M. & Segura, E. Membrane vesicles as conveyors of immune responses. *Nature Reviews Immunology* vol. 9 (2009).

9. Chivet, M., Hemming, F., Pernet-Gallay, K., Fraboulet, S. & Sadoul, R. Emerging role of neuronal exosomes in the central nervous system. *Front. Physiol.* **3 MAY**, (2012).

10. Bellingham, S. A., Guo, B. B., Coleman, B. M. & Hill, A. F. Exosomes: Vehicles for the transfer of toxic proteins associated with neurodegenerative diseases? *Front. Physiol.* **3 MAY**, (2012).

State-of-the art of EVs production

To date, several methods for the isolation of extracellular vesicles have been developed by the researchers at lab scale. They can be classified according to the working principle upon which they are based (Table 2).

The traditional methods used for EVs isolation are those based on the vesicles size and buoyant density, namely, ultracentrifugation, filtration techniques and gel filtration. The methods based on EVs solubility changes and/or aggregation as precipitation appeared later over the years. In addition, numerous methods for isolation of EV population based on highly specific interactions with the molecules exposed on the EV surface or microfluidic technologies have recently appeared.

Table 2: Classification of the methods for the isolation of extracellular vesicles according to their working principle.

Methods based on size and buoyant density

- **Ultracentrifugation-based techniques**
  o **Differential ultracentrifugation**
  o **Density gradient ultracentrifugation**
- **Size exclusion chromatography (SEC)**
- **Microfiltration/Ultrafiltration**
- **Flow field fractionation (FFF)**

Methods based on solubility changes and/or aggregate

- **Polymeric precipitation**

Methods based on charge

- **Anion exchange chromatography (AIEX)**
- **Electrophoresis**

Methods based on highly specific interactions on the EV surface

- **Affinity chromatography (AC)**
- **Immuno affinity capture**

Microfluidic technologies

The number of publications on EVs isolation is increased exponentially over the last decade. The 2000-2020 trend on the different EVs isolation methods worldwide adopted by researchers is obtained from PubMed website with the key word search "EVs isolation methods" (Figure 7).
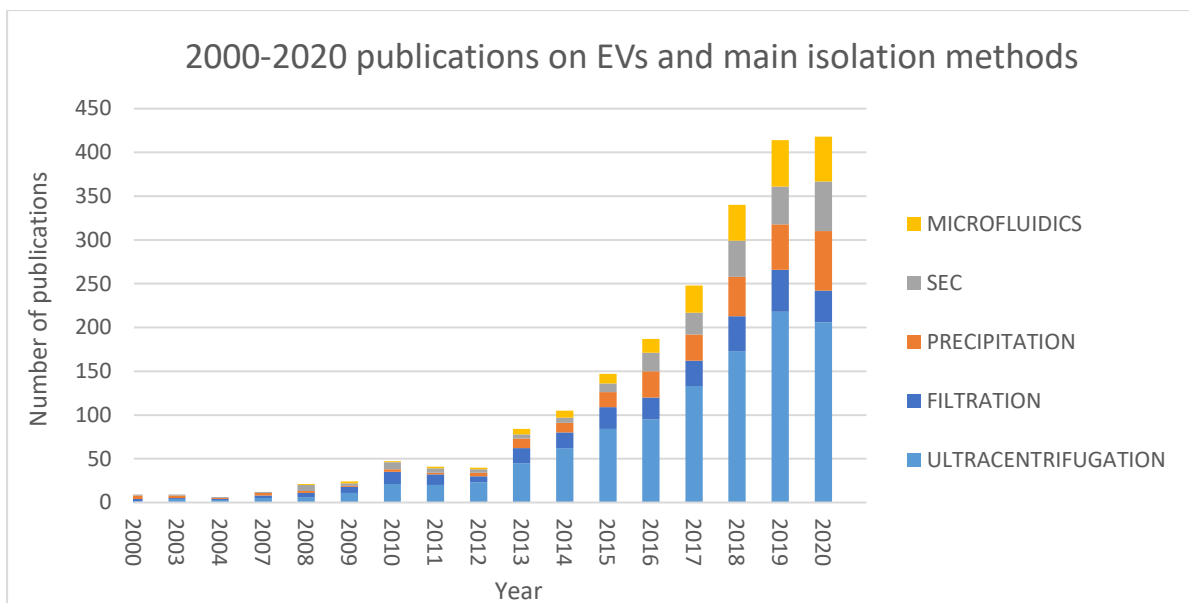
Figure 7: Number of publications on EVs isolation in recent years (PubMed)

Considering the year 2020, a pie chart with the worldwide distribution of the different primary methods used for EVs isolation is reported (Figure 8). It shows that ultracentrifugation remains by far the most widely used primary isolation method (49%), while the other half of the pie is distributed between precipitation (16%), gel filtration (14%), microfluidic technologies (12%) and filtration techniques (9%).
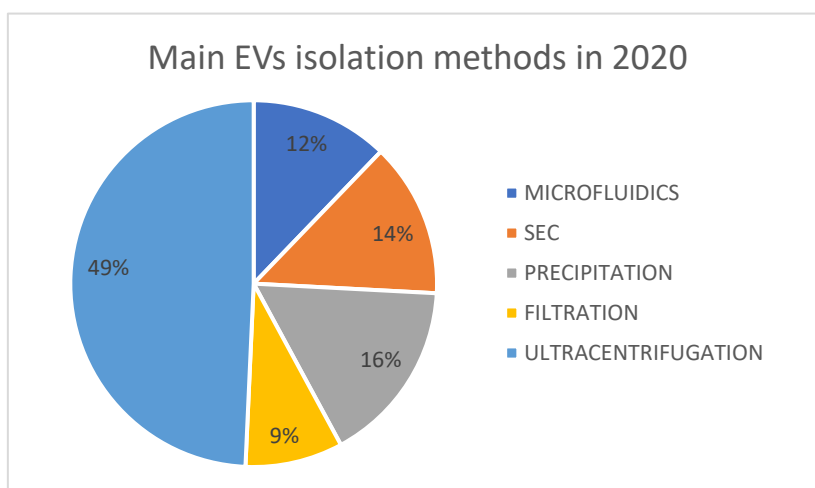
Figure 8: In 2020 the total number of publications on EVs isolation is 474. Among those, 206 papers used UC as primary EV isolation methods, 68 precipitation techniques, 57 SEC, 51 microfluidics technologies and 36 used filtration processes (PubMed).

It is noteworthy that the previous statistics refer only to the "primary" isolation method, while usually researchers use a combination of different techniques to obtain EVs preparations. In fact, according to a recent survey of the current worldwide practices for the isolation of EVs[1] over half (59%) of the respondents use a combination of different isolation techniques in their protocols.

2.1 Methods based on size and buoyant density

2.1.1 Differential ultracentrifugation (UC)

Ultracentrifugation is regarded as "the golden standard" for EVs isolation. To date, the majority of EVs have been isolated at lab scale from human cells grown in T-flasks and purified by ultracentrifugation-based methods[2]. Centrifugation allows the separation of particles according to their density differences, upon the application of a centrifugal force.

Differential ultracentrifugation for EVs isolation consists of multiple steps: first a low-speed centrifugation which removes high density particles like dead cells and apoptotic bodies, followed by higher speed spins to eliminate larger vesicles and debris. After, the supernatant is subjected to a high-speed ultracentrifugation run to pellet EVs. A typical UC-based workflow for EVs isolation is the following (Figure 9):
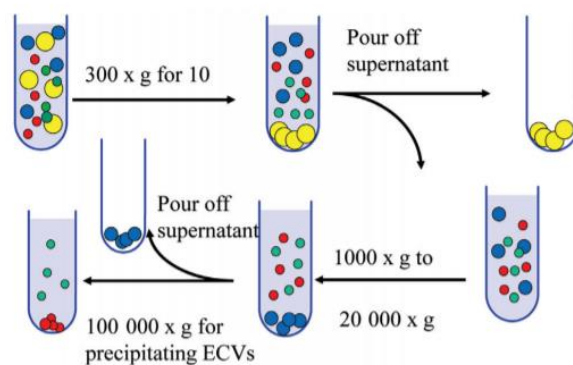
Figure 9: A typical UC protocol for EVs isolation by Momen-Heravi et al. [4]

- Centrifugation at 300 - 400 × g for 10 min to sediment the main portion of cells.
- Centrifugation of the supernatant at 2000 × g to remove cell debris. Pellet is discarded.
- Centrifugation of the supernatant at 10 000 × g to remove the aggregates of biopolymers, apoptotic bodies, and the other structures with the buoyant density higher than that of EVs. Pellet is discarded.
- Ultracentrifugation of the supernatant at 100 000 – 200 000 × g for 2 h to pellet EVs.
- The pellet of EVs is resuspended in phosphate buffered saline (PBS) and stored for further analysis.

Usually, two additional stages in EVs purification are carried out: washing and microfiltration. In the former the EV pellet is resuspended and ultracentrifuged several times to remove co-sedimented proteins and impurities. Microfiltration is performed using filters with pore diameters of 0.1, 0.22, or 0.45 μm to further purify the obtained EV preparation. Washing and microfiltration stages increase the purity of the target vesicles, but they also contribute to decrease their quantity.

The efficiency of EV isolation by ultracentrifugation is dependant on four main factors: viscosity of the sample, acceleration (g), type of rotor and its characteristics, centrifugation time[3,5,6].

- Viscosity
  A reduction in the viscosity of the sample causes an increase in the efficiency of isolation, as the higher the viscosity, the more difficult it would be for the vesicles to move through the sample.
- Acceleration (g)

The acceleration of the centrifuge, expressed in terms of relative centrifugal force (RCF or g force), determines the separation efficiency.

- Rotor – k factor

The k-factor of a rotor represents the relative pelleting efficiency of a rotor at maximum speed. The lower the k-factor, the better the pelleting efficiency of a rotor and the shorter the centrifugation time. The pelleting time is determined by the equation:

$$t=k/s$$

where t is the time [hr] required for centrifugation, s [S] is the sedimentation coefficient expressed in Svedberg units, and k is the k-factor. The sedimentation coefficient depends on the size and shape of the vesicle being isolated, and the viscosity of the sample media. The smaller the s, the longer it takes to pellet the particle.

- Rotor – type

Two types of rotors are commonly used for EVs isolation: swinging bucket (SW) and fixed-angle (FA) rotors (Figure 10). The SW rotor allows the tube to change angle during the run: the buckets are vertical when stopped and horizontal from the rotational axis when rotating. The FA rotor is fixed at a constant angle during the whole centrifugation run. As consequence of their geometry SW rotors generally have a longer sedimentation path length than FA rotors, which results in a lower pelleting efficiency (lower k value). The SW rotor, however, have a better resolution, making it more suitable for the separation of particles with small differences in size (similar sedimentation coefficients). On the other hand, the FA rotors are better suited for the separation of particles with big differences in the sedimentation coefficients.
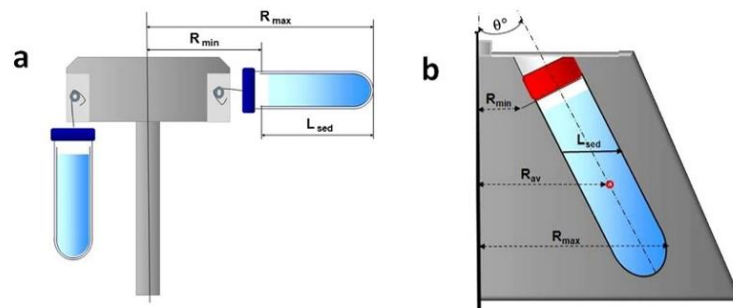
Figure 10: (a) "swinging bucket" and (b) "fixed angle" rotors of a centrifuge by Livshits et al.[6]

- Time

The centrifugation time is set considering the viscosity, the g-value, and the desired EV final purity. Longer runs allow to pellet greater quantities of exosomes as well as exosomal proteins and RNA. On the other hand, the duration shall be limited to preserve the functional integrity of the final product and reduce co-precipitation of impurities. In fact, extreme pellet condensation may cause aggregation thus making pellet impossible to resuspend.

As the UC isolation protocol is relatively easy to follow and does not require any specialized equipment apart from an ultracentrifugation unit (commonly found in most laboratories), it has been widely employed over the past 30 years to isolate exosomes from various sources such as cell culture media, human fluids, plants, bacteria and animal sources[7]. Being the most frequently used method in the field

it offers the best possibilities in terms of data comparison from published literature. Differential ultracentrifugation, in fact, contributed to most pioneering exosomes studies.

However, the usual UC protocol suffers from several drawbacks[3–5,7]. The resultant EVs yield is very low compared to the starting material and it may be highly variable, depending on the individual operator. The efficiency of the process is, in fact, affected by many factors and the composition of the isolated EV mixture is highly sensitive to the mentioned variety of experimental settings. This also means that EV mixtures obtained with different ultracentrifuges are highly variable and unreproducible. Often non-exosomal impurities are present: under a certain centrifugal force, all components with a certain buoyant density can be precipitated at the bottom of the tube. Consequently, often there is the need to subject the UC pellet to additional stages: these procedures are time-consuming and could further compromise the low EV yield.

Besides, the high forces applied during the final UC step may damage the integrity of EVs and cause aggregation. Commonly used ultracentrifugation tubes have a low volume capacity (5–20 mL). The use of centrifugal concentrator devices (e.g., Centricon®) can increase the process of volumes of up to 200 mL with a 5 mL loading capacity ultracentrifugation tube[7]. Nonetheless, implementation of UC on a large scale is challenging and currently it is limited to analytical and small-scale experimental biochemistry[3].

2.1.2 Density gradient ultracentrifugation (DG UC)

The purity of UC-based EVs preparations can be further increased using an additional density gradient step. In DG UC the sample is loaded in a centrifuge tube where a pre-constructed density gradient medium is present (Figure 11A). It has a progressively decreasing density from the bottom to the top of the tube. The tube is then subjected to an extended ultracentrifugation spin. Under the application of the centrifugal force solutes gradually move through the DG medium towards the bottom. They reach a static position in the medium layer having the same density.
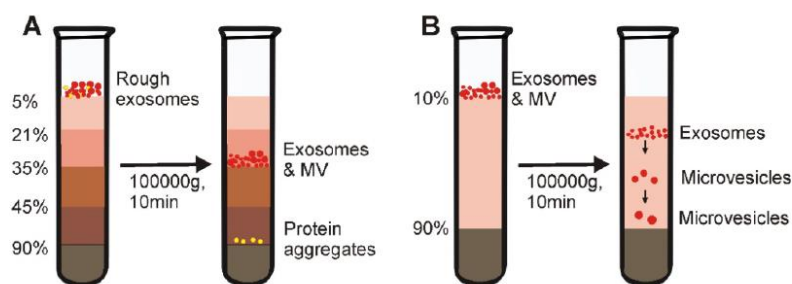
Figure 11: Isopycnic density-gradient UC (A) and Moving-zone gradient UC (B) by Yang et al.[7]

In isopycnic density-gradient UC the separation depends solely on the density difference between the different solutes in the sample: this means that it cannot separate substances with similar buoyant density to exosomes[7].

To overcome such limitation, moving-zone gradient UC (also called rate zonal centrifugation) has been developed, which separates particles by both size and density. It normally consists of two gradient medium sections (Figure 11B). The top layer medium has a density lower than all of the solutes of the sample while the bottom is a high-density cushion. As the density of the solutes are all greater than that of the gradient medium, after centrifugation, all solutes will be sequentially separated based on not only density, but also mass/size, thereby allowing the separation of vesicles of comparable density but varying size. This also means that, unlike isopycnic UC, all insoluble particles can be pelleted at the

bottom of the tube after prolonged centrifugation In moving-zone UC the centrifugation time must be optimized for efficient exosome isolation[7].

Sucrose and iodixanol (also known as OptiPrepTM) are the most common density gradient medium for exosome isolation[3].

As it can partially overcome co-precipitation of contaminants and apoptotic bodies found in the UC pellet, density gradient ultracentrifugation yield EV preparations with a higher purity as compared to a classic UC. It can increase purity of exosomes from larger vesicles such as apoptotic bodies, but also smaller ones (subcellular components) such as HIV-1 particles and virions[5].

A limiting factor of DG UC is the narrow loading zone (due to the presence of the DG medium) which limits the sample volume that can be loaded[3].

Overall, besides the EVs yield and purity improvements, this method still suffers the drawbacks associated to classical ultracentrifugation, as it still results in a considerable loss of EVs; it is complex, laborious, and time-consuming and it is inapplicable in a clinical setting.

2.1.3 Size exclusion chromatography (SEC)

Over the last few years size exclusion chromatography (SEC), also called gel-filtration, is becoming an increasingly popular method for EVs enrichment because it allows an efficient separation between vesicles and macromolecules present in biological samples, using mild physical conditions. As the components to be separated pass through a porous stationary phase they are fractionated according to their sizes and shapes. During SEC vesicles preserve their structural integrity, biological activity, and quantity, as they move with the fluid flow under a small differential pressure and almost do not interact with the fixed phase[9].

The knowledge acquired from SEC-based liposome isolation has been readily applied to exosome separation, as exosomes share many similar physical properties with liposomes[7].

SEC can be set up as gravity-flow or can be automated with FPLC systems, improving product consistency and data reproducibility by reducing user influence. The use of buffers with a high ionic strength (e.g. phosphate buffers as PBS) minimizes undesired interactions between the product and the stationary phase.

Commonly, cross-linked agarose beads (as Sepharose® and Sephacryl®) have been developed as stationary phase for EV isolation. In less than 10 years of development, companies have commercialized SEC kits designed specifically for exosome isolation such as qEV (iZON) and PURE-EVs (Hansa Biomed). They have been applied to separate EVs from various biofluids such as plasma, serum and cell culture[3,7].

Each resin has its own size exclusion limit that allow to obtain a specific EV population. For example, Sepharose®CL-4B resin with a size exclusion limit of 42 nm is more suitable for separating EVs from albumin, compared to Sepharose®CL-2B, with an exclusion limit of 75 nm[10].

SEC avoids important drawbacks associated with dUC-based exosomal isolation: aggregation and morphological changes in the extracted vesicles. It is considered a superior method to other conventional techniques as dUC also in terms of final purity: the EV fraction isolated by SEC usually displays a low content of non-EV proteins. For example, it has been found that SEC can separate EVs from high density lipoproteins (HDLs): they have similar densities but different sizes, being HDLs particles smaller than EVs. This means they can be separated through SEC but not with commons density-based isolation methods as dUC[13]. On the other hand, SEC can co-isolate EVs with other lipoproteins sharing the same size range with EVs, including chylomicrons (75-1200 nm), LDL (25nm) or VLDL (30-80nm).

One of the most important drawbacks of the method is the limit on the input sample volume, intrinsically set by the bed volume. For this reason, several groups have proposed using a concentration step (UC, UF) prior to use of SEC columns. Also, with SEC, the EVs fraction of interest is diluted during the process and a subsequent concentration step may be as well required. This additional step can further increase EV losses and the possibility of introducing environmental contaminants[7]. Furthermore, packing of SEC columns can be tedious, being a procedure highly affected by affected by operational error it can decrease the reliability of the method[10].

Although dUC is still the most common technique, SEC is increasingly being adopted in the field. In particular, it is mainly employed in combination with other techniques, allowing to overcome SEC limitations as well as to improve EV purity[7]. Usually, it is combined with initial centrifugation steps to remove cells and debris and ultrafiltration to manage sample volume. Also, anion exchange chromatography has been used to selectively remove lipoproteins after SEC separation[14].

2.1.4 Filtration techniques

Filtration is a popular size-based separation technique used for both EVs concentration and purification. Filtration techniques relies on the use of membranes with specified pore diameters to isolate particles of a certain size range, through the application of a driving force, usually pressure or centrifugal force. Microfiltration (MF) membranes have a pore size in the order of micrometers and when isolating EVs by MF, filters with pore sizes of 3, 0.8, 0.45, 0.22, and 0.1 μm are typically used. Ultrafiltration (UF) employs more selective membranes, with defined molecular weight cut-offs (MWCO) ranging from 10-600 kDa for most applications.

The recovery of exosomes based on filtration techniques can be performed through a diversity of isolation protocols. Microfiltration and ultrafiltration (UF) are often used in combination with other techniques, for example as a complement to ultracentrifugation protocols or as additional steps in gel filtration chromatography. However, MF and UF are also applicable as stand-alone techniques for EV isolation.

Both UF and MF membranes can be exploited in sequential MF/UF isolation protocols: they rely on a series of filtration steps for exosome enrichment. First, larger impurities (cells, cell debris, apoptotic bodies) are eliminated first by using filters with pore diameters of 0.8, 0.45, 0.22 and 0.1 μm, leaving a relatively vesicle-rich permeate. Smaller impurities (free proteins, contaminants) are then eliminated by using membranes with pores smaller than the target EVs (0.22 μm, 0.1 μm, 600 kDa, 500 kDa, 100 kDa); they are able to retain vesicles and collect impurities into a permeate waste. Thus, the EV fraction of a specified size is concentrated and purified.

Merchant et al.[15] proposed a microfiltration protocol for urinary exosomes using a 0.1μm low protein-binding membrane in hydrophilized polyvinylidene difluoride (VVLP) filter. They managed to easily isolate EVs from fresh urine samples and reported equivalent enrichment of EVs proteomes with reduced co-purification of abundant urinary proteins in comparison with other standard methods as ultracentrifugation.

Heinemann et al.[16] developed an optimized sequential UF/MF protocol for the isolation of exosomes from cell culture supernatants or body fluids. It involves 3-steps (Figure 12):

- Step 1) Dead-end prefiltration with a 0.11 μm mPES membrane. Cells and cell debris are filtered out while exosomes and free protein can pass through the filter. Microvesicles larger than 0.1 μm are also supposed to pass the filter due to their flexibility.

- Step 2) 5-times tangential flow filtration (TFF) with a 500 kDa MWCO mPES membrane to remove free proteins and contaminants and concentrate the sample.
- Step 3) Track-Etch filtration with a 0.1μm membrane in TE PC is performed for final exosome enrichment at very low pressure to filter out microvesicles larger than 0.1 μm.
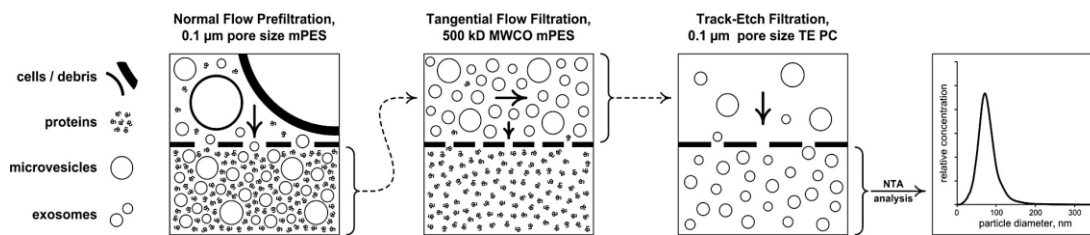

Figure 12: Schematic of the 3-step filtration protocol for the isolation of exosomes from cell culture supernatants or body fluid developed by Heinemann et al. [16]

Based on the sequential ultrafiltration protocol, many companies recently developed EVs isolation kits. ExoMirTM by Bio Scientific Corporation uses two membranes (200 nm and 20 nm) both placed in a syringe allowing rapid fractionation of exosomes and larger membrane-bound particles[17]. Also, ExoTIC (Exosome total isolation chip) developed by Liu et al.[18] is based on the same principle: it is a solid device that hosts a track-etched polycarbonate membrane (30 nm or 50 nm pore size) and a PES filter (200 nm pore size). It allows to purify intact EVs in the 30–200 nm size range from various biological media. Both kits contribute to make filtration-based isolation of exosomes a more reproducible and clinically friendly procedure.

In centrifugal UF centrifugation provides the force to rapidly remove solvents and small molecules through an ultrafiltration membrane. Centrifugal UF is usually carried out in centrifugal concentrators, centrifugation tubes packed with a membrane filter, usually suitable for small starting volume ranging from 100 μl to 100 ml (Sartorius Vivaspin centrifugal concentrators).

Cheruvanky et al.[19] demonstrated that urinary EVs can be rapidly enriched from human urine using a centrifugal concentrator with 100kDa nanomembranes, thus enriching vesicles by centrifugation at 3000 x g.

According to Lobb et al.[20] centrifugation-based filters (Centricon) have been shown to recover from CCM three times as many particles as pressure-driven membranes (BioMax). The low yield of the pressure-driven process is explained by the authors considering the non-specific absorption of a significant amount of exosomes to the membrane in the UF stirred cell. They also found out that centrifuge-based concentrator is the most appropriate device when working with volumes of 50-200 mL of conditioned media, while pressure-driven concentrating is more appropriate with volumes in excess of 400 mL due to the higher flow rate, and that exosome loss is only observed with the first 50-100 mL of CCM (once the membrane has been sufficiently ''blocked'' with particles, the yields of the two processes are comparable).

The main challenge with MF/UF is the clogging and trapping of vesicles (and therefore loss of exosomes) on the filter unit. The driving force is used to "push" the specimen through the membrane; however, protein molecules and newly formed aggregates of biopolymers and vesicles block the membrane pores as the sample is being concentrated, thereby slowing the process and increasing the concentration of contaminant molecules and resulting in partial loss of the target material. Membrane fouling is common and unavoidable to all filtration operations, but its formation can be limited in different ways. First, by the selection of a proper membrane's material, like in this case a material having low affinity for proteins (e.g. PES, PVDF). Also, the individuation of a suitable membrane cut off

plays a vital role. Fouling can be limited by starting with larger MWCO filters and moving to smaller ones though many filtration steps.

When filtration is performed in Tangential Flow Filtration (TFF) mode the feed flows tangentially over the membrane, and membrane fouling is significantly limited compared to dead-end mode. It can be controlled by reaching steady conditions that guarantee constant flux and cake thickness over time. Depending on the membrane pore size, TFF can be applied to isolate the desired product from larger particles by allowing it to permeate into the permeate stream or to purify the target product from smaller impurities when it is maintained in the retentate stream. Moreover, the same configuration can be applied for buffer exchange or for product concentration in the retentate stream. In fact, if the volume lost though transmembrane flow is resupplied to the feed as fresh buffer, TFF can be used for buffer exchange in diafiltration mode.

This flexibility, together with the short processing times, the scalability, and the adaptability to continuous operation, is industrially fully exploited in the field of liposome production, where TFF is considered as the standard purification method[21]. EVs and liposomes have a comparable structure and they are both made by a lipid bilayer membrane. Their similarities make TFF the most suitable candidate as unit operation for the large-scale production of EVs.

While SEC dilutes the product, TFF also concentrates EVs while purifying them. TFF can be thought of as a hybrid of concentration and purification strategies, highly suitable for large- scale EV isolation from diluted samples.

Besides, industrial-scale input volumes can be used as crossflow filtration units can hold volumes in the order of liters. Compared with UC, TFF offers several advantages, including mild pressure, time efficiency, scalability and absence of expensive and complex equipment. The advantages of TFF over UC have been demonstrated by Busatto et al.[22], where TFF has been applied to isolate EVs from cell culture medium with a 500 kDa PES hollow fiber membrane. EVs have been enriched and purified from scalable sample volume with high a recovery rate in a rapid, sterilized manner. Comparative assessment of TFF and UC revealed that the former concentrates EVs of comparable physicochemical characteristics, but with higher yield (5-fold higher), improved batch-to-batch consistency, less albumin contaminants in half the processing time (1 h).

By contrast, the study by Heath et al. [23] underlined that despite the higher purification yield of intact vesicles, TFF provides EVs with lower purity than UC. They detected a large amount of co-isolated proteins and lipid impurities, that would demand a further purification step, negatively impacting the processing time and overall yield.

Certainly, the diversity of isolation protocols used by different researchers considerably complicates comparison of the results obtained by different laboratories.

Besides, an aspect that should be further evaluated is the potential deformation and lysis of EVs caused by shear forces. The results obtained by Dimov et al.[24] on liposomes demonstrated that the shear stress on the filter does not alter the integrity of liposomes at optimal operational conditions, thus offering a gentler purification method in comparison with UC. In this context, the selection of an adequate TMP appear to be crucial.

To conclude, the work done by B Dehagani et al.[25] offer an example of an optimized TFF isolation protocol, for the concentration of EVs from large volumes of fluid, that involves the standardization of the membrane cleaning step (Figure 13).
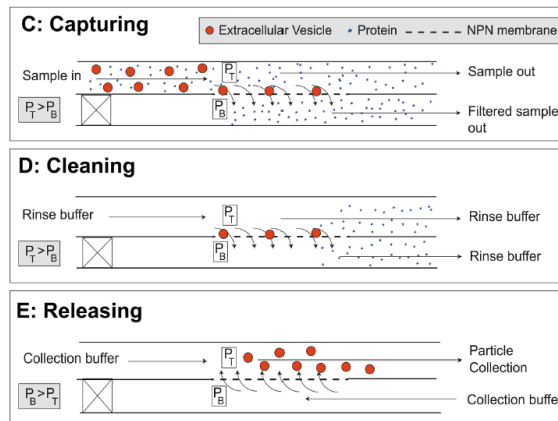
Figure 13: 3-Steps protocol (TFAC) developed by Dehagani et al.[25] for EVs isolation

The authors developed a filtration based microfluidic system termed as tangential flow for analyte capture (TFAC), which is a modified version of tangential flow filtration. In this 3-steps protocol: particles are first captured on the surface of a membrane in tangential flow, then washed under the same flow conditions with a cleaning buffer to remove contaminants; finally the TMP is reversed, releasing the particles from the membrane where they are then swept downstream and collected. According to the authors testing human plasma in TFAC mode resulted in capturing extracellular vesicles with minimal contamination.

2.1.5 Field Flow Fractionation (FFF)

Field-Flow Fractionation (FFF) is a size-based isolation technique that has been applied in the field of EV isolation. Asymmetric Flow Field-Flow Fractionation (AF4) is the most abundantly used sub-technique of FFF. In AF4 the separation is provided by the diffusion of particles as they flow in a thin sub-millimetric film of laminar flow confined in a narrow chamber with a membrane at the bottom. A force field is applied perpendicular to the laminar flow and drives the particles toward the UF membrane, which subsequently permeate according to their size (Figure 14). The feed flows in a parabolic shape as a constant laminar flow is employed[26].
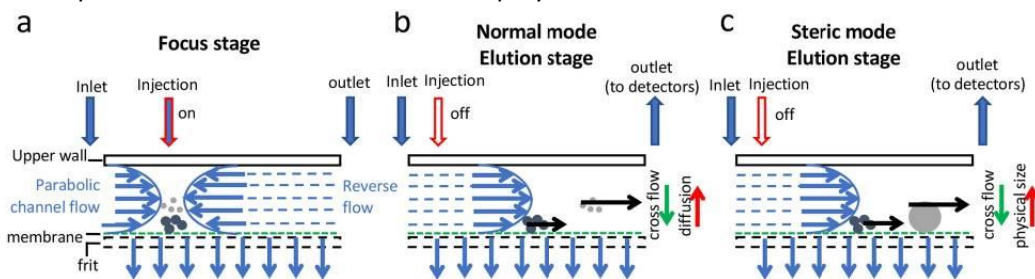
Figure 14: Schematic illustration of the AF4 working principle with the three main stages a) Focus stage b) normal mode Elution stage c) steric mode Elution stage by Zhang et al.[27]

It is a gentle technique that does not require a stationary phase, conversely to chromatographic separations. Besides, AF4 has a programmable cross-flow intensity which can be optimized to increase the separation efficiency, making the process very flexible. Contrary to the elution in SEC, the smaller particles elute first followed by the larger ones. This is because smaller particles have higher diffusion coefficient.

The major disadvantage of the method is the low sample volume input since the field and the membrane could get overloaded at high volumes. Usually, these devices are coupled with a on-line

detectors such as UV detectors, and dynamic light scattering (DLS) and multi-angle light scattering (MALS) for the detection of size distribution of particles[10,26].

AF4 can successfully separate EVs from lipoproteins and it is becoming attractive for the fractionation of EV subpopulations. Zhang and collegues[28] fractionated EVs into distinct subclasses – small exosomes (60–80 nm), large exosomes (90–120 nm), and discovered a new subpopulation of non-membranous nanoparticles that called "exomeres" (35 nm) from various cell types. According to them AF4 is highly reproducible, fast, simple, label-free and gentle. Moreover, they isolated different exosome subpopulations in a single AF4 run with real-time measurements of various physical parameters of individual particles, proving that AF4 can also be an important additional analytical tool.

2.2 Methods based on solubility changes

2.2.1 Polymeric precipitation

Precipitation methods for EVs isolation are the second most popular method after ultracentrifugation, as in 2020 about 16% of the publications relies on precipitation techniques as primary method for EV isolation (PubMed). Crowding reagents as hydrophilic polymers have been long used to precipitate proteins, nucleic acids and viruses virus particles[3].

Concerning EVs, polymeric precipitation is based on the formation of a mesh-like polymeric web that captures EVs, which are later pelleted at low centrifugal speeds. The crowding agent leads to a decrease in the solubility of the compounds in the solution, thus allowing to pelletize EVs at lower centrifugation speeds. In most methods, samples are incubated with PEG at 4°C for up to 12 h and centrifuged at low speed (usually at 1500 x g) to collect pelletized EVs in the buffer[3].

The most used crowding reagent is Polyethylene glycol (PEG), with various molecular weights. The advantages of PEG precipitation are simplicity and celerity as well as the possibility to work at physiological p-H values that results in milder effects on EVs structural integrity and biological activity. PEG is a cheap non-toxic, biocompatible and flexible material, but it should be separated from the EV enriched preparation, resulting in more costly and intensive downstream processing[4]

Since EVs are negatively charged, charge-based precipitation could also be performed in the presence of PEG and positively charged molecules such as protamine. PEG has also been used along with dextran to create a two-phase system for isolation that significantly decreased protein contamination. Some precipitation methods rely on hydrophobic interactions to aggregate EVs by "salting them out" using sodium acetate, even if these methods are highly non-specific[3].

Overall, the main advantages of the method are the simplicity, the possibility to process large volumes of fluids and the fact that it does not require specialized equipment. Typically, polymer precipitation-based exosome isolation is characterized by high yield (higher than 90%). This comes at a price, with the major disadvantage being the elevated levels of co-precipitation of non-EV proteins, protein complexes, lipoproteins, and nucleoproteins, as well as viral particles.[3]

To report a successful example of PEG precipitation Rider et al.[29] adapted a protocol for isolating viruses using PEG to EVs isolation and called it "ExtraPEG". They added 5-12% PEG solutions to the cell culture media; the resulting mixture is incubated overnight, centrifuged at low speed, followed by a single small-volume ultracentrifugation purification step. Their NTA results showed a linear relationship between the yield in vesicles and the concentration of PEG. By contrast, low PEG concentrations favor highly pure preparations. The authors found 8% PEG concentration to be the optimal value. They obtained a yield in exosomes comparable to the differential centrifugation

method, and superior to commercially available purification methods. Furthermore, proteomic analysis revealed that 97% of the proteins detected are associated with vesicles.

Recently, many commercial kits for precipitation have been developed like ExoQuick (Systems Biosciences), Total Exosome Isolation (Life Technologies), ExoPrep (HansaBioMed), Exosome Purification Kit (Norgen Biotek) and miRCURY Exosome Isolation Kit (Exiqon). They are reported to isolate EVs with different quality and efficiency.

Exoquick, for example, is a rapid EV isolation system that can process also very small sample volumes (100 µl). It contains a proprietary polymer that precipitates exosomes overnight after mixing with a biofluid, refrigeration and low speed centrifugation. A modified ExoQuick protocol was proposed by Alvarez et al.[30] for isolating EVs from urine. The modifications to the standard protocol comprise centrifugation at a higher speed, DTT treatment of sample, heating for THP depolymerization, a larger volume of ExoQuick solution and longer incubation with polymer solution. The modified method gives larger amount of EVs and isolates larger amount of mRNA compared with the standard ExoQuick protocol.

Both Exosome RNA Isolation Kit (Norgen, Biotek Corp.) Total Exosome Isolation (Thermo Fisher Scientific) are reported to yield high EV content and low concentration of contaminating proteins.[31,32] Despite being user-friendly and guarantee high reproducibility, these kits are also very expensive, and their efficiency is usually not taken from granted by researchers.

According to Andreu et al. [33] the quality and yield of the EVs and mRNA isolated using self-prepared PEG 6000 optimized solution is comparable to the commercial reagents but with the cost of procedure being considerably lower.

2.3 Methods based on charge

2.3.1 Anion exchange chromatography (AIEC)

Zeta potential measurements on EVs determined that they do possess a negative charge (-10 to -50 mV). Anion exchange chromatography is currently gaining growing interest in the field of EVs isolation as an option in both large and small scales[2]. It is already a well-established bioprocessing technique for the separation of proteins and viruses. The method exploits the interactions between the negative charges on the EV membrane and an anion exchanger with positively charged functional groups. The stationary phase is able to retain the vesicles inside the column and bound vesicles can be eluted by using a high ionic strength elution buffer.

Heath and colleagues[23] demonstrated the applicability of the AIEC technique using a monolithic column with quaternary amine functionality (strong anion exchanger) for the isolation of cell-derived EVs. The method required shorter isolation time (less than 3 hr for 1 L of cell culture supernatant) compared to UC and yielded intact EVs with higher purity compared to TFF. The method accomplished to efficiently remove FBS-derived proteins, as bovine serum albumin (BSA) and apolipoprotein A. Additionally, the macroporous monolithic column allowed to operate at flow rates up to 10 mL min^{-1}, demonstrating the potential to overcome the throughput limitations of chromatography resins.

Kosanovi'c et al.[34] isolated EVs from amniotic fluid using using diethylaminoethyl cellulose resin (weak anion exchanger). They optimized separation and elution conditions and found out that a higher concentration of NaCl (1 M vs 0.2 M) as elution buffer resulted in larger cell-derived vesicles. Despite the versatility and scalability of AIEC, its applications in EV research as an individual technique is mostly limited to cell culture so far [10]. More complex biological matrices, such as blood and plasma, are challenging for ion-exchange methods due to the presence of high amounts of other negatively

charged biomolecules. The method can, however, be used in combination with other techniques to increase EV purity.

2.3.2 Electrophoresis

Electrophoresis technique exploits the differential mobility of the particles under the application of an electric field due to their charge-to-size ratio. Agarose gel electrophoresis is a well-established method for the separation of RNA, DNA, and proteins. It is a new-born technique in the field of EVs isolation, nonetheless very promising.

Zhang et.al.[35] proposed a method for the separation of EVs in plasma using agarose gel electrophoresis based on their differences in size and zeta potential properties with lipoproteins contaminants. Usually, the separation of EVs from certain viscous biofluids, such as plasma, are difficult due to the presence of lipoproteins which have similar dimensions as that of EVs. The authors evaluated the average diameters and zeta potentials of lipoproteins as well as EVs and formulated a protocol for agarose gel electrophoresis based on their size and z-potential ratios. Lipoproteins are classified with respect to their densities as very low density (VLDL), low density (LDL), and high density (HDL). From electrophoresis track assays, it was observed that the EVs migration is slower than HDL but faster than LDL and VLDL in 1% agarose gel with Tris buffer (Figure 15C). This method achieved high recovery rates in less than 3 hours.
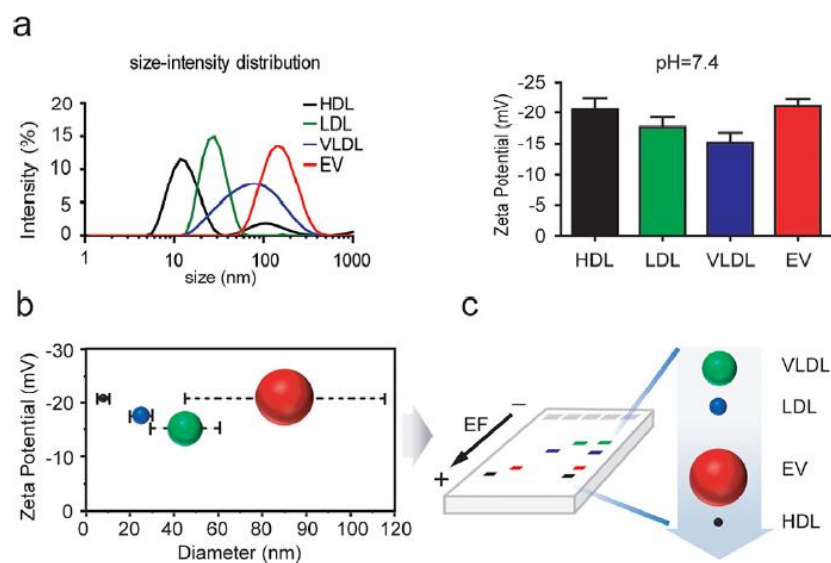

Figure 15: A) Size and B) zeta potential comparison of common lipoproteins with EVs. C) The migration of the lipoproteins and EVs under electric field on an agarose gel by Zhang et al. [35]

Overall, as for AIEX, all the separations based on electrical charge have the same major problem: they can lead to co-isolation of all the negatively charged biomolecules. This limitation can be overcome by combining electrophoresis with other techniques, based on size or density differences. In this context membrane-based processes are very attractive.

Yang et al. [36] recently developed a method for the isolation of lemon-derived EVs (LDEVs) that combines an electrophoretic technique with a 300 kDa cut-off dialysis bag for the isolation of PDEVs (ELD). The working principle is shown in Figure 16: upon the application of an electric field, impurities and non-vesicular proteins were able to pass through the 300kDa membrane, while lemon vesicles were retained and thus purified. The electrophoretic buffer was changed every 30 min, and the

electrophoretic direction was also reversed to avoid membrane pores being blocked by the vesicles. They obtained a preparation highly enriched in lemon vesicles in just 2.5 hours, demonstrating that ELD was an efficient method for the isolation of LDEVs, being time-saving and without the need of special equipment.
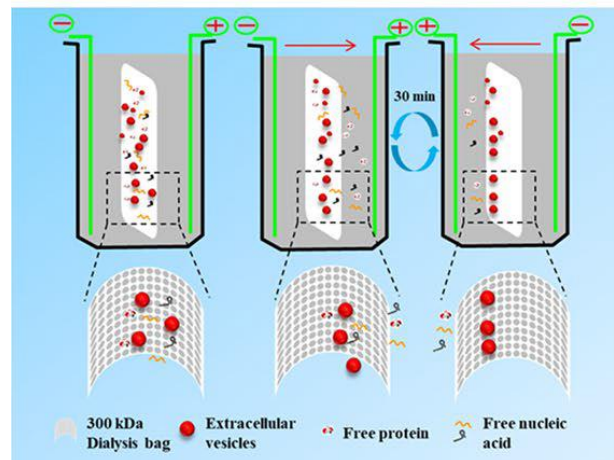

Figure 16: ELD method working principle by Yang et al. [36]

The main drawback for electrophoretic separations is the heat generated during the process due to the huge amount of electric field necessary for efficient separation. This can be potentially detrimental to vesicles. Marczak et al.[37] tacked the problem combining electrophoresis with an ionic membrane process, in a continuous setup carried out in a microfluidic chip (Figure 17).
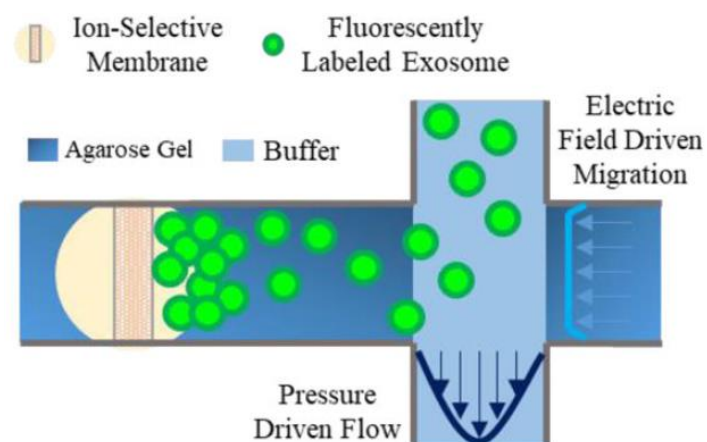

Figure 17: Microfluidic cell set-up with electrophoresis and an ion selective membrane by Marczak et al. [37]

The cationic membrane attracts the negatively charged EVs as they flow over the gel under the influence of an electric field. Purification is achieved exploiting the big agarose gel pores that efficiently trap cell debris while smaller vesicles easily reach the membrane. The cationic membrane allows for exosomes concentration and isolation, while electrophoresis allow for their purification. A comparison was carried out with the golden standard ultracentrifugation as well as the commercial precipitation reagent Exoquick. The authors found a recovery rate between 70-80% while in comparison, from the same source, UC and Exoquick had 6% and 11% respectively.

2.4 Methods based on affinity interactions

2.4.1 Immuno affinity capture

Immunoaffinity-based isolation strategies relies on specific reversible interactions between an immobilized ligand and a surface molecule of EVs. Lipids, proteins, and polysaccharides are exposed on the surface of EVs. All these substances are potential ligands for manifold molecules, including antibodies, lectins, and lipid-binding proteins.

For effective immunoaffinity-based exosome isolation, first ligands recognizing exosome-specific markers need to be fixed on a solid surface (Figure 18). The sample is then incubated with the ligand-conjugated solid matrices and exosomes are enriched onto such solid matrices. Finally, through an elution step, free exosomes can be collected[7].
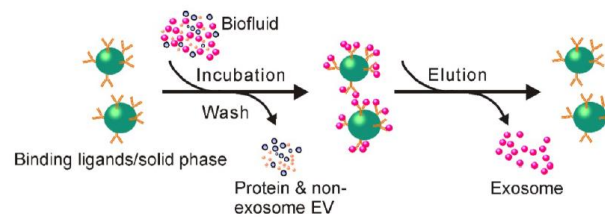

Figure 18: Schematic of immunoaffinity-based exosome isolation by Yang et al. [7]

To date, different affinity approaches have been exploited for EV isolation: they can be categorized into two groups, namely affinity chromatography and immunocapture, based on isolation mechanism[10]. Considering the matrices, small-scale substrates, such as magnetic beads, microfluidic chips, plastic plates, cellulose filters, membrane affinity filters or monolithic columns s have been used over the past few years[2].

Antibody-antigen interactions are the most exploited and several antibody-based affinity-capture beads are available for the purification of EV. The most used antibodies target tetraspanin proteins as EVs markers. The tetraspanin protein family is most prevalently associated with mammalian EVs and, in particular, CD9, CD63, CD81, and CD82 are found in EVs from nearly any mammalian cell type[38].

Zhao et al.[39] have developed a microfluidic device (ExoSearch chip) for continuous exosome isolation and detection from human plasma using magnetic beads conjugated with three antibodies against common exosomal markers (CD9, CD81, and CD63) for immunocapture and fluorescence-labeled tumor markers (CA- 125, EpCAM, and CD24) for probing.

Other affinity methods use exosome-binding molecules such as heat shock protein[40] and heparin[41], or markers from EVs parent cells such as epithelial cellular adhesion molecule (EpCAM)[42], that are often overexpressed on tumor-derived exosomes. As demonstrated by Rupp et al.[43], an EpCAM antibody-coated magnetic bead system allowed the specific isolation of tumor-originated exosomes from not only cell culture medium but also various types of clinical samples. Collecting exosomes of specific origin not only facilitates the study of their parental cells, but also provides important indicators for disease diagnosis (for example, through the detection of EpCAM exosomes is possible to assess the existence of EpCAM related cancers). Interestingly, through specific biomarkers, immunoaffinity capture represents an ideal platform for isolating defined subpopulations of exosomes with specific origins.

The most important advantages of affinity-based approaches for EV isolation include high specificity and selectivity for EVs of interest besides a reduced isolation time and easy procedures, making them highly attractive and suitable for clinical applications and diagnostic purposes.

Nonetheless, affinity methods in the field of EVs isolation are still at the infancy of their development. In the current state-of-the-art none of these approaches have yielded pure EVs preparations due to the limited knowledge regarding specific surface biomarkers of EVs[44].

A problem related to affinity methods is the harsh and non-physiological elution buffer used to separate exosomes from ligands. Elution could irreversibly damage the structure and biological function of the collected EVs. It is worth to notice, however, that the denatured exosomes can still be acceptable for diagnosis purposes (e.g. via assessing genetic and protein contents of exosome)[7]. However successful elution of intact EVs and their subpopulations have been shown in studies with antibodies immobilized in monolithic columns[45].

Monolithic columns have several advantages over particulate-based supports for the separation of large biomolecules, including low back pressure and convective mass transfer rather than diffusive transport, enabling high flow rates and short separation times due to large and interconnected pores. Multia et al.[45] isolated platelet-derived EVs from human plasma through immunoaffinity chromatography method using a polymeric monolithic disk column (Figure 19). The method could easily isolate intact CD9 + and CD61 + EVs from plasma in under 30 min in a single step.
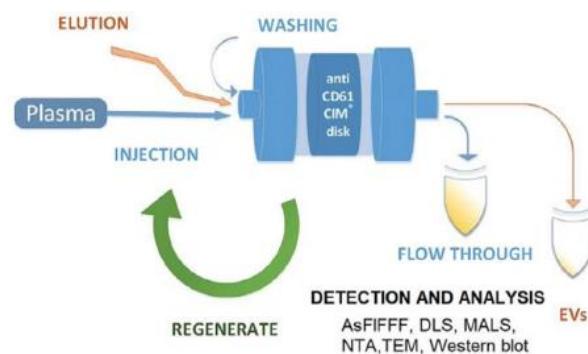

Figure 19: immunoaffinity monolithic disk column for CD61 + EV isolation from plasma developed by Multia et al. [45]

Another issue for immunoaffinity methods is the specific isolation of only a subset of exosomes, the ones that possess the protein markers recognized by the selected antibody, rather the total exosome population[7].

Additionally, isolation can be affected by nonspecific binding, competitive inhibition and cross-reactivity of antibodies. Antibodies development and production is costly and this, together with their limited shelf life, significantly compromises their application, especially for large scale exosome preparation.

An interesting option recently adopted by some groups[45,46] is the substitution of antibodies with cheaper and more stable aptamers. Aptamers are short single stranded DNA or RNA sequences, that can specifically recognize and bind to their targets in an antibody-like manner. Unlike traditional antibodies aptamers can be produced by in vitro chemical synthesis and exhibit several advantages such as low batch to- batch variation, easy scaling up, extended shelf life, low or no immunogenicity and easy chemical modification to improve binding properties.

Concluding, efforts should be directed towards the identification of specific EV biomarkers, the development of protocols with mild elution conditions that do not deteriorate the EV quality, and the design of stationary phases that are both compatible with EVs and easy to functionalize.

2.5 Microfluidic technologies

The recent advances in microfabrication science led to the development of microfluidic devices, compact units composed of a network of microchannels that aims to control the fluid flow in the microscale. Microsystem devices allow for a highly efficient and precise separation of micro or nano-sized particles inside a certain volume of fluid. At micro- and nano- scale, in fact, fluids possess distinctive properties, with the frictional forces that dominates the kinetic forces. This offers the possibility to precisely tune and manipulate several parameters related to the process and the materials.

These devices are commonly referred to as *Lab-on-Chip (LOC)*, meaning that they are able to reproduce several laboratory processes on a single integrated micrometric platform, a *chip*.

Thus, they offer high accuracy and specificity in EVs isolation and, compared to other conventional methods, they allow for a substantial decrease in the necessary amount of sample, reagents, and time required for experiment while increasing the automation level of the process.

Microfluidic EV isolation techniques are based on different working principles, including affinity capture and capture based on the physical or mechanical characteristics of EVs as size, density, compressibility, viscoelasticity, etc.

The most relevant microfluidic techniques recently developed for EVs isolation are microfluidic filtration, immunoaffinity capture, chip centrifugation, acoustic separation, viscoelastic flow, and hydrodynamic flow.

Microfluidic filtration (Mf-F) is a very promising tool for the continuous separation and enrichment of EVs based on the specific EVs size. Davies et al.[47] developed two kinds of Mf-F devices, pressure- and electrophoresis-driven, that separate cells, debris and small EVs from blood through a nanoporous membrane with an adjustable pore size (Figure 20). The limitation of pressure-driven Mf-F is that the pores become blocked after obtaining approximately 4 µL of filtrate. Electrophoresis avoids this problem and increases the separation efficiency and purity.
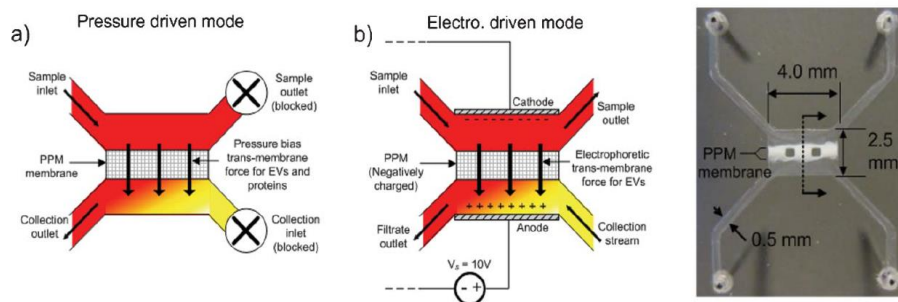
Figure 20: Microfluidic filtration system by Davies et al. [47]

Also, microfluidic double-filtration approaches were developed. Liang et al.[48] constructed a double-filtration Mf-F system comprising a filter with a pore size of 200 nm to remove cells and large impurities and a second filter with a pore size of 30 nm that allows proteins to pass through (Figure 21). This system achieves high throughput and yield, in comparison with ultracentrifugation, for isolation of 30–200 nm EVs.

Figure 21: Microfluidic double-filtration system by Liang et al. [48]

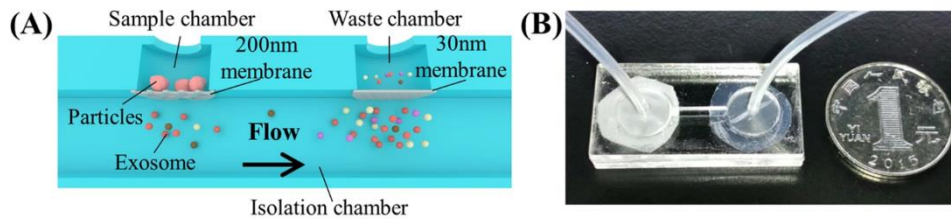Immunoaffinity-based separation of EVs is carried out in microfluidic devices made by microchannels coated with antibodies or introducing antibody-coated magnetic beads in the microchip (Figure 22). These methods are very promising for the separation of specific subset and subpopulation of exosomes. Thus, microfluidic immunoisolation methods is considered a very promising and powerful alternative method for conventional tumor biopsy.
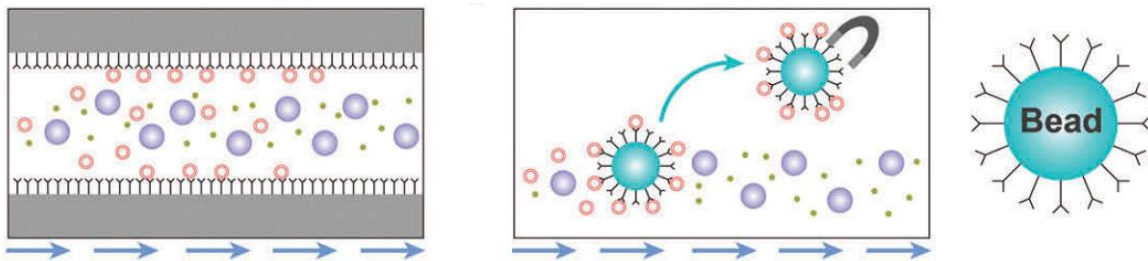

Figure 22: Microfluidic devices a) with inner surface coating with capture antibodies and b) functionalized capture beads by Guo et al.[49].

Viscoelastic microfluidics separation relies on the difference between elastic forces imposed on particles with different sizes in a viscoelastic medium. Poly(ethylene oxide) (PEO) and poly-(vinylpyrrolidone) (PVP) solutions are two frequently biocompatible synthetic polymers used as viscoelastic media. The inertial forces are extremely small and negligible in these high-viscosity fluids, whereas elastic force is the dominant lateral force exerted on particles and it causes particles migration[50].

Liu et al.[51] devised a size-dependent viscoelastic microfluidic system to extract exosomes from cell culture media or serum with separation purity and recovery rate of more than 90 and 80%, respectively. A PEO solution was used to induce viscoelastic forces on the EVs in a controllable manner in 50x20 μm isolation channels (Figure 23). The elastic lift force exerted on nanoparticles causes size-dependant displacements: larger nanoparticles migrate faster and are collected from the middle outlet while smaller ones migrate slower and are collected from side outlets.
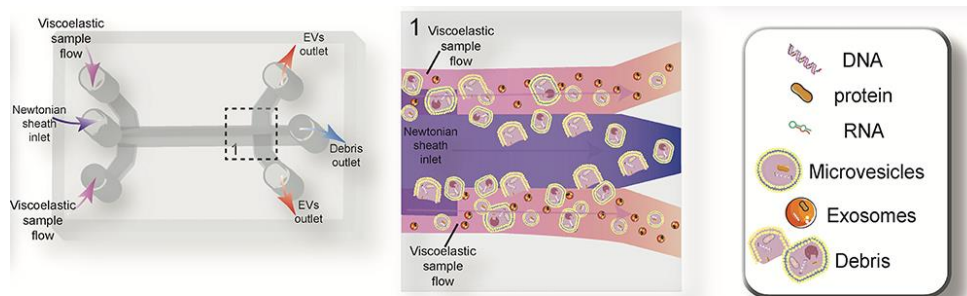

Figure 23: EVs microfluidic viscoelastic separation by Liu et al. [50]

Microfluids are revolutionizing research methodologies and are incredibly powerful diagnostic tools. However, some problems are yet to be resolved; for example, the analyzed sample can block channels, the sample input volume is considerably lower compared to the traditional methods, thus their applicability is limited to very specific small-scale applications.

2.6 Summary table

A summary reporting advantages and disadvantages for each of the discussed methods for EV isolation is presented in Table 3.

Table 3: Method principle, time, scalability potential, cost, advantages and disadvantages for the most used EV isolation techniques.

	Method principle	Time	Advantages	Disadvantages	Scala bility	Cost
Differential centrifugation (UC)	Sedimentation of biomolecules according to density using high g-force	140 - 600 min [52,53]	- Easy protocol; - Absence of additional chemicals; - Most established method for comparison of data.	- Low throughtput; - Efficiency affected by many factors; - Low and operator-dependent yield; - Low reproducibility; - Possible damage of EVs; - Long duration; - Limited to analytical and small-scales.	+	€€€€
Density gradient ultracentrifugation (DG UC)	Separation according to density in a pre-constructed density gradient medium	250 min – 2 days [53]	- Increase in EVs purity compared to UC; - Absence of additional chemicals.	- Complexity; - Low throughput; - Efficiency affected by many factors; - Low and operator-dependent yields; - Time consuming; - Low reproducibility; - Possible damage of EVs; - Limited to analytical and small-scale.	++	€€€
Size exclusion chromatography (SEC)	Separates by hydrodynamic volume	1 ml/min [20]	- Reproducibility; - Reduced contamination; - Gentle method; - Prevents EV aggregation; - No additional chemicals; - Insensitive to high viscosity.	- Low resolution; - Limitations on sample volume; - Dilution of EV isolates; - Co-isolation of same-size particles.	++++	€€
Filtration (MF/UF)	Uses membranes with specific pore sizes	130 min [54]	- Simple procedure; - Time efficient; - Relatively gentle; - No additional chemicals; - No limitations on sample volume.	- Membrane clogging; - Loss of sample and aggregation; - Low purity; - Possible deformation of vesicles.	++++	€
Flow Field Fractionation (FFF)	Flow modulated by a force field applied perpendicular to the flow	45-60 min [10]	- Reproducible; - Removal of lipoproteins; - Non-invasive;	- Low input volume	+	€€

Polymeric precipitation	Solubility changes by adding a crowding agent	8-12 hr [10]	- Inexpensive; - Simple; - Gentle method; - High yield.	- Need to remove the crowding agent; - High contamination; - Time-consuming.	+++	€
Anion exchange chromatography (AIEX)	Separation based on charge	180 min [23]	- Scalability; - Short processing time; - Structural and biological integrity or EVs; - Higher purity than TFF.	- Co-isolation of other negatively charged biomolecules; - Final concentration step may be required.	++++	€€
Electrophoresis	Separation based on electrophoretic mobility in an electric field	60-120 min [37]	- Easy control; - Fast and efficient; - Non invasive.	- Sample heating due to electric field; - Co-isolation of other negatively charged biomolecules; - Combination with others techniques may be required.	+++	€
Immuno-affinity techniques	Capture EVs using antibodies	240 min [53]	- Increased purification efficiency; - Target specific population; - Great potential in diagnostics.	- Costly - Harsh and difficult elution - Limited knowledge of EVs markers; - Isolation of a subset of EVs; - Non specific binding; - Competitive inhibition.	++	€€€€
Microfluidic (Mf)	Flow manipulation in microscale	60-120 min [55]	- Specificity and selectivity; - Low energy and material requirements; - Quick and efficient.	- Low sample loading; - Possible blockage due to system clogging.	++	€€€

2.7 Optimization and scale-up strategies

Most of the current methods for the isolation of extracellular vesicles share a common weakness: the very low yield in vesicles. According to Haraszti et al.[56] a dose of 10^9–10^{11} exosomes per mouse is typically necessary for a single test in mice models. This quantity is approximately yielded from one liter of conditioned culturing media, with current practices as UC. The low EV yields severely limit the preclinical and clinical development of exosome technologies in medicine, as well as their industrial translation for other applications, as in food nanotechnologies and cosmetics.

Thus, the research in the field should address the development and optimization of an isolation method that is easily scalable and in compliance with good manufacturing practices (GMP), in order to support large-scale manufacturing. In this context, considering upstream processing, yields improvements can be achieved by changing the EV source and/or the bioreactor systems, in case of EVs from cell culture supernatant.

Concerning the choice of the biological source, EV production cannot rely on a single cell line. This feature is in contraposition with mAbs production, that almost completely relies on Chinese hamster ovary (CHO) cell lines, chosen as the standard protein expression system due to their immortality, rapid growth and easy handling[2]. Concerning EVs, the choice of the biological source is highly dependent on the desired application, since the functions of EVs are strictly linked to the mother cell functions and phenotype.

So far, most EVs are produced from human bodily fluids and different types of human cells including stem cells, dendritic cells, mast cells, macrophages, epithelial cells, and cancer cells (Figure 24).
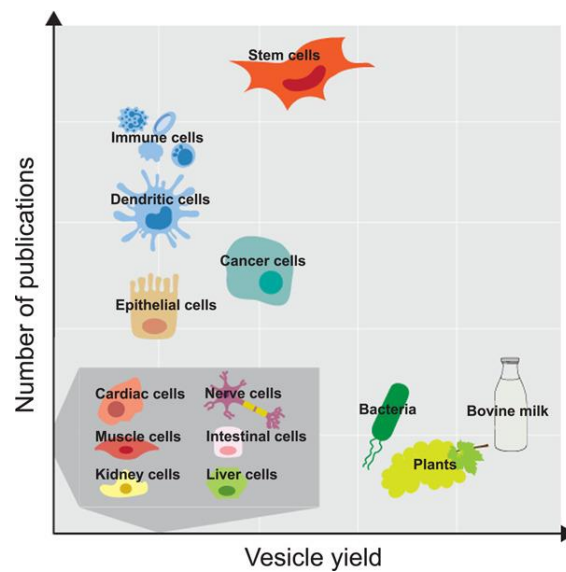

Figure 24: Most common sources of therapeutics EVs vesicles and the corresponding productivity by Paganini et al [2].

The cultivation of human cells can be challenging for several reasons[2]. First, after repeated subculturing human cells undergo the process of senescence and stop dividing. To overcome this issue they need to replaced or immortalized. Secondly, most human cells are adherent, so the maximum achievable yield is limited by the available surface area for their growth. Besides, issues related to their expensiveness, low input volumes available, as well as safety and ethical compliances, may arise.

Indeed, even if some applications require specific human cell lines and their use cannot be avoided, these complications encouraged researchers to explore alternative EV sources, as animal and plant sources. Due to their cheapness and availability, they allow to easily isolate EVs from large volumes of fluid, leading to improved yields. Besides, since they are common components of our diet, milk and plants derived-vesicles are also intrinsically biocompatible and safe. Other important therapeutic benefits are discussed in detail in Chapter 3.

In case of cell culture, it is crucial to optimize the upstream processing conditions, as the bioreactor setup and the composition of the cell culture medium. Concerning the bioreactor system, the possible scale-up approaches directly come from the development in the field of stem cell expansion. In Figure 25 is reported a schematic representation of the current and future technologies used for upstream processing of secreting-EVs stem cells. The simplest expansion approach is based on the substitution of single T-flasks with multi-layered cell culture flasks to provide a bigger surface area for cell expansion.
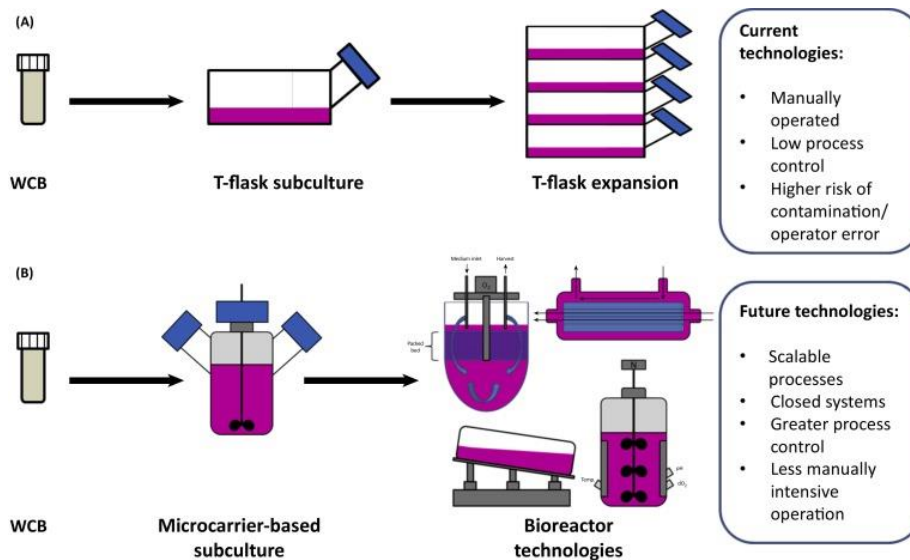
Figure 25: Current and future technologies for upstream processing of stem cells for EVs production by Colao et al.[57].

These, however, are lab-scale batch culturing systems that do not allow to monitor the homogeneity of the culturing conditions. In this context, research efforts into scaling up cell culture have focused on bioreactor systems that permit to maximize surface area, such as microcarriers in stirred bioreactors or hollow-fiber bioreactors[57]. They offer greater process control, requires less manually intensive operations and allow to process large amounts of fluids. Hollow fiber bioreactors, for example, can host 100-fold more cells than common T-flasks and allow for constant circulation of the fresh medium in the fibers[2].

Also, the use of stirred-tank bioreactors with microcarriers, the current system of choice for MSC cultivation, has been explored in the field of mammalian EVs production. Microcarriers, typically spherical, provide a high surface area to volume ratio for cell growth and yield to a considerably greater productivity compared to common 2D static cultures[2]. In stirred-tank bioreactors impellers are used to enhance mixing and maintain homogeneous culture conditions and the system can be easily monitored and controlled.

Finally, concerning downstream processing, yields improvements can be achieved by changing and/or optimizing purification techniques. Hence, the knowledge previously acquired in the development of other bioprocesses, as stem cells, liposomes and monoclonal antibodies (mAb) production, can be exploited in order to speed up the production of novel EVs therapeutics. In this context, Paganini et al.[2] provide a handful parallelism between EV, mAb and liposome production (Figure 26).
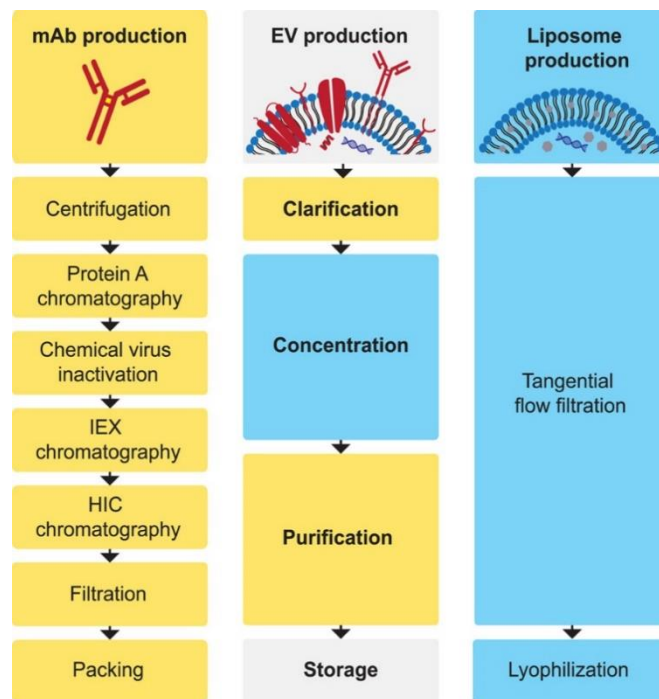
Figure 26: Flow diagrams of the typical platform purification process for mAbs, liposomes, and EVs [2].

The unit operations used for mAbs and liposomes can be potentially applied in the downstream processing of EVs. In particular, the strategies adopted for mAbs production could be potentially exploited for EVs clarification and purification steps, while liposome production through TFF could be potentially applied on large scale for EVs concentration.

According to Paganini et al., this approach could yield to a purification strategy similar to that used for viral vectors, which exhibit similar attributes of EVs in terms of size and morphology. In this process, high purity level is achieved by combining chromatography with filtration techniques. Specifically, after cell lysis, clarification, DNA digestion and virus inactivation steps, viral vectors are purified by ion exchange chromatography, concentrated by UF, dialyzed, further purified by SEC, newly concentrated by UF, and finally dialyzed before storage[2].

Also, according to Colao et al.[57] tangential flow filtration (TFF), followed by affinity capture (that targets EV-specific surface proteins) and final polishing steps, are most promising approaches for the clinical development of high-purity exosome therapies (Figure 27). The chromatographic steps should deplete the culture medium-derived proteins (as FBS), and a final buffer exchange step should allow washing and concentration of the product before formulation or secondary manufacturing.
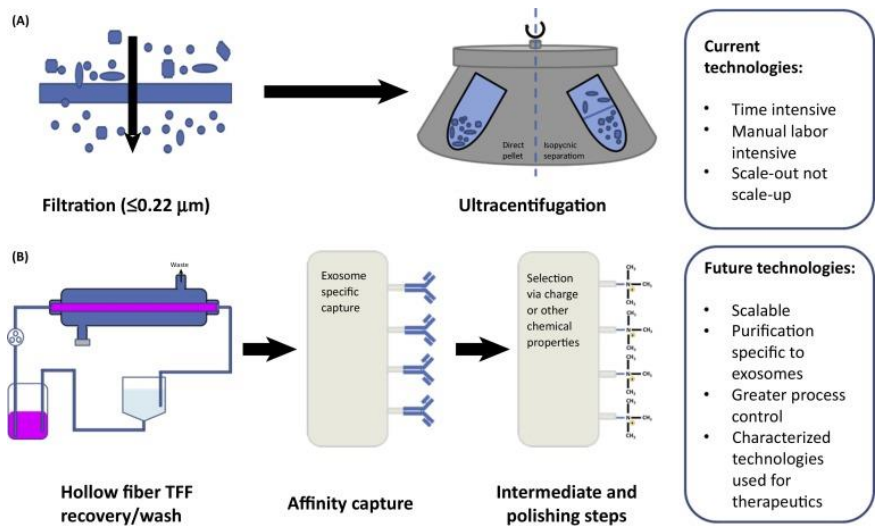
Figure 27: Current and future technologies for downstream processing of therapeutics EVs by Colao et al.

Chapter 2 references

1. Gardiner, C. *et al.* Techniques used for the isolation and characterization of extracellular vesicles: Results of a worldwide survey. *J. Extracell. Vesicles* **5**, (2016).

2. Paganini, C. *et al.* Scalable Production and Isolation of Extracellular Vesicles: Available Sources and Lessons from Current Industrial Bioprocesses. *Biotechnology Journal* vol. 14 (2019).

3. Konoshenko, M. Y., Lekchnov, E. A., Vlassov, A. V. & Laktionov, P. P. Isolation of Extracellular Vesicles: General Methodologies and Latest Trends. *BioMed Research International* vol. 2018 (2018).

4. Momen-Heravi, F. *et al.* Current methods for the isolation of extracellular vesicles. *Biological Chemistry* vol. 394 (2013).

5. Sidhom, K., Obi, P. O. & Saleem, A. A review of exosomal isolation methods: Is size exclusion chromatography the best option? *International Journal of Molecular Sciences* vol. 21 (2020).

6. Livshits, M. A. *et al.* Erratum: Isolation of exosomes by differential centrifugation: Theoretical analysis of a commonly used protocol (Scientific Reports (2016) 5 (17319) (DOI:10.1038/srep17319)). *Scientific Reports* vol. 6 (2016).

7. Yang, D. *et al.* Progress, opportunity, and perspective on exosome isolation - Efforts for efficient exosome-based theranostics. *Theranostics* vol. 10 (2020).

8. GE Healthcare. GE Handbook - Size Exclusion Chromatography. *GE Healthc.* (2018).

9. Popovic, M. & de Marco, A. Canonical and selective approaches in exosome purification and their implications for diagnostic accuracy. *Translational Cancer Research* vol. 7 (2018).

10. Liangsupree, T., Multia, E. & Riekkola, M. L. Modern isolation and separation techniques for extracellular vesicles. *J. Chromatogr. A* **1636**, (2021).

11. Arntz, O. J. *et al.* An optimized method for plasma extracellular vesicles isolation to exclude the copresence of biological drugs and plasma proteins which impairs their biological characterization. *PLoS One* **15**, (2020).

12. Mol, E. A., Goumans, M. J., Doevendans, P. A., Sluijter, J. P. G. & Vader, P. Higher functionality of extracellular vesicles isolated using size-exclusion chromatography compared to ultracentrifugation. *Nanomedicine Nanotechnology, Biol. Med.* **13**, (2017).

13. Yuana, Y., Levels, J., Grootemaat, A., Sturk, A. & Nieuwland, R. Co-isolation of extracellular vesicles and high-density lipoproteins using density gradient ultracentrifugation. *J. Extracell. Vesicles* **3**, (2014).

14. Van Deun, J. *et al.* Integrated Dual-Mode Chromatography to Enrich Extracellular Vesicles from Plasma. *Adv. Biosyst.* **4**, (2020).

15. Merchant, M. L. *et al.* Microfiltration isolation of human urinary exosomes for characterization by MS. *Proteomics - Clin. Appl.* **4**, (2010).

16. Heinemann, M. L. *et al.* Benchtop isolation and characterization of functional exosomes by sequential filtration. *J. Chromatogr. A* **1371**, (2014).

17. Doyle, L. & Wang, M. Overview of Extracellular Vesicles, Their Origin, Composition, Purpose, and Methods for Exosome Isolation and Analysis. *Cells* **8**, (2019).

18. Liu, F. *et al.* The Exosome Total Isolation Chip. *ACS Nano* **11**, (2017).

19. Cheruvanky, A. *et al.* Rapid isolation of urinary exosomal biomarkers using a nanomembrane ultrafiltration concentrator. *Am. J. Physiol. - Ren. Physiol.* **292**, (2007).

20. Lobb, R. J. *et al.* Optimized exosome isolation protocol for cell culture supernatant and human plasma. *J. Extracell. Vesicles* **4**, (2015).

21. Worsham, R. D., Thomas, V. & Farid, S. S. Potential of Continuous Manufacturing for Liposomal Drug Products. *Biotechnology Journal* vol. 14 (2019).

22. Busatto, S. *et al.* Tangential Flow Filtration for Highly Efficient Concentration of Extracellular Vesicles from Large Volumes of Fluid. *Cells* **7**, (2018).

23. Heath, N. *et al.* Rapid isolation and enrichment of extracellular vesicle preparations using anion exchange chromatography. *Sci. Rep.* **8**, (2018).

24. Dimov, N., Kastner, E., Hussain, M., Perrie, Y. & Szita, N. Formation and purification of tailored liposomes for drug delivery using a module-based micro continuous-flow system. *Sci. Rep.* **7**, (2017).

25. Dehghani, M., Lucas, K., Flax, J., McGrath, J. & Gaborski, T. Tangential Flow Microfluidics for the Capture and Release of Nanoparticles and Extracellular Vesicles on Conventional and Ultrathin Membranes. *Adv. Mater. Technol.* **4**, (2019).

26. Gandham, S. *et al.* Technologies and Standardization in Research on Extracellular Vesicles. *Trends in Biotechnology* vol. 38 (2020).

27. Zhang, H. & Lyden, D. Asymmetric-flow field-flow fractionation technology for exomere and small extracellular vesicle separation and characterization. *Nat. Protoc.* **14**, (2019).

28. Zhang, H. *et al.* Identification of distinct nanoparticles and subsets of extracellular vesicles by asymmetric flow field-flow fractionation. *Nat. Cell Biol.* **20**, (2018).

29. Rider, M. A., Hurwitz, S. N. & Meckes, D. G. ExtraPEG: A polyethylene glycol-based method for enrichment of extracellular vesicles. *Sci. Rep.* **6**, (2016).

30. Alvarez, M. L. Isolation of urinary exosomes for RNA biomarker discovery using a simple, fast, and highly scalable method. *Methods Mol. Biol.* **1182**, (2014).

31. Dash, M., Palaniyandi, K., Ramalingam, S., Sahabudeen, S. & Raja, N. S. Exosomes isolated from two different cell lines using three different isolation techniques show variation in physical and molecular characteristics. *Biochim. Biophys. Acta - Biomembr.* **1863**, (2021).

32. F., R. *et al.* Comparative miRNA analysis of urine extracellular vesicles isolated through five different methods. *Cancers (Basel).* **8**, (2016).

33. Andreu, Z. *et al.* Comparative analysis of EV isolation procedures for miRNAs detection in serum samples. *J. Extracell. Vesicles* **5**, (2016).

34. Kosanović, M., Milutinović, B., Goč, S., Mitić, N. & Janković, M. Ion-exchange chromatography purification of extracellular vesicles. *Biotechniques* **63**, (2017).

35. Zhang, Y. *et al.* High-Efficiency Separation of Extracellular Vesicles from Lipoproteins in Plasma by Agarose Gel Electrophoresis. *Anal. Chem.* **92**, (2020).

36. Yang, M., Liu, X., Luo, Q., Xu, L. & Chen, F. An efficient method to isolate lemon derived extracellular vesicles for gastric cancer therapy. *J. Nanobiotechnology* **18**, (2020).

37. Marczak, S. *et al.* Simultaneous isolation and preconcentration of exosomes by ion concentration polarization. *Electrophoresis* **39**, (2018).

38. Théry, C., Zitvogel, L. & Amigorena, S. Exosomes: Composition, biogenesis and function. *Nature Reviews Immunology* vol. 2 (2002).

39. Zhao, Z., Yang, Y., Zeng, Y. & He, M. A microfluidic ExoSearch chip for multiplexed exosome detection towards blood-based ovarian cancer diagnosis. *Lab Chip* **16**, (2016).

40. Ghosh, A. *et al.* Rapid isolation of extracellular vesicles from cell culture and biological fluids using a synthetic peptide with specific affinity for heat shock proteins. *PLoS One* **9**, (2014).

41. Balaj, L. *et al.* Heparin affinity purification of extracellular vesicles. *Sci. Rep.* **5**, (2015).

42. Zhou, Y. G. *et al.* Interrogating Circulating Microsomes and Exosomes Using Metal Nanoparticles. *Small* **12**, (2016).

43. Rupp, A. K. *et al.* Loss of EpCAM expression in breast cancer derived serum exosomes: Role of proteolytic cleavage. *Gynecol. Oncol.* **122**, (2011).

44. Thery, C. *et al.* Minimal information for studies of extracellular vesicles 2018 (MISEV2018): a position statement of the International Society for Extracellular Vesicles and update of the MISEV2014 guidelines. *J. Extracell. vesicles* **7**, (2018).

45. Multia, E., Tear, C. J. Y., Palviainen, M., Siljander, P. & Riekkola, M. L. Fast isolation of highly specific population of platelet-derived extracellular vesicles from blood plasma by affinity monolithic column, immobilized with anti-human CD61 antibody. *Anal. Chim. Acta* **1091**, (2019).

46. Zhang, K. *et al.* Rapid Capture and Nondestructive Release of Extracellular Vesicles Using Aptamer-Based Magnetic Isolation. *ACS Sensors* **4**, (2019).

47. Davies, R. T. *et al.* Microfluidic filtration system to isolate extracellular vesicles from blood. *Lab Chip* **12**, (2012).

48. Liang, L. G. *et al.* An integrated double-filtration microfluidic device for isolation, enrichment and quantification of urinary extracellular vesicles for detection of bladder cancer. *Sci. Rep.* **7**, (2017).

49. Guo, S. C., Tao, S. C. & Dawn, H. Microfluidics-based on-a-chip systems for isolating and analysing extracellular vesicles. *Journal of Extracellular Vesicles* vol. 7 (2018).

50. Talebjedi, B., Tasnim, N., Hoorfar, M., Mastromonaco, G. F. & De Almeida Monteiro Melo Ferraz, M. Exploiting Microfluidics for Extracellular Vesicle Isolation and Characterization: Potential Use for Standardized Embryo Quality Assessment. *Frontiers in Veterinary Science* vol. 7 (2021).

51. Liu, C. *et al.* Field-Free Isolation of Exosomes from Extracellular Vesicles by Microfluidic Viscoelastic Flows. *ACS Nano* **11**, (2017).

52. Théry, C., Clayton, A., Amigorena, S. & Raposo, and G. Isolation and Characterization of Exosomes from Cell Culture Supernatants. *Curr. Protoc. Cell Biol.* (2006).

53. Greening, D. W., Xu, R., Ji, H., Tauro, B. J. & Simpson, R. J. A protocol for exosome isolation and characterization: Evaluation of ultracentrifugation, density-gradient separation, and immunoaffinity capture methods. in *Methods in Molecular Biology* vol. 1295 (2015).

54. Salih, M., Zietse, R. & Hoorn, E. J. Urinary extracellular vesicles and the kidney: Biomarkers and beyond. *American Journal of Physiology - Renal Physiology* vol. 306 (2014).

55.   Meng, Y. *et al.* Microfluidics for extracellular vesicle separation and mimetic synthesis: Recent advances and future perspectives. *Chemical Engineering Journal* vol. 404 (2021).

56.   Haraszti, R. A. *et al.* Exosomes Produced from 3D Cultures of MSCs by Tangential Flow Filtration Show Higher Yield and Improved Activity. *Mol. Ther.* **26**, (2018).

57.   Colao, I. L., Corteling, R., Bracewell, D. & Wall, I. Manufacturing Exosomes: A Promising Therapeutic Platform. *Trends in Molecular Medicine* vol. 24 (2018).

Plant-derived extracellular vesicles

The existence of multivesicular bodies (MVBs) secreted from plant cells was first proposed in 1967 in two independent papers by Halperin et al.[1] and Marchant et al.[2] They were the first to suggest that the fusion of MVBs with the plasma membrane might result in the release of exosome-like vesicles into the extracellular space in fungi and higher plants.

Nowadays it is widely recognized (primarily confirmed by TEM microscopy) that plants release "exosome-like" extracellular vesicles. Plant EVs structure resemble that of vesicles of animal origin, as they are lipoprotein structures of heterogeneous dimensions released by vegetal cells, which carry numerous bioactive substances including lipids, proteins, and miRNAs.[3]

Although EVs biogenesis has not been fully clarified, their role in cross-kingdom interactions has been widely studied as it has been the starting point of the researchers' interest in the field.[4] The studies on mammalian EVs unravel that, besides their role in intraspecies communication, EVs might also be a mode of communication between unrelated species. Examples of EV-mediated interactions between mammalian and parasites[5], mammalian and bacteria[6], bacteria and plants[7], plants and parasites[8,9] are reported in literature.

In the context of the interactions between mammalian and plants, the presence of EVs in our plant-based diets has raised a lot of questions about their influence on our health. In fact, the discovery that plants do contain various types of vesicles spontaneously lead to the observation that, as we eat every day, these vesicles are continuously put in contact with our intestinal tract. Recent data suggest that EVs from food might have relevant biological role on our digestive tract and might contribute to the homeostasis of the whole body.[4]

In the last decade, the role of plant miRNAs as a functional component of food with therapeutic effects has been hypothesized. In the past, the beneficial properties of some plant species were exclusively attributed to some functional phytocomponents such as polyphenols, alkaloids, saponins, tannins, vitamins, and minerals[10]. In addition to those, it is now demonstrated that plant miRNAs are absorbed by the mammalian digestive tract and can regulate mammalian genes.[11] In this context, due to their miRNA content, plant EVs are gaining attention as a novel class of cross-kingdom modulators, able to mediate animal-plant interactions at the molecular level.

3.1 PDEVs biogenesis and their role in plant physiology

As already mentioned, the plant EVs biogenesis is unclear. It is thought that PDEVs biogenesis starts in plant cells with the formation of *endosomes*, which matures in *multivesicular bodies* (MVBs) (Figure 28).
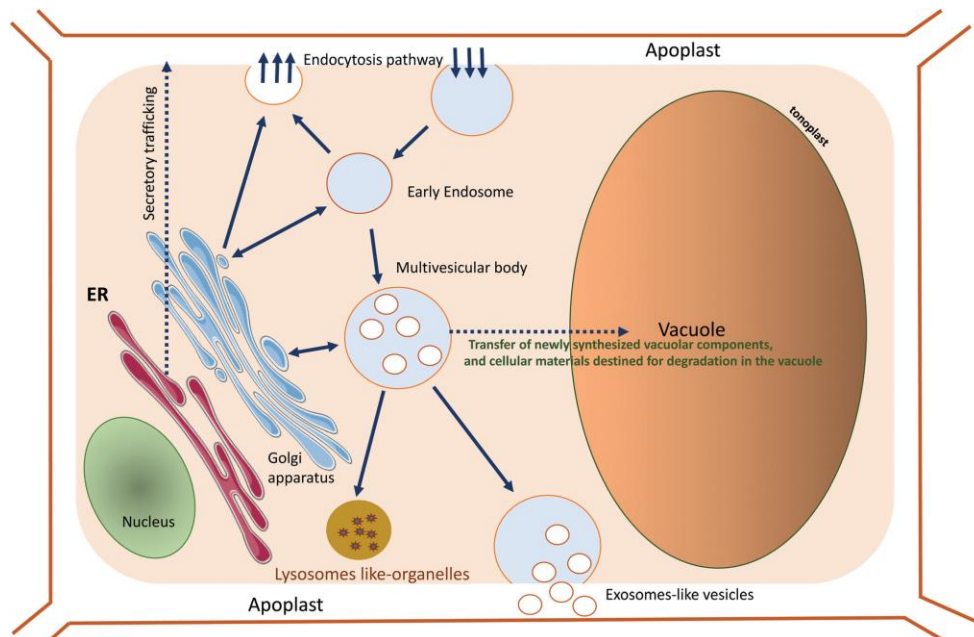
Figure 28: Schematization of PDEVs biogenesis process through MVB fusion with the plasma membrane and the release of exosome-like vesicles [4].

MVBs are spherical endosomal organelles containing small vesicles formed by inward budding of the limiting membrane. Their internal vesicles are able to actively and selectively incorporate genetic material as RNAs. It is thought that MVBs fuse with the plasma membrane in an exocytic manner, leading to release their contents, including internal vesicles, into the extracellular space[13].

Recent studies have provided three lines of evidences about this mechanism in plants, as reported by An et al.[14]:

-   Vesicles having the same morphology as MVB internal vesicles have been observed in extracellular spaces in various types of plant cells and in various plant species by TEM[15].
-   Co-occurrence of MVBs and paramural vesicles has been observed in processes of cell proliferation, cell differentiation, and cell response to abiotic and biotic stress.
-   Identical molecular components, such as arabinogalactan proteins[17], have been immunolocalized in both MVBs and paramural bodies.

Despite these evidences, a conclusive demonstration of MVB-mediated secretion of exosomes in plants still does not exist.

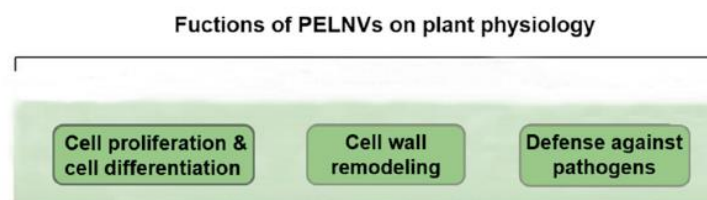Plant MVBs are thought to execute at least three crucial roles on the plant physiology (Figure 29).

Figure 29: Summary of the main supposed functions of PDEVs on plant physiology.[13]

As they can deliver their content to either the central cell vacuole or extracellular space, they are supposed to be involved in cell proliferation, differentiation and response to environmental stress.[4] Besides the incorporation of nutrients from the apoplast, plant MVBs are supposed to sequestrate damaged membranes and deleterious materials originating from oxidative stress.[4]

Also, in several studies these nanovesicles appear to be enriched in cell wall remodeling enzymes and defense proteins. Cell wall remodeling enzymes were detected in EVs from sunflower[18], tomato[19] and A. *thalian leaves*[20]. Proteins involved in biotic and abiotic stress responses were detected in the latter two studies, as well as in olives EVs[21]. Considering the defense against pathogens, PDEVs secretion appear to be enhanced in response to bacterial/parasite infections, and so it can be considered pathogen-inducible in plants, suggesting the relevant immunological role of PDEVs.[12,20]

3.2 Composition of PDEVs

Proteomic and lipidomic profiling of PDEVs have been attempted in several plant species in order to both characterize these structures and allow a comparison of their composition with that of mammalian vesicles. Some protein and lipid families have been found to be recurring in vesicles isolated from different species. Nonetheless, the knowledge of specific marker of plant vesicles is still missing. PDEVs proteins can be mainly categorized into transmembrane proteins and cytosolic proteins. The most characteristic protein families detected in several PDEVs are heat shock proteins (HSPs), annexins and aquaporins, as described in Table 4.

Table 4: Main protein families detected in different PDEVs via proteomic profiling [3].

Protein families in PDEVs	Type	Role	References
Heat Shock Proteins (HSPs)	Membrane proteins	- Proteins induced in cells undergoing stress; - Role in plant growth, development and for nutrient's internalization.	- HSP70, HSP90 found in Citrus limon EVs.[22] - HSP70, HSP80 highly expressed in four citrus species EVs.[23] - HSP60, HSP70 in sunflower EVs.[18] - HSP60, HSP70, HSP90 in grapefruit EVs.[24]
Annexins	Membrane proteins	- Critical role in EV biogenesis (MVB generation and budding of the intraluminal vesicles)	Found in EVs from Citrus species[22,23], sunflower[18] and leaf apoplast[20].
Aquaporins (AQPs)	Transmembrane proteins	- They constitute channels for water transport across the membrane; - Involved in the regulation of cell turgor.	Detected in EVs from citrus fruits[22,23], grapefruit[25] and broccoli[26].

As for animal EVs, also plant vesicles content reflects the composition of the mother cells, considering both the conditions in which the plant lives and the specific plant species composition.[3] Therefore, besides the main protein families reported above, proteins associated to stress response as well as

proteins involved in ROS (Reactive Oxygen Species) pathways have been detected in different plant species by different groups[20,21].

The lipids present in PDEVs regulate the stability of the vesicles and demonstrate an active biological activity in mediating vesicles' processes. The main lipid families found in PDEVs are reported in Table 5.

Table 5: Main lipid families detected in different PDEVs via lipidomic profiling [3].

Lipid families in PDEVs	Type	Role	References
Phosphatidic acid (PA)	Both exogenous (dietary) and endogenous origins	Formation and dynamics of cell membranes; Activator of cellular signaling pathways.	- PA was first found in the extracellular fluid of sunflower seeds[18]; - Grape EVs found to be enriched in PA (53.2%)[25]; - PA found in ginger vesicles (43%)[27].
Phosphatidylethanolamine (PE)	Membrane phospholipid	Membrane fusion.	PE found in grape[25] and grapefruit[24] EVs.
Phosphatidylcholine (PC)	Membrane phospholipid	Anti-inflammatory role, showing protective effect against inflammatory bowel disease.	PC found in grapefruit[24] and ginger[27] EVs.
Galactolipids	Glycolipid found in edible plants	Anti-inflammatory effects[28] and anti-tumoral effects[29].	Ginger EVs enriched in monogalactosylmonoacyl-glycerol and digalactosyldiacylglycerol.[30]

In addition to the lipid species discussed above, edible plant EVs are a source of other bioactive phytochemical compounds with attributed beneficial properties to human health, like naringenin in grapefruit-EVs[24], shogaol in ginger EVs[31] and sulforaphane from broccoli-EVs[32].

Plant EVs contain also genetic material, as miRNAs. Xiao et al.[33] identified 418 miRNA profiles of PDEVs from 11 different edible fruits and vegetables and divided them into three classes according to their distribution. They found out that the most abundant miRNAs in PDEVs can potentially regulate the expression of inflammatory cytokines and cancer-related genes in vitro. There are many evidences of the interaction of vesicle-associated plant miRNA with mammalian cells.

Zhang et al.[11] proposed that ingested plant miRNAs are absorbed by the gastrointestinal epithelial cells of consuming animals, which subsequently package them into EVs. EVs protect miRNAs from degradation and deliver them to distant cells, where they are capable of interaction with endogenous RNAs and regulation of their expression. Specifically, the authors identified plant miR168a, normally contained in rice, in the Chinese human serum. Their results indicate that plant miR168a is able to modulate mouse liver target gene expression and increase plasma LDL cholesterol levels. Also, Wang et al.[34] detected exogenous RNA sequences from foods in human plasma. In particular, they identified RNA sequences from cereal, soybeans, tomato and grape.

Several studies attempt to compare protein, lipid and nucleic acids composition profiles of plant and mammalian EVs. For example, Ju et al.[25] reported that grape exosome-like nanoparticles contained 96 miRNAs and 28 identified proteins. In comparison, mammalian exosomes typically contain 100–300 miRNAs and more than 1000 proteins[35]. PDEVs have a lower protein content in comparison to mammalian exosomes and, considering that among transmembrane proteins CD63, CD81, and CD9 have been identified as markers of mammalian EVs, they were found to differ also in terms of protein composition.[30] Concerning lipids, mammalian exosomes are generally rich in cholesterol and sphingomyelin but have only low levels of phosphatidylethanolamine and phosphatidic acid[35]. Overall, the RNA, lipid and protein profiles in plant vesicles differ from those found in mammalian exosomes.

3.3 PDEVs biological properties and applications

Plant EVs applications in nanomedicine and nutraceutics are based on their intrinsic biological properties (immunological modulation effects, anti-tumor activity, regenerative effects, hepatoprotection effects) and on their use as nano-vehicles to ship therapeutic compounds (Figure 30, Figure 31).
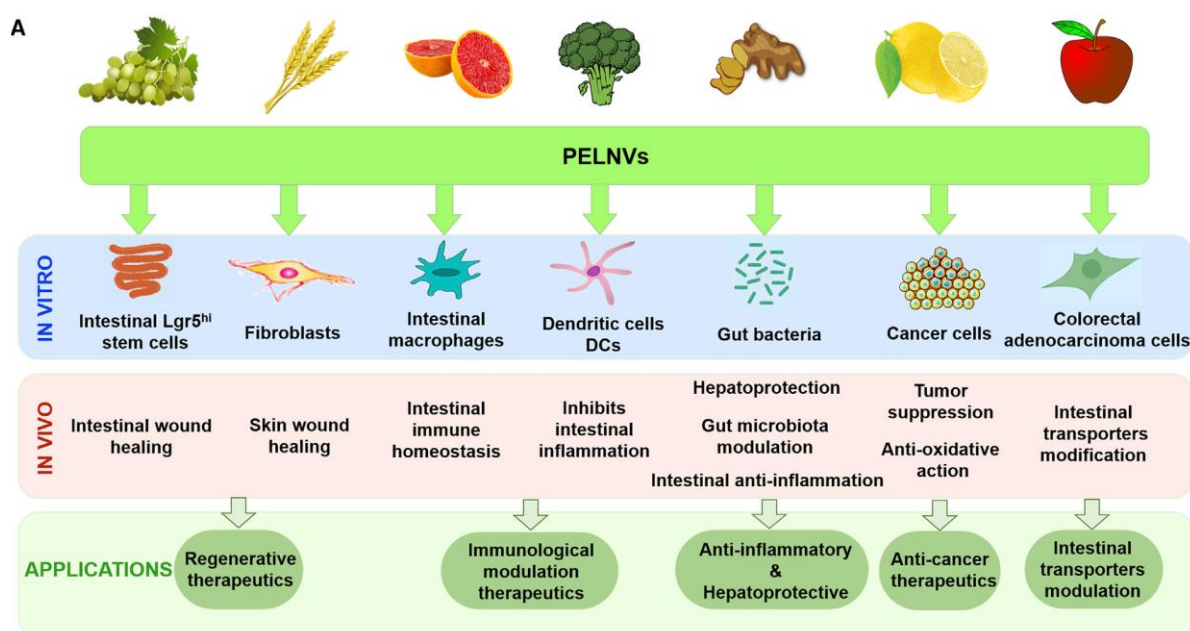

Figure 30: Summary of the biological functions and applications of EVs derived from plants. [13]

Alongside with their potential use as drug delivery systems, PDEVs can be exploited as nano-therapeutics for diseases due to their pristine biological functions.

Anti-inflammatory properties

Inflammation is a part of the innate immunity mechanism: if left uncontrolled, it can evolve into acute or chronic inflammatory diseases. Plant vesicles have been found to exert an anti-inflammatory effect by regulating the immunological response of hosts. After internalization into the host's recipient cells, PDEVs trigger a cascade of intracellular signaling mechanisms, which modulate cellular responses and bring about tissue homeostasis. First, they have revealed their immunological regulating effects on the gastrointestinal haemostasis.[13] Wang et al.[24] demonstrated that grapefruit-derived vesicles are able to

fortify the anti-inflammatory capability of intestinal macrophages. In fact, in the recurrent inflammatory disorders of intestine such as colitis, macrophages lose their tolerogenic traits. In the study, grapefruit vesicles uptaken by macrophages were able to alleviate dextran sulfate sodium (DSS)-induced colitis in mice with no toxicity. Moreover, in the same study, miRNAs of ginger- and grapefruit-derived vesicles were also reported to target the genes in gut probiotic *Lactobacillus rhamnosus* in mice gut alongside favoring their proliferation and consequently prompting anti-microbial immunity of the gut. Similar studies on broccoli[32], grapes, and carrots[36] have also been reported.

Anti-tumor Activities

Several studies have revealed the role of plant vesicles in inhibiting tumor cell proliferation. Zhang et al.[30] ginger-derived EVs showed their anti-tumor action in colitis-associated cancer. They were able to diminish pro-inflammatory cytokines associated with cancer onset and progression and suppress intestinal epithelial cell proliferation and apoptosis. Also, vesicles isolated from lemon-juice by Raimondo et al.[22] inhibit the growth of different types of tumor cells by tumor targeting, oxidative stress reduction, and by activating a TRAIL-mediated apoptotic cell death mechanism.

Recently, Cao et al. [37]purified EVs from ginseng roots and demonstrated that these vesicles induce apoptosis of murine melanoma cell by inducing reactive oxygen species generation. The results provided in this study suggest that plant EVs may contribute to the immune response to tumors, carrying out a crucial immuno-modulation effect.

Regenerative Effects

In one of the first studies on PDEVs (2013) Ju et al.[25] isolated grape-derived vesicles (GELNs) and explored their role on DSS-induced colitis in mice. It was shown that they have the capability to diffuse through and enter intestinal stem cells *in vivo* and induce the proliferation of Lgr5hi intestinal stem cells and regenerate the intestinal epithelial tissue. Moreover, they showed that GELNs can regulate the expression of pluripotent stem cell markers, thus increasing the level of genes related to stem cell growth.

Also, ginger-derived EVs isolated by Zhang et al.[30] showed to promote intestinal wound healing by regulating the expression of proteins as hemopexin, HSP, axin, and kinesin.

Interestingly, the effect of plant vesicles has recently been evaluated on in vitro skin regeneration models, suggesting new potential applications. Sahin et al.[38] isolated vesicles from wheat-grass and studied their potential use in wound healing through in-vitro studies. Wheat-derived EVs induced skin regeneration by triggering proliferation in a dose-dependent manner on epithelial, endothelial, and dermal fibroblasts. They also stimulated collagen type I expression.

Hepatoprotection

Zhuang et al.[31] studied the use of ginger-derived EVs to cure liver damages induced by alcohol in mice. Liver deterioration can be caused by alcohol-derived metabolites that stimulate ROS generation, pro-inflammatory cytokines, transforming growth factor, TNF-a, and collagen.[13] Ginger-derived EVs are found to contribute to hepatoprotection by suppressing ROS generation. Besides, shogaols and other bioactive EVs can stimulate the expression of liver detoxifying and antioxidant agents, like the nuclear factor Nrf2.
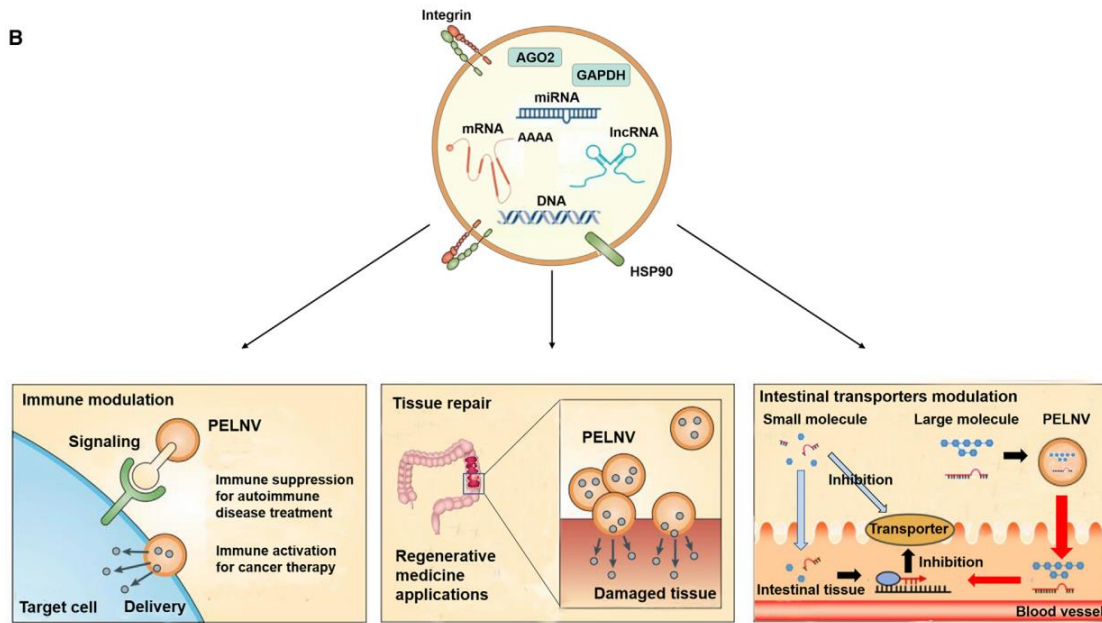
Figure 31: Therapeutic mechanisms of PELNVs in immunological modulation, tissue repair, and intestinal transporters modulation. [13]

3.4 PDEV isolation techniques

Since plant NPs are evolving as alternative therapeutics against several diseases, it is essential to develop isolation and purification methods compatible with advantageous production costs and suitable for scalability. Vegetal EVs allows their purification from large volumes and being a very cheap source of materials, their industrial application is regarded as extremely feasible. Besides, data from literature shows that plant-derived vesicles can be produced at higher yields. To make an example conventional dUC isolates an average $0.5–1.5 \times 10^{13}$ particles from 1 L of mammalian cell culture medium or 3–4 µg protein per 10^6 cells.[39] Chen et al.[40] isolated $0.5–2 \times 10^{14}$ particles per kg of ginger root using the gUC method, which is about 10 times more than that obtainable in current mammalian production systems.
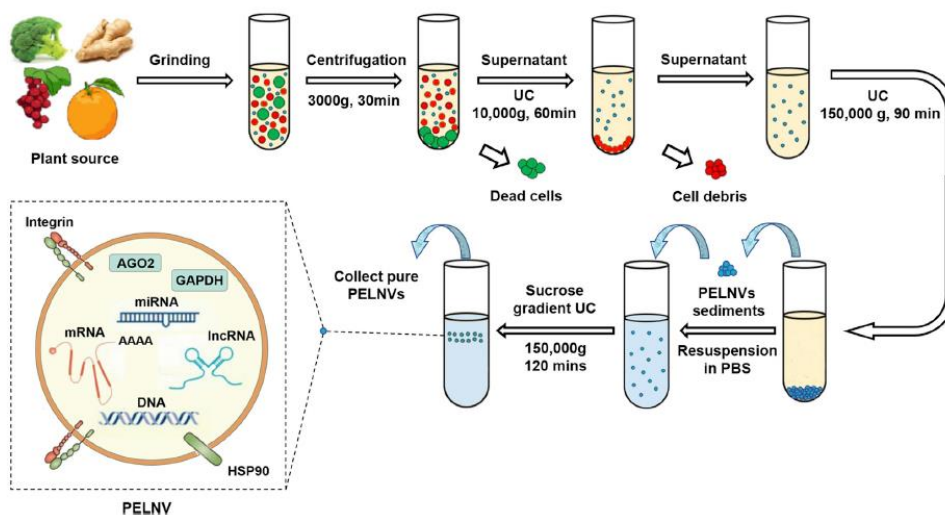

Figure 32: Isolation and Preparation of PELNVs through differential UC and density gradient UC [13].

As already discussed in Chapter 2, the differential ultracentrifugation (UC) technique has acquired the benchmark status in isolation and purification of EVs. The isolation of PDEVs can be very challenging since plants are complex matrices. Also, the different organs such as fruit, leaf, seed, and root have different physical structures and tissue types.

To date, the dUC isolation protocol is mostly applied for the isolation of plant vesicles. The starting point is the extraction of the plant juice that is then put through a series of centrifugation steps with gradually enhancing speed (Figure 32). At every step, the pellet is discarded and the supernatant is further processed. In the final step the supernatant is subjected to a further higher speed UC run of at least 100000 x g to obtain a n EVs-rich pellet. The pellet containing PDEVs is subsequently resuspended and washed in a small amount of phosphate-buffered saline (PBS). The vesicle yield obtained after the basic procedure of differential UC is usually contaminated with nucleic acids and protein agglomerates[13]. Therefore, for further purification, homogenized suspension is subjected to sucrose gradient ultracentrifugation at an elevated speed greater than 150000 x g for 120 min.

To obtain the ultra-pure PDEVs the high-speed UC run can be repeated several times. Although this benefits in achieving purity of PDEVs, it reduces the PDEVs yield concentration. Besides, repeated pelleting of PDEVs, under high centrifugal force of differential UCs, may result in compromising the vesicles structural integrity and cause agglomeration.[13]

To date, the vast majority of PDEVs have been isolated through dUC methods. A comprehensive Table with the main results obtained so far in the isolation of PDEVs have been reported from literature is presented in Appendix I.

In case of mammalian exosomes, several alternative purification methods have been developed to replace the use of ultracentrifugation, such as ultrafiltration and polymer-based precipitation methods.

The main drawback of the dUC method in the isolation of PDEVs from the highly complex matrix is the low efficiency to separate the vesicles from the co-sedimenting impurities. This usually negatively influences not only the reproducibility but also the downstream analysis and the applications. The combination of dUC/gUC generally solves this problem and results in purer fraction than dUC alone. Thus, dUC/gUC has only been limitedly applied in the plant field because it is time-consuming and includes multiple washing and pelleting steps that can negatively affect the final vesicle yields.

As alternative to dUC/gUC for the isolation of plant vesicles Kalarikkal et al.[41] developed a polyethylene glycol-6000 (PEG6000) based ginger EVs purification method. Using different PEG6000 concentrations the authors were able to recover between 60% to 90% of EVs compared to UC method. PEG-EVs exhibit almost identical composition, size and zeta potential to UC derived vesicles. PEG is an approved food additive, so this precipitation method can provide a scalable and cost-effective alternative to purify PDEVs.

Even though the precipitation method is easy and cheap, it has some drawbacks such as co-purification of non-EVs proteins and requirement of additional clean-up steps.[47]

Another alternative to dUC is the use of SEC as purification step as alternative to gUC. Up to now, this way has only been explored by Bokka et al.[43] in the isolation of tomato-derived nanovesicles.

The authors compared the performances of dUC/SEC and dUC/gUC methods and they found out that while gUC was proven to be more useful in the separation of different vesicle populations, SEC was more efficient in the removal of the co-purifying impurities, and thus improved the purity of the preparations and enabled them for subsequent downstream analysis. The authors also pointed out that both methods required concentrated samples for the separation.

Among all the mentioned methods, filtration techniques are quick and easy and have a great potential in the biomanufacturing of plant vesicles. To date, the method has just been used in combination with dUC and further work should be addressed in the development of filtration techniques that can represent suitable alternative to UC, and not just additional purification steps.

A potential alternative to UC, still almost completely unexplored, is the exploitation of the negative superficial charge that the majority of PDEVs display. As already discussed in Chapter 2, Yang et al.[48] combined membrane dialysis purification with electrophoresis to isolate exosomes from lemons. This provided for a quick separation with appreciable homogeneity in the size and morphology.

Chapter 3 references

1.   Halperin, W. & Jensen, W. A. Ultrastructural changes during growth and embryogenesis in carrot cell cultures. *J. Ultrasructure Res.* **18**, (1967).

2.   MARCHANT, R., PEAT, A. & BANBURY, G. H. THE ULTRASTRUCTURAL BASIS OF HYPHAL GROWTH. *New Phytol.* **66**, (1967).

3.   Pucci, M. & Raimondo, S. Plant extracellular vesicles: the safe for bioactive compounds. *Adv. Biomembr. Lipid Self-Assembly* (2020) doi:10.1016/bs.abl.2020.04.002.

4.   Rome, S. Biological properties of plant-derived extracellular vesicles. *Food Funct.* **10**, (2019).

5.   Szempruch, A. J. *et al.* Extracellular Vesicles from Trypanosoma brucei Mediate Virulence Factor Transfer and Cause Host Anemia. *Cell* **164**, (2016).

6.   Svennerholm, K. *et al.* Escherichia coli outer membrane vesicles can contribute to sepsis induced cardiac dysfunction. *Sci. Rep.* **7**, (2017).

7.   Ionescu, M. *et al.* Xylella fastidiosa outer membrane vesicles modulate plant colonization by blocking attachment to surfaces. *Proc. Natl. Acad. Sci. U. S. A.* **111**, (2014).

8.   Hou, Y. *et al.* A Phytophthora Effector Suppresses Trans-Kingdom RNAi to Promote Disease Susceptibility. *Cell Host Microbe* **25**, (2019).

9.   Rutter, B. D. & Innes, R. W. Extracellular vesicles as key mediators of plant–microbe interactions. *Current Opinion in Plant Biology* vol. 44 (2018).

10.   Tungmunnithum, D., Thongboonyou, A., Pholboon, A. & Yangsabai, A. Flavonoids and Other Phenolic Compounds from Medicinal Plants for Pharmaceutical and Medical Aspects: An Overview. *Medicines* **5**, (2018).

11.   Zhang, L. *et al.* Exogenous plant MIR168a specifically targets mammalian LDLRAP1: Evidence of cross-kingdom regulation by microRNA. *Cell Res.* **22**, (2012).

12.   Li, X. *et al.* Biogenesis and function of multivesicular bodies in plant immunity. *Frontiers in Plant Science* vol. 9 (2018).

13.   Dad, H. A., Gu, T. W., Zhu, A. Q., Huang, L. Q. & Peng, L. H. Plant Exosome-like Nanovesicles: Emerging Therapeutics and Drug Delivery Nanoplatforms. *Molecular Therapy* vol. 29 (2021).

14.   An, Q., Van Bel, A. J. E. & Hückelhoven, R. Do plant cells secrete exosomes derived from multivesicular bodies? *Plant Signal. Behav.* **2**, (2007).

15.   Marchant, R. & Robards, A. W. Membrane systems associated with the plasmalemma of plant cells. *Ann. Bot.* **32**, (1968).

16.   Chafe, S. C. Cell wall formation and 'protective layer' development in the xylem parenchyma of trembling aspen. *Protoplasma* **80**, (1974).

17.   Herman, E. M. & Lamb, C. J. Arabinogalactan-rich glycoproteins are localized on the cell surface and in intravacuolar multivesicular bodies. *Plant Physiol.* **98**, (1992).

18.   Regente, M. *et al.* Vesicular fractions of sunflower apoplastic fluids are associated with potential exosome marker proteins. *FEBS Lett.* **583**, (2009).

19.   Gonorazky, G. *et al.* Phosphatidylinositol 4-phosphate is associated to extracellular lipoproteic fractions and is detected in tomato apoplastic fluids. *Plant Biol.* **14**, (2012).

20. Rutter, B. D. & Innes, R. W. Extracellular vesicles isolated from the leaf apoplast carry stress-response proteins. *Plant Physiol.* **173**, (2017).

21. Prado, N. *et al.* Nanovesicles are secreted during pollen germination and pollen tube growth: A possible role in fertilization. *Molecular Plant* vol. 7 (2014).

22. Raimondo, S. *et al.* Citrus limon-derived nanovesicles inhibit cancer cell proliferation and suppress CML xenograft growth by inducing TRAIL-mediated cell death. *Oncotarget* **6**, (2015).

23. Pocsfalvi, G. *et al.* Protein biocargo of citrus fruit-derived vesicles reveals heterogeneous transport and extracellular vesicle populations. *J. Plant Physiol.* **229**, (2018).

24. Wang, B. *et al.* Targeted drug delivery to intestinal macrophages by bioactive nanovesicles released from grapefruit. *Mol. Ther.* **22**, (2014).

25. Ju, S. *et al.* Grape exosome-like nanoparticles induce intestinal stem cells and protect mice from DSS-induced colitis. *Mol. Ther.* **21**, (2013).

26. Martínez-Ballesta, M. del C. *et al.* Plasma membrane aquaporins mediates vesicle stability in broccoli. *PLoS One* **13**, (2018).

27. Teng, Y. *et al.* Plant-Derived Exosomal MicroRNAs Shape the Gut Microbiota. *Cell Host Microbe* **24**, (2018).

28. Maeda, N., Kokai, Y., Hada, T., Yoshida, H. & Mizushina, Y. Oral administration of monogalactosyl diacylglycerol from spinach inhibits colon tumor growth in mice. *Exp. Ther. Med.* **5**, (2013).

29. Bruno, A. *et al.* Selective in vivo anti-inflammatory action of the galactolipid monogalactosyldiacylglycerol. *Eur. J. Pharmacol.* **524**, (2005).

30. Zhang, M. *et al.* Edible ginger-derived nanoparticles: A novel therapeutic approach for the prevention and treatment of inflammatory bowel disease and colitis-associated cancer. *Biomaterials* **101**, (2016).

31. Zhuang, X. *et al.* Ginger-derived nanoparticles protect against alcohol-induced liver damage. *J. Extracell. Vesicles* **4**, (2015).

32. Deng, Z. *et al.* Broccoli-Derived Nanoparticle Inhibits Mouse Colitis by Activating Dendritic Cell AMP-Activated Protein Kinase. *Mol. Ther.* **25**, (2017).

33. Xiao, J. *et al.* Identification of exosome-like nanoparticle-derived microRNAs from 11 edible fruits and vegetables. *PeerJ* **2018**, (2018).

34. Wang, K. *et al.* The Complex Exogenous RNA Spectra in Human Plasma: An Interface with Human Gut Biota? *PLoS One* **7**, (2012).

35. Zhang, M., Viennois, E., Xu, C. & Merlin, D. Plant derived edible nanoparticles as a new therapeutic approach against diseases. *Tissue Barriers* vol. 4 (2016).

36. Mu, J. *et al.* Interspecies communication between plant and mouse gut host cells through edible plant derived exosome-like nanoparticles. *Mol. Nutr. Food Res.* **58**, (2014).

37. Cao, M. *et al.* Ginseng-derived nanoparticles alter macrophage polarization to inhibit melanoma growth. *J. Immunother. Cancer* **7**, (2019).

38. Şahin, F. *et al.* In Vitro Wound Healing Activity of Wheat-Derived Nanovesicles. *Appl. Biochem. Biotechnol.* **188**, (2019).

39. Lobb, R. J. *et al.* Optimized exosome isolation protocol for cell culture supernatant and human plasma. *J. Extracell. Vesicles* **4**, (2015).

40. Chen, X., Zhou, Y. & Yu, J. Exosome-like Nanoparticles from Ginger Rhizomes Inhibited NLRP3 Inflammasome Activation. *Mol. Pharm.* **16**, (2019).

41. Kalarikkal, S. P., Prasad, D., Kasiappan, R., Chaudhari, S. R. & Sundaram, G. M. A cost-effective polyethylene glycol-based method for the isolation of functional edible nanoparticles from ginger rhizomes. *Sci. Rep.* **10**, (2020).

42. Wang, Q. *et al.* Delivery of therapeutic agents by nanoparticles made of grapefruit-derived lipids. *Nat. Commun.* **4**, 1867 (2013).

43. Bokka, R. *et al.* Biomanufacturing of Tomato-Derived Nanovesicles. *Foods* **9**, (2020).

44. Fujita, D. *et al.* Apple-Derived Nanoparticles Modulate Expression of Organic-Anion-Transporting Polypeptide (OATP) 2B1 in Caco-2 Cells. *Mol. Pharm.* **15**, (2018).

45. Zhao, Z., Yu, S., Li, M., Gui, X. & Li, P. Isolation of Exosome-Like Nanoparticles and Analysis of MicroRNAs Derived from Coconut Water Based on Small RNA High-Throughput Sequencing. *J. Agric. Food Chem.* **66**, (2018).

46. Stanly, C., Moubarak, M., Fiume, I., Turiák, L. & Pocsfalvi, G. Membrane transporters in citrus clementina fruit juice-derived nanovesicles. *Int. J. Mol. Sci.* **20**, (2019).

47. Iravani, S. & Varma, R. S. Plant-Derived Edible Nanoparticles and miRNAs: Emerging Frontier for Therapeutics and Targeted Drug-Delivery. *ACS Sustain. Chem. Eng.* **7**, (2019).

48. Yang, M., Liu, X., Luo, Q., Xu, L. & Chen, F. An efficient method to isolate lemon derived extracellular vesicles for gastric cancer therapy. *J. Nanobiotechnology* **18**, (2020).

Plant-EVs as drug delivery systems

"To liberate the drug at the right time in a right amount of concentration at a specified target site"

*(*Vijaya Shanti and Mrudula, 2011)

The definition given by Shanti and Mrudula[1] highlights the two key aspects that characterize an ideal drug delivery vehicle. It has the aim to bring a drug inside the human body, allowing site specificity and a time-controlled release. Drug therapies need vehicles that permit a high delivery efficiency to a certain target site, without generating toxicity or host immune response[2].

To date, many types of particulate nanoscale DDS have been developed: organic nanoparticles such as liposomes, micelles, dendrimers, polymeric and lipid nanoparticles, and inorganic vehicles as quantum dots and metal nanoparticles (Figure 33).
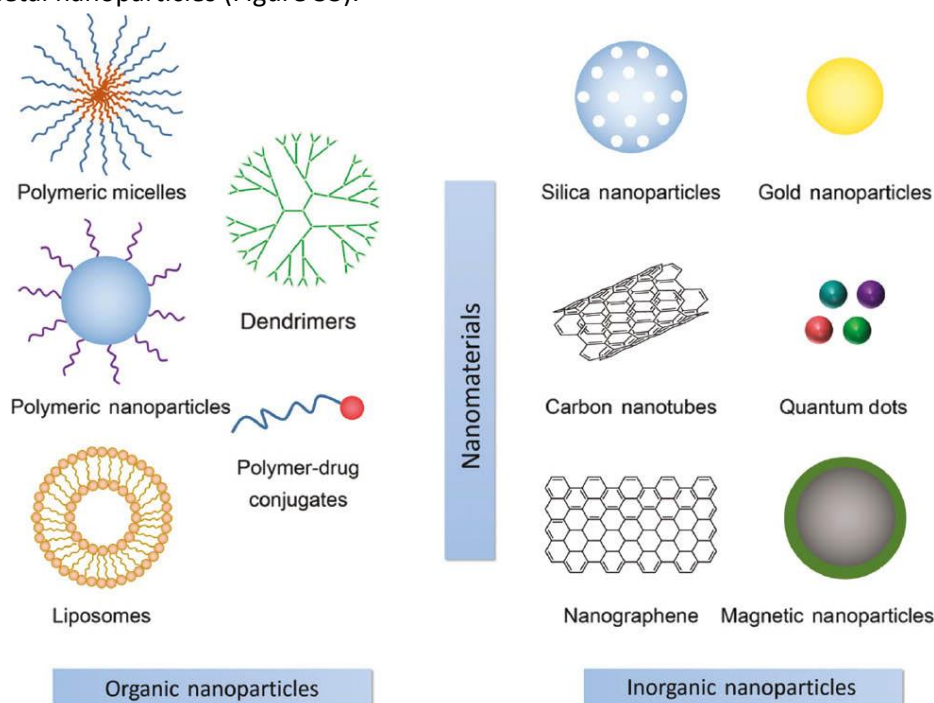
Figure 33: Schematic structures of the main types of nanoparticles developed for DDS [3]

These systems need to overcome two main issues when in contact with the human body: the cytotoxicity of the materials, and the rapid clearance by the reticuloendothelial system (RES) or the mononuclear phagocyte system (MPS)[4].

Compared with synthetic nanoparticles, endogenous DDS have recently shown promising results in enhancing drug delivery and therapeutic efficacy because of their native in vivo biocompatibility[5]. Extracellular vesicles are among those systems and they are considered excellent candidates for the delivery of drugs and compounds. EVs can be loaded with exogenous therapeutic drugs such as proteins, miRNAs, siRNAs and expression vectors, to achieve superior effects against diseases, but also in nutraceutics and cosmetics by enhancing the beneficial action of natural bioactive molecules[6].

The use of EVs as DDS can reduce the systemic toxicity of many drugs while extending the circulation time and thereby increasing their therapeutic efficiency. Several reports have reported the advantages of using exosomes as nanocarriers. These advantages include:

- Native biocompatibility
- Ability to penetrate mammalian barriers (like the blood-brain barrier) without inducing inflammatory response or necrosis[7].
- Small size for penetration into deep tissues[8].
- Slightly negative zeta potential for long circulation[9,10].
- Deformable cytoskeleton and similarity to cell membranes[11].
- Increased capacity to escape degradation or clearance by the immune system[12].

EVs isolated from fruits and plants (PDEVs) are gaining a growing attention in the field of DDS due to a very important (but obvious) observation: they are ingested everyday by humans and so they can be considered intrinsically safe[5]. In addition, fruit, plants, but also animal products, are the most advantageous sources in terms of cheapness and scalability, considering their potential clinical and industrial use.

A phase I clinical trial for the use of exosomes derived from fruit to deliver curcumin to the colon for the treatment of colon cancer is currently underway[13].

According to Rome[2] there are three main PDEV-based nanoplatforms that can be used for the delivery of pharmaceutical or natural agents: re-engineered EVs made by lipids from plant-derived EVs (Figure 34A), pristine plant-derived EVs (Figure 34B) and coated PDEVs (Figure 34C).
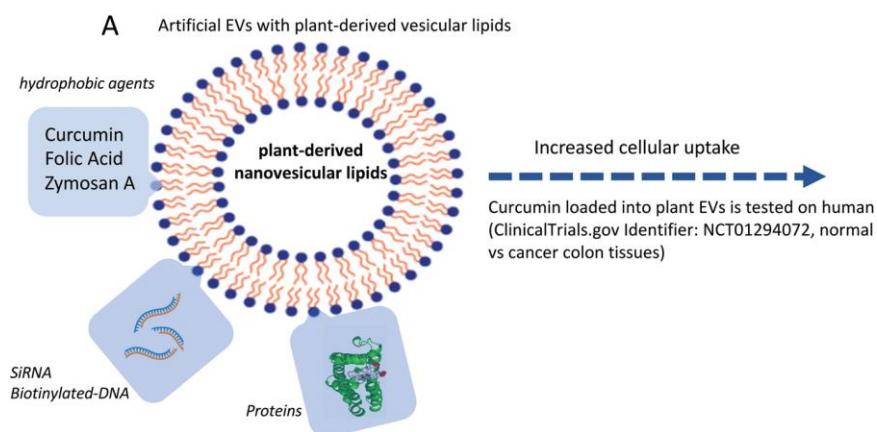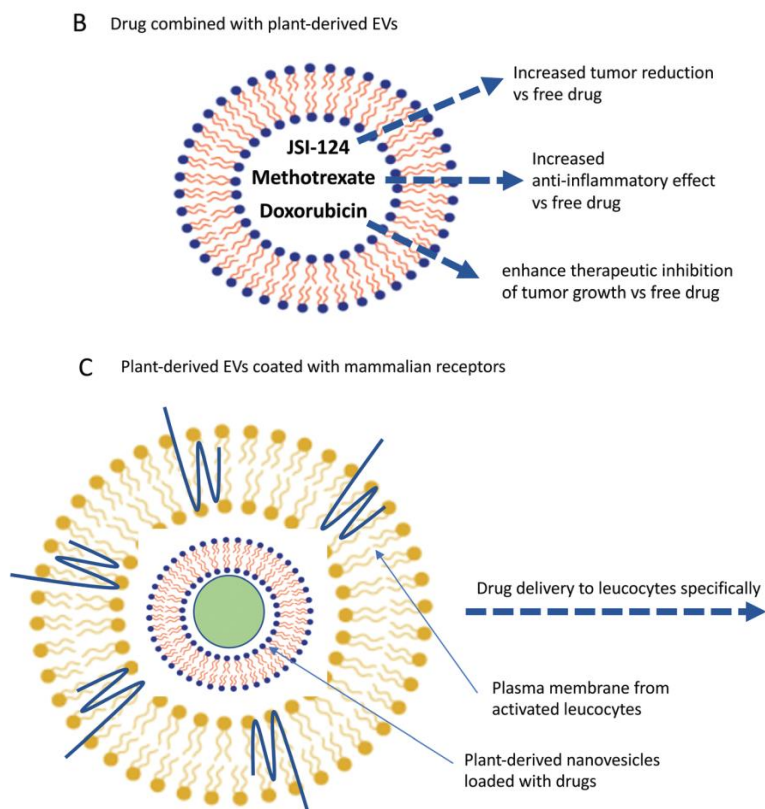
Figure 34: Plant-derived EVs as DDS. (A) Re-engineered EVs made by lipids from plant-derived EVs; (B) Pristine plant-derived EVs; (C) Plant-derived EVs coated with mammalian membranes which specific receptors [2].

Plant-derived EVs can be loaded with drugs in their pristine form (Figure 34B). EVs ability to bind hydrophobic agents is exploited, increasing their bioavailability and thus their cellular uptake[2].

There are two main cargo loading techniques for drugs encapsulation: passive and active cargo loading. In Table 6 are reported the main techniques that have been recently explored for exosomes encapsulation[5].

Table 6: EVs for cargo delivery by Luan et al. [5].

		Advantages	Disadvantages	Model drugs
I) Passive loading	a) Incubation of exosomes and free drugs	Simple Do not compromise membrane integrity	Low drug loading efficiency	Doxorubicin[60] Paclitaxel[48] Catalase[44] Paclitaxel[58]
	b) Incubation of the donor cells with free drugs	Simple Do not compromise membrane integrity	Low drug loading efficiency Drugs may cause cytotoxicity to the donor cells	
II) Active loading	a) Sonication	High drug loading efficiency	Compromise membrane integrity	Catalase[44]
	b) Extrusion	High drug loading efficiency	Compromise membrane integrity	Porphyrin[50]
	c) Freeze/thaw	Medium drug loading efficiency Liposome-exosome fusion	Aggregations	Porphyrin
	d) Electroporation	Loading with large molecules such as siRNA, miRNA	Aggregations	let-7a miRNA[66] MAPK1 siRNA[52]

4. 1 Passive cargo loading

The passive drug loading technique is based on the simple incubation of PDEVs at a certain temperature: EVs are incubated with drugs, and the drugs diffuse into the exosomes along the concentration gradient (Figure 35). This strategy relies on diffusion action, hydrophobic/hydrophilic and electrostatic interactions between the drug molecule and the vesicles lipid bilayer (Figure 36)[5].
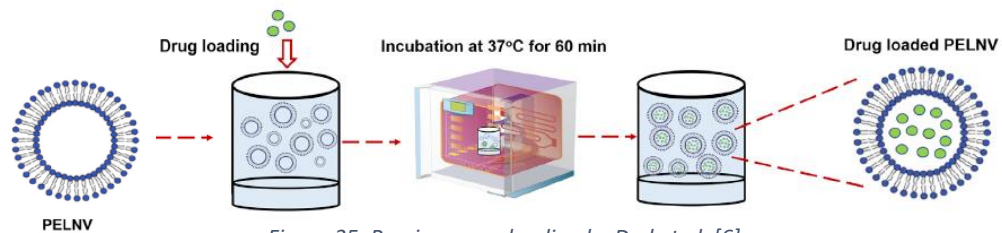

Figure 35: Passive cargo loading by Dad et al. [6]

One important parameter that affects the loading efficiency is the hydrophobicity of the drug molecules. Hydrophobic drugs interact with the lipid bilayer of the vesicle membrane[5]: in particular, hydrophobic drugs are incorporated in the internal cavity of the lipid bilayer while hydrophilic compounds are encapsulated in the internal aqueous space of the vesicles.
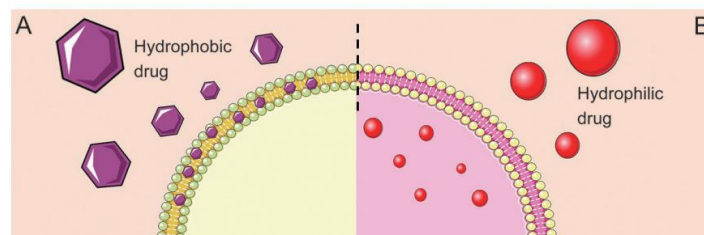

Figure 36: Hydrophobic/hydrophilic interactions between drugs and EVs phospholipidic membrane by Luan et al. [5]

Most of EVs displays a negative superficial charge. It can be exploited in both active and passive cargo loading techniques to attract positively charged drugs (e.g. doxorubicin) and so support the load of the drug. Also, negatively (e.g. RNAs, DNAs) and neutrally charged compounds (e.g. curcumin, folic acid) are commonly encapsulated in EVs. In this case, the lipophilic properties of these compounds allow for their encapsulation by bypassing the effects of the adverse electrostatic interactions.

Some natural compounds have a beneficial effect on health, but their potential cannot be fully exploited due to their poor solubility and bioavailability. For example, curcumin is a model hydrophobic drug for encapsulation. Despite having numerous bioactive and therapeutic properties (anti-inflammatory, anti-cancer, antioxidant properties), the poor solubility of curcumin, due to its hydrophobicity and preferential interaction with lipid membranes, remains a major barrier in its bioavailability and clinical efficacy. To date, a variety of technologies have been developed to increase curcumin bioavailability, through encapsulation in liposomes, polymeric nanoparticles, biodegradable microspheres, cyclodextrin, and hydrogels and recently, also mammalian exosomes were tested[2].

Through overnight incubation Vashisht et al.[14] achieved passive curcumin loading in milk exosomes, obtaining a loading efficiency of 70.46%. They investigated the stability of free curcumin and exosomal curcumin in PBS and in vitro digestive processes though spectrophotometry readings. Curcumin encapsulated into exosomes was found to be more soluble and stable as compared to free curcumin (Figure 37). Their results suggested that while free curcumin is highly susceptible to pH change and

leads to the destruction of its structure under in vitro digestion, curcumin encapsulated in exosomes is stable at optimum temperature, high and low pH, and resistant to different enzymatic treatments. Sun et al.[15] studied the enhanced anti-inflammatory activity of curcumin encapsulated in EL-4-exosomes (murine tumor cell line) towards activated myeloid cells in vivo. The study indicated that curcumin delivered by EVs is more stable and more concentrated in blood.

All together these results suggest that EVs released from mammalian cells (e.g.; exosomes from intestinal cells or outer membrane vesicles OMV from gut microbiota) might naturally participate in an increase in the bioavailability of some hydrophobic and poorly soluble components ingested from our food, spontaneously increasing their entrance into mammalian cells and promoting their beneficial action on health[2].
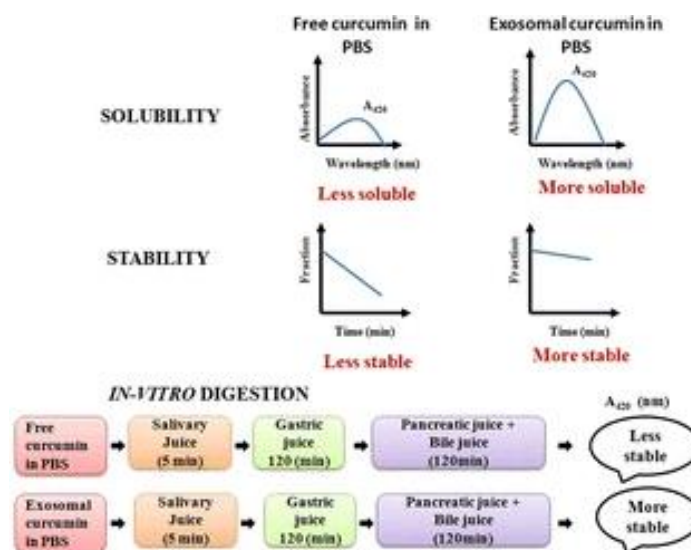

Figure 37: Enhanced solubility and stability of exosomal curcumin in PBS than free curcumin in PBS and against digestive processes in the study by Vashisht et al. [14]

Another method for passive cargo loading is based on the incubation of the drug with the EVs donor cells. Through this approach the cells accumulate the desired bioactive compound and then secrete exosomes that already possess these compounds[5].

4.2 Active cargo loading

Active cargo loading is based on strategies that temporarily disrupt the EVs membrane so that the desired compounds could easily diffuse into the vesicles during the membrane deformation. The membrane can be disrupted by sonication, extrusion, and freeze-thaw cycles[5]. After the bioactive compound is loaded into the EVs, the membrane integrity can be restored to its initial integrity. In their study Kim et al. [16] observed that the membrane integrity of the exosomes was restored within an hour when the exosomes are incubated at 37 °C. However, the potential damage to the EVs structure and their targeting features due to the membrane disruption process is a remarkable concern. On the other hand, the main advantage in the use of active cargo loading techniques is the considerable increase in the loading capacity, in comparison to passive loading, while preserving the method's simplicity[17]. Fuhrmann et al. [18] used sonication to disrupt the EVs membrane and they reported an increase in the mammalian EVs loading capacity of hydrophilic porphyrins by up to 11 times when compared to passive cargo loading.

Also, there is a considerable interest in miRNAs, siRNAs and DNAs encapsulation for gene therapies. In this context, electroporation is the most used technique for active siRNA and miRNA loading onto EVs [19–21]. Electroporation creates small pores in the EVs membrane through application of an electrical field to exosomes suspended in a conductive solution. This method is mostly used for loading siRNA or miRNA into EVs, because these molecules are relatively large and cannot diffuse into the exosome spontaneously, as in the case of small hydrophobic molecules [5].

Plant derived EVs have a size ranging from 50 to 500 nm and one of the most difficult task is to obtain a uniform EVs size distribution, crucial for their exploitation for drug delivery. Hence, PDEVs can be re-engineered in order to formulate uniform-sized nanoparticles.

Nanolipids can be extracted from plant-derived EVs and then used to reconstitute artificial EVs loaded with drugs to increase their cellular uptake into mammalian cell [2]. However, Akuma et al. [17] observed that the lipid nanocarriers are not exosomes, in structure and function, but they have the benefits of a natural, food-derived delivery system.

Loureiro et al. [22] extracted nanolipids from grape-derived-EVs by through the "Bligh and Dyer technique", a liquid-liquid extraction process and then processed through a 200-nm liposome extruder in order to obtain re-assembled uniform-size nanovectors (Figure 38).

Using the same re-engineering approach Zhang et al. [23] loaded doxorubicin into nanovesicles derived from ginger-EVs. Lipids extracted from ginger-EVs re-assembled themselves in nanostructures through sonication and the loading of doxorubicin was favored by electrostatic interaction. The encapsulation prompted the drug release in a pH-dependent manner to treat colon cancer.
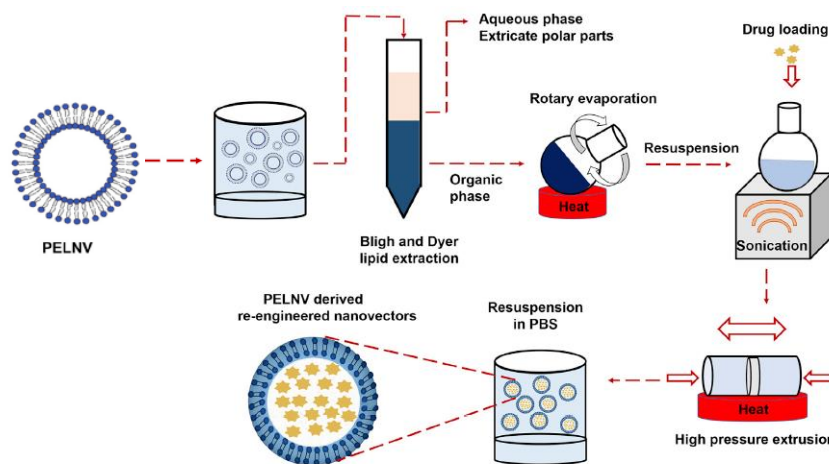

Figure 38: Re-engineering method for PDEVs by Loureiro et al. [22] with active cargo loading procedure [6].

Lipids from grape fruit-EVs (GF-EVs) were extracted by Wang et al. [7] and used to reconstitute artificial vesicles. These were able to bind hydrophobic agents such as curcumin, folic acid and Zymosan A, without altering their activities. In addition, they could deliver biotinylated-DNA and proteins, and functional siRNA into recipient cells in vitro.

PDEVs-derived nanovectors also offer the possibility of tailoring their surface with specific bioactive molecules that can be immobilized onto their surface [6]. In the aforementioned study by Zhang et al. [24] the action of ginger-EVs-derived nanostructures loaded with doxorubicin toward colon cancer was enhanced by conjugating the vesicles with a targeting ligand, folic acid.

Besides, the delivery efficiency plant-derived EVs loaded with drugs can be further increased by coating them with membranes from mammalian origin containing specific receptors (Figure 34C).

Wang et al. [25] coated grapefruit-derived EVs with membranes of activated leukocytes enriched in receptors capable of targeting the inflammatory tissue. In vivo, these coated GF-EVs were able to reduce tumor growth in two tumor models and to inhibit the inflammatory effects of dextran sulfate sodium-induced mouse colitis.

Despite these strategies, most targeting achievements of PDEVs and PDEVs-derived nanostructures are though their natural biodistribution. PDEVs, in fact, intrinsically express some lipids and cell adhesion molecules on their surface, such as phosphatidic acid, that naturally promote binding to certain recipient cells[26].

Chapter 4 references

1. Bheemidi, V. S., Tiruckovela, M. & Varanasi, P. K. An imperative note on novel drug delivery systems. *Journal of Nanomedicine and Nanotechnology* vol. 2 (2011).

2. Rome, S. Biological properties of plant-derived extracellular vesicles. *Food Funct.* **10**, (2019).

3. Zhou, Q., Zhang, L. & Wu, H. Nanomaterials for cancer therapies. *Nanotechnology Reviews* vol. 6 (2017).

4. Haque, S., Whittaker, M. R., McIntosh, M. P., Pouton, C. W. & Kaminskas, L. M. Disposition and safety of inhaled biodegradable nanomedicines: Opportunities and challenges. *Nanomedicine: Nanotechnology, Biology, and Medicine* vol. 12 (2016).

5. Luan, X. *et al.* Engineering exosomes as refined biological nanoplatforms for drug delivery. *Acta Pharmacologica Sinica* vol. 38 (2017).

6. Dad, H. A., Gu, T. W., Zhu, A. Q., Huang, L. Q. & Peng, L. H. Plant Exosome-like Nanovesicles: Emerging Therapeutics and Drug Delivery Nanoplatforms. *Molecular Therapy* vol. 29 (2021).

7. Wang, Q. *et al.* Delivery of therapeutic agents by nanoparticles made of grapefruit-derived lipids. *Nat. Commun.* **4**, 1867 (2013).

8. Vader, P., Mol, E. A., Pasterkamp, G. & Schiffelers, R. M. Extracellular vesicles for drug delivery. *Advanced Drug Delivery Reviews* vol. 106 (2016).

9. Malhotra, H. *et al.* Exosomes: Tunable nano vehicles for macromolecular delivery of transferrin and lactoferrin to specific intracellular compartment. *J. Biomed. Nanotechnol.* **12**, (2016).

10. Rupert, D. L. M., Claudio, V., Lässer, C. & Bally, M. Methods for the physical characterization and quantification of extracellular vesicles in biological samples. *Biochimica et Biophysica Acta - General Subjects* vol. 1861 (2017).

11. Hood, J. L. & Wickline, S. A. A systematic approach to exosome-based translational nanomedicine. *Wiley Interdiscip. Rev. Nanomedicine Nanobiotechnology* **4**, (2012).

12. Hood, J. L. Post isolation modification of exosomes for nanomedicine applications. *Nanomedicine* vol. 11 (2016).

13. Investigating, S. *et al.* Study Investigating the Ability of Plant Exosomes to Deliver Curcumin to Normal and Colon Cancer Tissue. *Clinicaltrials.Gov* (2011).

14. Vashisht, M., Rani, P., Onteru, S. K. & Singh, D. Curcumin Encapsulated in Milk Exosomes Resists Human Digestion and Possesses Enhanced Intestinal Permeability in Vitro. *Appl. Biochem. Biotechnol.* **183**, (2017).

15. Sun, D. *et al.* A novel nanoparticle drug delivery system: The anti-inflammatory activity of curcumin is enhanced when encapsulated in exosomes. *Mol. Ther.* **18**, (2010).

16. Kim, M. S. *et al.* Development of exosome-encapsulated paclitaxel to overcome MDR in cancer cells. *Nanomedicine Nanotechnology, Biol. Med.* **12**, (2016).

17. Akuma, P., Okagu, O. D. & Udenigwe, C. C. Naturally Occurring Exosome Vesicles as Potential Delivery Vehicle for Bioactive Compounds. *Frontiers in Sustainable Food Systems* vol. 3 (2019).

18. Fuhrmann, G., Serio, A., Mazo, M., Nair, R. & Stevens, M. M. Active loading into extracellular vesicles significantly improves the cellular uptake and photodynamic effect of porphyrins. *J.*

Control. Release **205**, (2015).

19. Zhang, M., Wang, X., Han, M. K., Collins, J. F. & Merlin, D. Oral administration of ginger-derived nanolipids loaded with siRNA as a novel approach for efficient siRNA drug delivery to treat ulcerative colitis. *Nanomedicine* **12**, (2017).

20. Alvarez-Erviti, L. *et al.* Delivery of siRNA to the mouse brain by systemic injection of targeted exosomes. *Nat. Biotechnol.* **29**, (2011).

21. Wahlgren, J. *et al.* Plasma exosomes can deliver exogenous short interfering RNA to monocytes and lymphocytes. *Nucleic Acids Res.* **40**, (2012).

22. Loureiro, J. A. *et al.* Resveratrol and grape extract-loaded solid lipid nanoparticles for the treatment of Alzheimer's disease. *Molecules* **22**, (2017).

23. Zhang, M. *et al.* Edible ginger-derived nanoparticles: A novel therapeutic approach for the prevention and treatment of inflammatory bowel disease and colitis-associated cancer. *Biomaterials* **101**, (2016).

24. Wang, Q. *et al.* Delivery of therapeutic agents by nanoparticles made of grapefruit-derived lipids. *Nat. Commun.* **4**, (2013).

25. Wang, Q. *et al.* Grapefruit-derived nanovectors use an activated leukocyte trafficking pathway to deliver therapeutic agents to inflammatory tumor sites. *Cancer Res.* **75**, (2015).

26. Wang, X., Devaiah, S. P., Zhang, W. & Welti, R. Signaling functions of phosphatidic acid. *Progress in Lipid Research* vol. 45 (2006).

Experimental part

Materials and methods

The experimental work is based upon the development of a membrane-based process for the isolation and purification of extracellular vesicles (EVs) from lemon juice.

A diafiltration process represents the core part of the purification strategy, thus the work proceeds with the selection of the best process set-up configuration, as well as the selection of a proper membrane, in terms of materials and cut-offs.

The process is then optimized addressing the main hindrance associated to filtration processes, that is the membrane's gel layer formation and the resulting product losses.

In the following chapter the main techniques and instrumentations used in the experimental part of the work are described. The main focus is placed upon the description of the filtration cells, Amicon® *dead-end* stirred cell and Minitan-S *tangential flow filtration* system used to perform diafiltration and their process set-up.

Size exclusion chromatography (SEC) is employed extensively within the work as main analytical techniques. Thus, a detailed description of the used HPLC and FPLC systems, as well as the chromatography columns adopted, is presented.

The obtained EVs preparations are successively characterized by means of dynamic light scattering measurements (DLS) and total protein's quantification through BCA assay.

Finally, curcumin is employed as model drug to test the ability of encapsulation of the phospholipidic vesicles.

5.1 Materials

Materials for filtration

- Lemons
- Achillea lemon juice (100% biological lemon juice)
- PBS phosphate saline buffer 0,1 M, p-H=7.4 filtered with a 0,45 μm paper filter

Microfiltration membranes

- Sartorius Sartobind Q, average pore size 3 μm
- Sartorius Regenerated Cellulose, average pore size 0,45 μm

Ultrafiltration membranes

- F400R PVDF membrane, MWCO 250 kDa
- Sigma Aldrich PES membrane, MWCO 100kDa
- Merck Millipore RC membrane, MWCO 300kDa

Materials for SEC-HPLC analysis

- HPLC Plus water
- PBS phosphate saline buffer 0,1 M, p-H=6.7 prepared with HPLC Plus water
- Yarra SEC-2000 column by Phenomenex®

Materials for SEC-FPLC analysis

- Demi water filtered with a 0,45 μm paper filter
- PBS phosphate saline buffer 0,1 M, p-H=7.4 filtered with a 0,45 μm paper filter
- Sepharose CL-2B resin
- BioRad Econo-Column

-   BioRad Econo-Column flow adaptor

Materials for curcumin encapsulation
-   Curcumin from Sigma Aldrich
-   Methanol
-   PBS phosphate saline buffer 0,1 M, p-H=7.4 filtered with a 0,45 µm paper filter

Materials for BCA analysis
-   Pierce™ BCA Protein Assay Kit by Thermo Fisher scientific
-   PBS phosphate saline buffer 0,1 M, p-H=7.4 filtered with a 0,45 µm paper filter
-   Bovine Serum albumin 2 mg/ml

5.2 Methods and instrumentation

5.2.1 Preparation of samples from citrus limon fruit

Biological lemons are bought from different local shops (Bologna), to obtain a "homogeneous" feed, given the distinctive characteristics of different species of lemons and the different maturity stages. The selected fruits came from Spain, South Italy (Sicily) and South Africa (Figure 39).

Figure 39: Different lemons were bought from local markets.

Firstly, lemons are carefully hand-peeled with a knife to remove the skin and the pith, the white part of the peel. Subsequently a common extractor is used to squeeze lemons and obtain lemon juice (Figure 40).

Figure 40: Tristar juice extractor

To evaluate the influence of the extractor and the lemon's source in the process yield, trials are also made using other two different feeds:

- Lemons squeezed with a kitchen electrical juicer.
- Commercial lemon juice (Succobene limone 100%, 330 ml) by Achillea. It is a commercial lemon juice made by 100% lemon juice from biological Sicilian lemons.

5.2.2 Centrifugation

5.2.3 Ultracentrifugation

5.2.4 Filtration techniques

After the first centrifugation at 5000 rpm for 50 minutes, different clarification protocols based on a preliminary microfiltration process have been evaluated. Different parameters are considered:

- Dilution factor;
- MF membrane's material and average pore size;
- Need of an additional centrifugation step, at higher speed;
- Dead-end versus cross-flow mode using different cells;
- Type of buffer used as diluent.

Concerning the purification stage, diafiltration is chosen as technique for the purification of vesicles from other contaminants. For this purpose, both stage (batch) diafiltration in *dead-end* mode and constant volume diafiltration in *cross-flow* mode are carried out. In this case the parameters considered are:

- UF membrane's material and molecular weight cut offs (MWCO);
- Number of stages/number of diavolumes required to achieve a certain purification;
- Dead-end versus cross-flow mode using different cells;

The main parameters controlled during diafiltration experiments are:

- The flux through the membrane, measured indirectly by measuring the volume of permeate collected over time.
- The distribution of species between retentate and permeate, by means of SEC-FPLC and SEC-HPLC analyses.
- Membrane fouling and EVs losses in the cake/gel.

5.2.4.1 Theoretical notes of filtration

There are two main configurations for filtration processes: *dead-end* and *cross-flow* mode. In dead-end filtration the feed flows perpendicularly to the membrane due to the convective motion imposed by the driving force. In this configuration the permeate flux decreases progressively over time, as the thickness of the cake/gel formed over the membrane surface increases (Figure 43a). As membrane fouling becomes predominant, conditions for filtration get progressively unsustainable over time as the cake thickness increases indefinitely and the permeate flux approach zero.
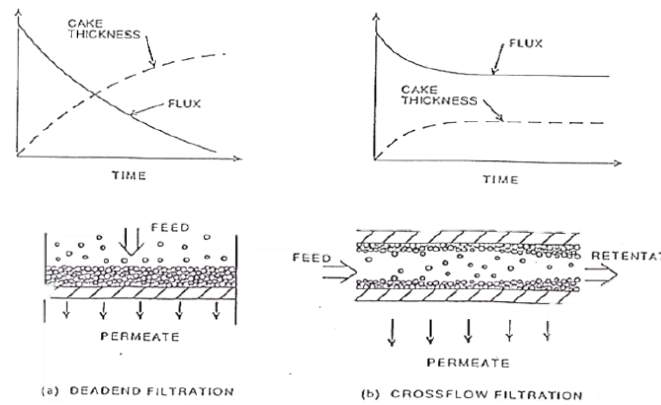
Figure 43: Dead-end (a) and cross-flow (b) modes for filtration. Flux and cake thickness trend over time.

In *cross-flow* mode (Figure 43b) the feed flows tangentially over the filtration surface. In this configuration the tangential component of the flow over the membrane disrupts the formation of the concentration polarization layer that builds up as species are rejected by the membrane. With TFF it is possible to identify conditions for which both the flux and transmembrane pressure are steady with time. Ideally, under these conditions, filtration can continue indefinitely.

Both ultrafiltration and microfiltration processes are predominantly controlled by the concentration polarization effect. The concentration polarization phenomenon is the solute concentration accumulation at the surface of the membrane c_w compared to that in the bulk solution c_b, throughout the separation process. The solute is transferred by convection into the boundary layer and then, being retained and concentrated over the membrane, it diffuses back to the bulk solution due to the concentration gradient. According to the "film theory" the counter-diffusive flux is localized on a "film" having a certain thickness δ (Figure 44).
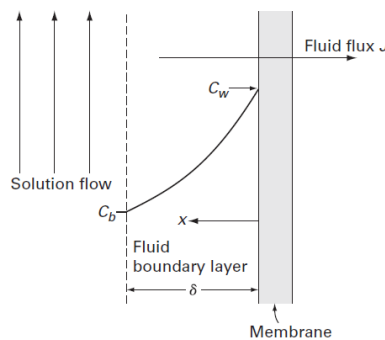
Figure 44: Schematic representation of the boundary layer in crossflow filtration with a dissolved solute in the feed [4].

At steady state, the rate of convective mass transfer of solute toward the membrane surface is equal to the rate of mass transfer of the solute counter-diffusion.

$$J_v c = -\mathcal{D}\frac{dc}{dx} \qquad (2)$$

By integrating equation (2) over the film thickness δ, by assuming total density and diffusion coefficient $\mathcal{D}$ to be constant over the film, the following solution is obtained:

$$\frac{J_v}{k_L} = ln\frac{c_w}{c_b} \qquad (3)$$

Where:

- $k_L = \frac{\mathcal{D}}{\delta}$ solute mass transfer coefficient [m/s];
- J_v volumetric flux [m³/(m²h)];

The ratio $\frac{c_w}{c_b}$, often called "polarization modulus", indicates the extent of concentration polarization and it is exponentially dependent on k_L (and so $\mathcal{D}$, δ) and J_v. It is possible to observe that concentration polarization assumes a highly relevant role in pressure-driven processes as the permeate flux increases, for example in the case of membrane with high solvent permeability. This phenomenon can be compensated by increasing the mass transfer coefficient, leading to a decrease in the concentration polarization effect, or increase dilution of the sample to be filtered. It is noteworthy that especially for high molecular weight molecules concentration polarization can become critical, since those molecules have a small diffusion coefficient $\mathcal{D}$.

At high concentration polarization levels, the solubility of the solute can be exceeded, resulting in the precipitation of the solute and the formation of solids or gel layer on the membrane surface. In UF, as the TMP increases, the concentration over the membrane increases up to a maximum value called "gel concentration". It is the maximum concentration achievable in an UF process. In gel conditions but the feed-side resistance to mass transfer is determining, i.e. the concentration polarization effect. If a total rejection to the solute is assumed, equation (1) becomes:

$$\frac{J_{vg}}{k_L} = ln\frac{c_g}{c_b} \qquad (4)$$

In this situation, the flux is asymptotic and not dependent on pressure, but it depends only on the mass transfer coefficient and the bulk concentration. c_g is usually calculated experimentally for a certain solution, even if some approximate values are tabulated in literature. The gel model can be applied also to MF, even if the physical phenomena is the formation of a cake rather than a gel, and the cake mass transfer mechanism is convective rather than diffusive.

5.2.4.2 Batch vs Constant volume diafiltration

Diafiltration is employed as technique for desalting as well as buffer exchange of solutions. It can be performed in a batch (discontinuous) or constant volume (semi continuous or continuous) mode. In batch diafiltration the sample is first concentrated to a fixed volume, then diluted back to its original starting volume with water or buffer. The process is repeated until the remaining solvent/impurities are lowered in concentration to the desired value. As shown in Figure 45, the sample is generally diluted with an equal volume of buffer (dilution factor equal to 2).
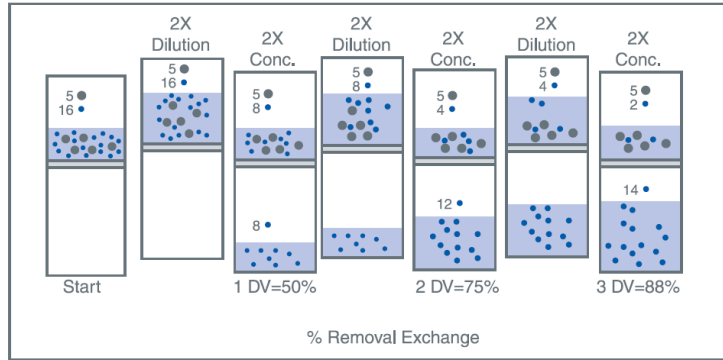
- Large molecules – bigger than pores in membrane
- Small molecules – salts or solvent

Figure 45: Discontinuous diafiltration – sequential dilution.[5]

The final product, after diafiltration, is at the same volume and concentration as when diafiltration started.

Assuming no rejection of contaminants and considering a batch volume V_0 with contaminant concentration c_0 undergoing a volume reduction X, after one batch concentration the component has concentration $c = c_0 X$ and volume $V = V_0/X$. After dilution back to the original volume V_0 the concentration is again $c = c_0$ and the volume of permeate generated is $V_P = V_0 - V_0/X$. After n stages:

$$\frac{c}{c_0} = X^{-n} \qquad (5)$$

$$V_P = nV_0(1 - \frac{1}{X}) \qquad (6)$$

Constant volume diafiltration involves washing out impurities, and in general low molecular weight species, in the retentate by adding new buffer at the same rate as filtrate is being generated (Figure 46). As a result, the retentate volume and product concentration does not change during the process. The filtrate volume generated is usually referred to in terms of "diafiltration volumes": when the volume of filtrate equals the starting retentate volume, 1 diavolume (DV) has been processed.
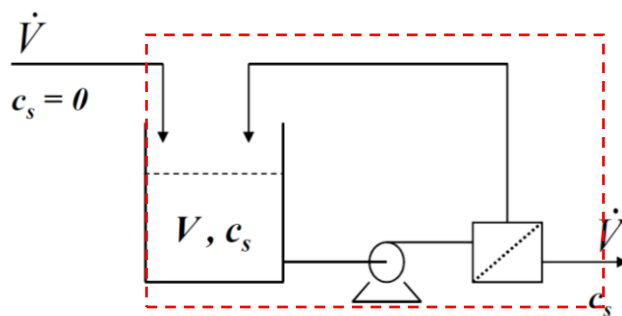
Figure 46: Constant volume diafiltration process configuration

Doing a mass balance on the solute s that is being removed (over the filtration system highlighted in Figure 46):

$$\frac{\partial n_i}{dt} = -\sum n_i^{\dot{o}ut} \qquad (7)$$

Assuming constant density:

$$\frac{\partial c}{\partial t} V = -\dot{V} c(t) \rightarrow \frac{\partial c}{c} = -\frac{\dot{V}}{V} dt \qquad (8)$$

By integrating from t=0 when $c_s = c_0$ and a generic time t:

$$ln\left(\frac{c}{c_0}\right) = -\frac{\dot{V}(t)}{V} = -\frac{V_P(t)}{V} \qquad (9)$$

If the membrane offers a certain rejection to the solute, the rejection coefficient R should be introduced in the equation:

$$ln\left(\frac{c}{c_0}\right) = \frac{\dot{V}(t)}{V}(1 - R) \qquad (10)$$

In diafiltration is important to find the optimum dilution conditions to maximize productivity. If from one hand concentration before diafiltration reduces the required diafiltration buffer required and saves time, on the other hand as the product becomes concentrated, the viscosity increases, and the filtrate flux decreases. The filtrate flux rate varies inversely as the natural log of the concentration factor: the flux declines as the bulk product concentration increases. Therefore, although it might take significantly less volume to diafilter a concentrated sample, it could take considerably more time compared to a less concentrated sample.

5.2.4.3 UF/MF dead-end cell

Amicon® Ultrafiltration Stirred Cell 8200 by Merck Millipore is used for pressure driven dead-end filtrations for both clarification and purification stages. The cell is set up is shown in Figure 47 and the cell specifications are reported in Table 11.
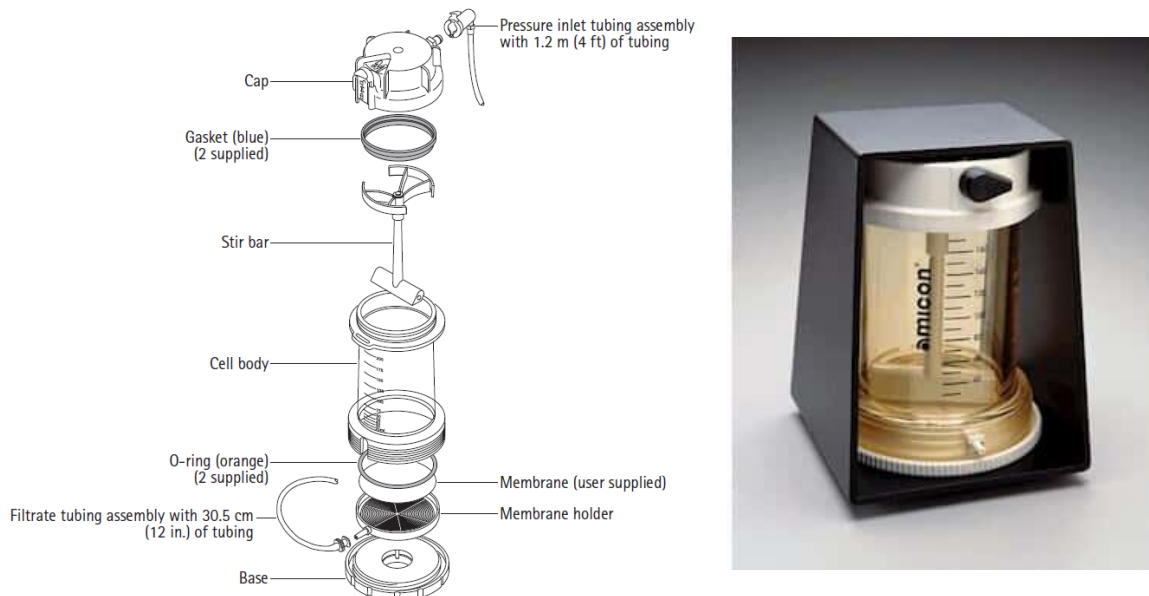
Figure 47: Schematic illustration (left) and picture (right) of the Amicon® UF/MF stirred cell 8200 model with a 200 ml cell capacity.[6]

Stirred Cell model 8200	
Cell capacity	200 mL
Minimum Process volume	5 mL
Nominal Membrane Diameter	63.5 mm
Effective Membrane Area	28.7 cm^2
Hold up volume	1.2 mL
Retaining stand base dimensions	9 x 9 cm
Retaining stand height	12.8 cm
Max Operating Pressure	75 psi

The cell is made by a cylindrical polysulfone body having a maximum working volume of 200 mL, inside of which a magnetic stirrer bar is mounted. The membrane housing can host membrane sheets having 63.5 mm of diameter, corresponding to an effective filtration area equal to 28.7 cm^2. The total filtration area, equal to 31.65 cm^2, is reduced due to the presence of the silicone rubber o-ring that seals the membrane evenly in the bottom of the holder. The membrane housing is screwed to the bottom part of the container and to the upper cap. The latter is connected to the external compressed air line through a pipe of 6.4 mm in diameter that allow the application of the desired driving force. Once a certain pressure is applied, the system is kept under pressure through an external retaining stand (shown in black in Figure 47). The system is placed above a magnetic stirrer that provides the rotation of the magnetic bar at the filtration interface, thus providing mechanical agitation. The working system in concentration/discontinuous diafiltration mode is schematized in Figure 48.
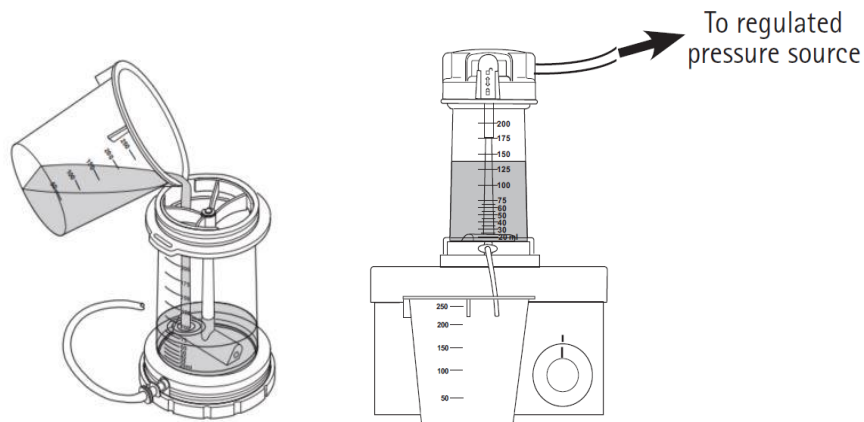
Figure 48: Amicon® Stirrer cell under batch concentration/diafiltration working conditions. First the solution to be filtered is added to the cell, that is subsequently sealed and connected to the compressed air pressure source. The system is placed above a magnetic stirrer that provides the rotation of the magnetic bar at the filtration interface, during the process. [6]

The stirred cell can be operated in either a concentration or diafiltration mode. In concentration mode, gas pressure is applied directly to the stirred cell and the solution is concentrated up to the desired value. The product of interest can be in the retentate as well as in the permeate. Diafiltration is conducted at constant volume. The system is charged with the solution and an equal amount of buffer (considering a dilution factor of 2). At each stage the process is stopped once the initial volume is reached and an equal volume of fresh buffer is added again. Both the operations are conducted at a TMP = 1.5 bar and stirring at 200 rpm. These values are selected to guarantee the filtration to be as gentle as possible, in order to preserve vesicles' integrity.

The pressure-driven filtration coupled with magnetic stirring allow to partially limit the concentration polarization effect. In fact, in the case of dead-end filtration, the turbulences generated by stirring at the filtration interface increases the mass transfer coefficient k_L, decreasing the concentration polarization effect and the subsequent fouling of the membrane.

5.2.4.4 Constant volume TFF diafiltration

Constant volume diafiltration is carried out in cross flow mode, in the Minitan™-S tangential flow ultrafiltration system by Merk Millipore. The system is shown in Figure 49 and the specifications are reported in Table 12.

Table 12: MiniTan-S UF system specifications [7]*.*

Materials	Acrylic manifolds with stainless steel end plates.
Dimensions	15.2 cm L x 11.4 cm W x 12 cm H
Filter area	30 cm^2 single membrane sheet
Volume	100 ml to 500 ml
Tubing size	1/4 OD to 1/8 ID
Retentate Flow	300-500 ml/min
Hold-up Volume	20-30 ml depending on tubing configurations
Pressure	1.75 – 2.1 bars maximum with silicone tubing
Temperature	50°C maximum
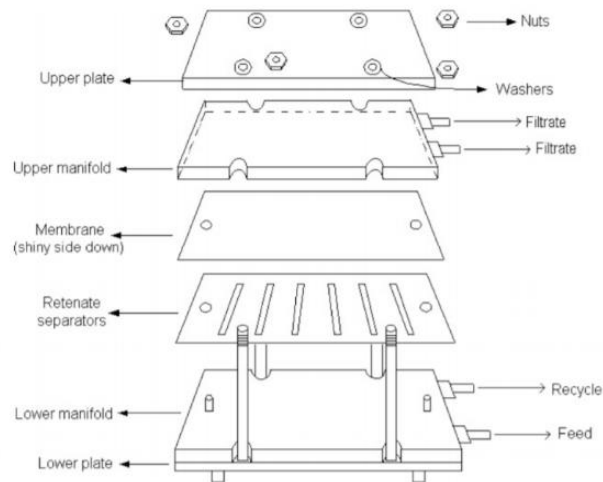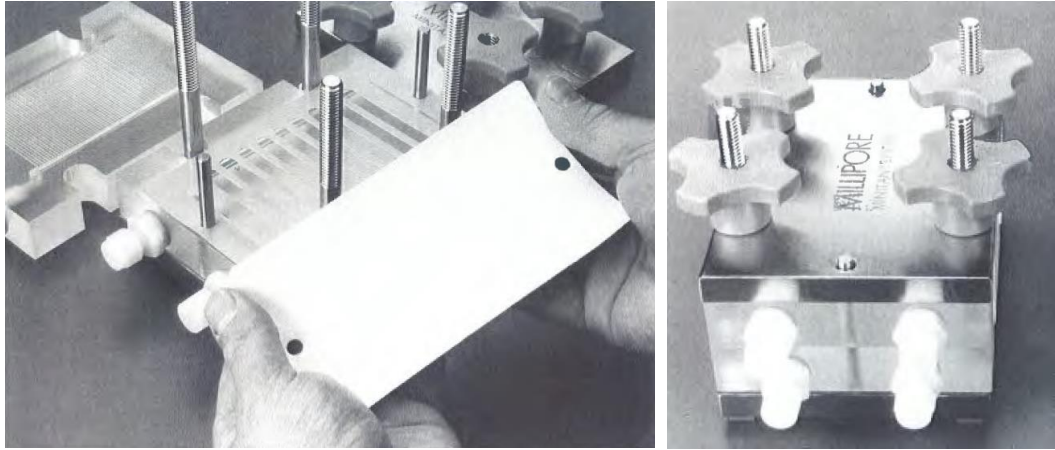
Figure 49: Minitan-S membrane sheet (upper left) and filtration apparatus (upper right). Exploded-view diagram of the Minitan-S system assembly and flow path (bottom). [7]

The system uses a single 30 cm^2 membrane sheet to perform filtrations. The membrane is placed between two open-flow silicone separators that provide a gasket seal and control the flow of fluids, determining the active area of filtration. Open-flow silicon separators are recommended for processing high concentration of suspended solids or large particles. These are enclosed between the acrylic upper and lower manifold and two stainless steel plates. The flow path is provided by the retentate and filtrate channel present in the lower and upper manifolds, respectively. The whole system is secured through four hand wheels.

A one pump configuration is used exploiting FPLC system and its P-900 pump system. The process flow diagram is shown in Figure 50.
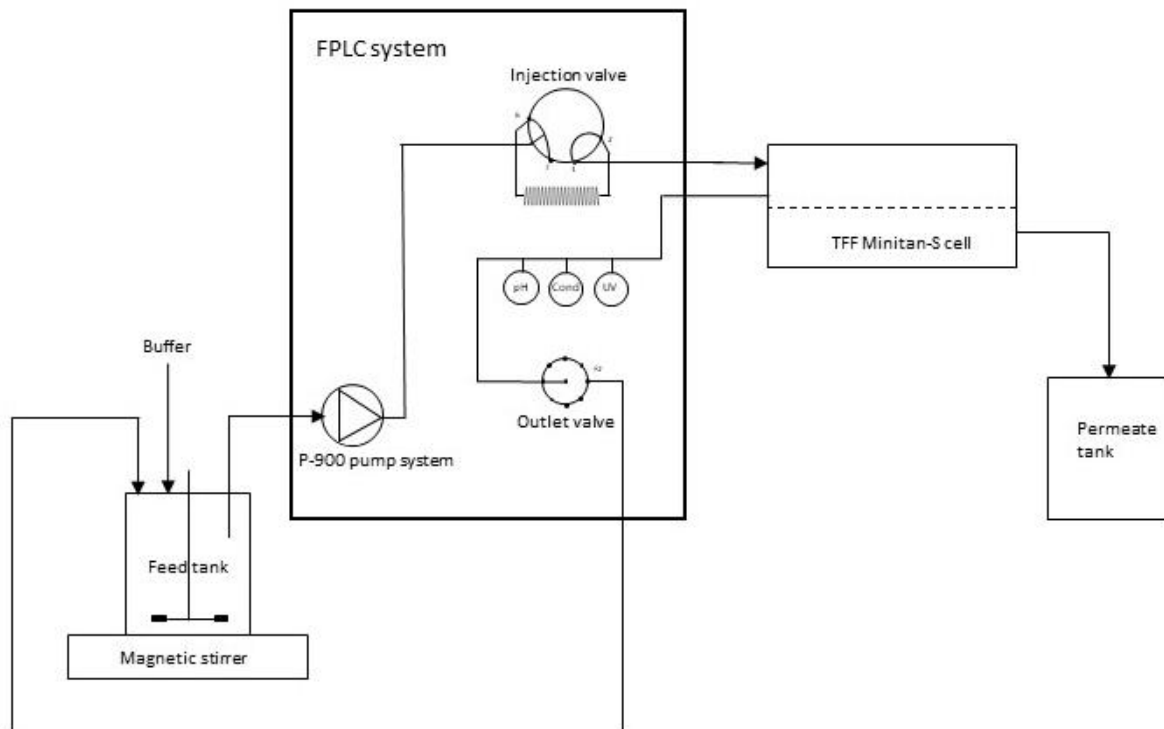
Figure 50: Process flow diagram of the lab-scale diafiltration apparatus setup using FPLC system and Millipore MInitan-S TFF cell

The feed reservoir is placed upon a magnetic stirrer to provide mechanical agitation through an impeller (200 rpm) and submerged in an ice bath kept at 6°C. FPLC pump draws sample solution from the feed reservoir and pumps it into the Minitan cell through plastic piping. The feed flow passes through the system injection valve in inject mode, with a 2ml sample loop. This is aimed at providing additional pressure drops, and so additional driving force for the process. As the solution passes through the Minitan particles larger than the MWCO sweep across the surface of the filter and are recirculated back to the sample reservoir. Water, salts, particles and impurities smaller than the MWCO pass through the cell and are collected into the permeate reservoir (a 200 ml graduated cylinder). The retentate is recirculated back to the FPLC system, and UV signal, conductivity and p-H are detected, before exiting through the FPLC outlet valve and finally the feed tank. As the system is operating in diafiltration mode, fresh buffer is continuously added by hand to the feed tank (as 5 ml of permeate are collected, 5 ml of buffer are added). The process is carried out at constant pressure (1.5 bar) through FPLC software Unicorn™ that allows to set a "Pressure-controlled" flow mode. It is a feedback tuning instruction that can be used when running the system pump in manual mode. It allows to set a pressure set point and a minimum allowed flowrate. This choice is motivated by the need to keep gentle conditions during the operation, to preserve vesicle's integrity that could otherwise be compromised by higher pressures. Unicorn™ software also allows on-line monitoring of retentate-side parameters as p-H, conductivity, pump flowrate, temperature, pressure, UV-signal at different wavelengths (260 nm, 280 nm).

5.2.5 Curcumin encapsulation

Curcumin is chosen as *model drug* to test encapsulation into lemon EVs through passive cargo loading techniques. It is a very powerful and beneficial compound to human health, although curcumin low

bioavailability and poor solubility strongly limits its use in many applications. Curcumin has a relatively low water solubility (under neutral or acidic conditions), but it can be directly dissolved in oils and some organic solvents due to its lipophilic nature. Some common organic solvents often used to solubilize curcumin prior to encapsulation are ethanol, methanol and acetone. Curcumin loading is achieved when the organic solvent – curcumin – EVs mixture comes in contact with water and curcumin loaded particles are spontaneously formed due to curcumin hydrophobic nature.

Encapsulation of curcumin is carried out on different EVs preparations:

- <u>SAMPLE A</u>: EVs isolated by membrane techniques and purified by TFF diafiltration. The retentate collected after 3 diavolumes is used.
- <u>SAMPLE B</u>: EVs isolated by differential ultracentrifugation method (method 1).
- <u>SAMPLE C</u>: EVs isolated by SEC. Injection of 2 ml of the permeate of the 3µm filtration in the SEC-FPLC column with Sepharose CB-2L stationary phase. The peak with retention volume between 36 and 50 ml is collected.

By using a series of blank sampling, encapsulation is monitored as lost free-curcumin in solution. A UV-visible spectrophotometer allows the detection of the amount of curcumin uptaken, as difference in absorbance. The spectrophotometric readings are performed at 425 nm, peak of the curcumin UV-Vis absorption spectra, using a Shimadzu UV-1601PC UV-Visible Scanning Spectrophotometer. The chosen organic solvent is methanol.

Curcumin stock solution and calibration curve

A 150 µg/ml stock solution of curcumin in methanol is obtained and stored at 4°C in amber glassware to avoid curcumin photodegradation. Standard solutions are prepared by serial dilution of the stock solution with PBS in order to obtain a concentration range between 5–150 µg/ml and build a calibration curve. Absorbance is measured at 425 nm and a standard calibration curve is obtained by plotting the absorbance over the concentration of standard curcumin solutions and interpolating the experimental points.

Determination of Stability of Free Curcumin and loaded Curcumin

To estimate and compare the stability of free curcumin and loaded curcumin, degradation curves over time are built. To this purpose, solutions of identical concentrations of curcumin in PBS and EVs-loaded curcumin are prepared and incubated in the dark at 37 °C water bath. At regular time intervals (30, 60, 90, 120, 130 minutes) samples are collected and absorbance is measured at a wavelength of 425 nm. The fold reduction of the curcumin concentration at each time point was compared to the beginning.

Loading of curcumin on lemon EVs

Equal amounts of curcumin stock solution are added to the EVs preparations (samples A, B, C). The final concentration of curcumin in each sample is 14 µg/ml. The preparations are centrifuged at 10 000 x g for 20 minutes to favor encapsulation and pellet unbound curcumin. The supernatant is stored in a light resistant container at 4°C and incubated overnight. The day after the preparations are subjected to another centrifugation run and analyzed through a spectrophotometric analysis at 425 nm. The curcumin concentration is determined using the curcumin calibration curve. A system of blanks is

prepared to this purpose. The loading efficiency (%) of curcumin in the Cur-EVs preparations is estimated through a simple mass balance over curcumin:

$$Loading\ efficiency\ \% = \left(\frac{Amount\ of\ encapsulated\ curcumin}{Total\ amount\ of\ curcumin\ added}\right) * 100 \qquad (11)$$

5.2.6 Size exclusion chromatography (SEC)

Size exclusion chromatography is a common technique used for biomolecules separation based on the differential distribution of the components in a sample between a mobile and a stationary phase. Specifically, in SEC, the component's fractionation depends on the size and shape of the components. The stationary phase is comprised of porous beads packed into a column while the mobile phase is a buffer running through the column. Sample components partition between the stationary and mobile phases based on their size-based accessibility to the pores of the stationary phase. Small particles, such as proteins, with small hydrodynamic radii, can enter the pores to various degrees, thus resulting in late elution. Components with large hydrodynamic radii, including EVs, are excluded from entering the pores, travel quicker along the column and so are eluted first. The access to the pores is limited only by steric hindrance (Figure 51).
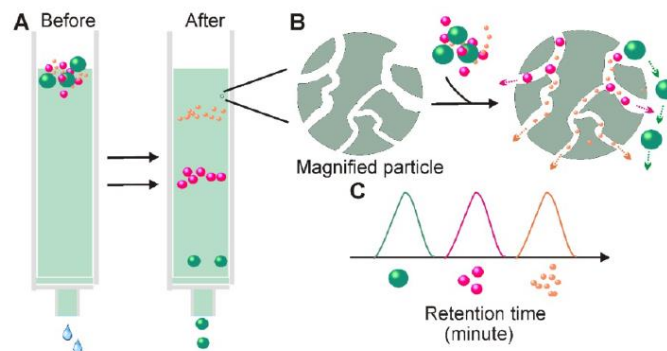
Figure 51: Principle for Size-exclusion chromatography-based exosome isolation. [8]

The separated components are visualized as peaks in a chromatogram, a plot of the volume of the mobile phase eluted through the column versus the detector signal. Each identified peak is relative to a certain substance, eluted at a certain time. From the analysis of the chromatogram is possible to obtain:
- The retention time of a certain compound, correspondent to the peak symmetry axis, that is the time required to the component to flow through the column;
- The height of the peak, proportional to the concentration of the compound in the sample;
- The area of the peak, proportional to the amount of substance separated.

The final resolution, the degree of separation between peaks, is influenced by many factors (Table 13):

Table 13: Factors affecting SEC resolution, the degree of separation between peaks.[9]

Medium-related factors	-	Particle size
	-	Particle uniformity
	-	Match between pore size and analyte size

Column-related factors	-	Bed height
	-	Column packing quality
Experimental-related factors	-	Flow rate
	-	Sample volume: column volume
	-	Viscosity of the mobile phase

Resolution is a function of the medium selectivity, i.e. the medium pore size distribution. After selection of SEC medium, sample volume and column dimensions are the two most critical parameters that will affect the resolution of the separation.

The separation efficiency depends on the volume of the analyzed sample: it should not exceed 1/20 to 1/15 of the column volume [9]. Smaller sample volumes help to avoid overlap if closely spaced peaks are eluted.

The height of the packed bed affects both resolution and the time taken for elution. The resolution in SEC increases with the square root of bed height. Doubling the bed height gives an increase in resolution equivalent to √2 = 1.4 (40%).

Also, the flow rate plays a role. Optimal column efficiency is found at lower linear velocities, hence decreasing the flow rate leads to a higher quality SEC fractionation. Finally, packing quality is another crucial parameter: the goal is to achieve a homogeneous pore size distribution across the column.

5.2.6.1 ÄKTA purifier-100 FPLC system

SEC is used both as analytical and preparative technique for lemon EVs, in a Fast Protein Liquid Chromatography (FPLC) system. The used FPLC system is ÄKTA FPLC purifier-100 by GE Healthcare (now Cytiva). It is a fully automated liquid chromatography system designed for research and lab scale applications. It allows flow rates up to 100 ml/min and pressures up to 5 MPa. The system consists of a compact separation unit that includes different modules and components and a computer running UNICORN^{TM} software to control the separation units. The main unit is composed by three superimposed modules (Figure 52):

- System of pumps P-900, high performance rotary piston pumps that can reach a maximum pressure of 100 bar and a maximum flowrate of 100 ml/min. The pumps are equipped with 2 pump modules, A and B.
- Monitor UV-900, a high precision on-line monitor for measuring UV absorption at multiple wavelengths covering an interval from 190 to 700 nm.
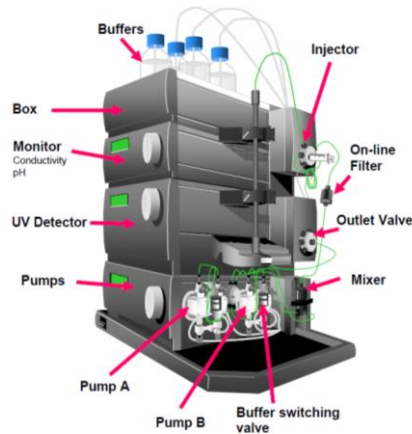- Monitor p-H/C-900, on-line combined monitor for measuring conductivity and p-H.

Figure 52: FPLC system AKTA purifier with the main three modules, pumps P-900, Monitor UV-900 and Monitor pH/C-900 [10].

Besides the modules there are other accessories like a mixer, the gradient proportionating valve for buffer switching, the injection valve, the outlet valve, on-line filter and the chromatographic column. The flow path between the different modules and components is shown in Figure 53.
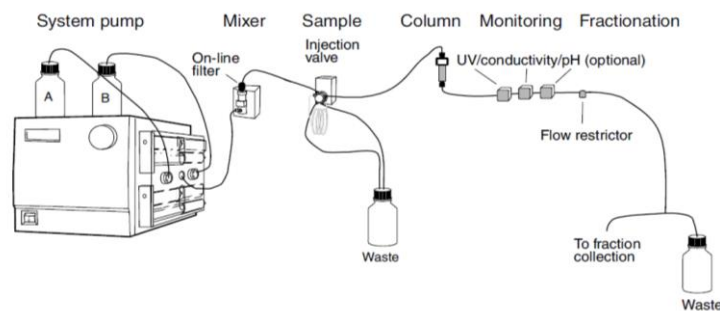

Figure 53: Flowpath through the FPLC system Akta purifier.[10]

The pump system has two pump modules, A and B. Each pump module has two pump heads in titanium allow, they are identical but actuated in opposite phase to each other giving a continuous flow with minimal pulsations. Each pump has an inlet check valve connected to a manifold from which the solvent is drawn up from the buffer tank (Figure 54). The outlet check valve houses a purge valve to allow purging of air or unwanted eluents and allows to pump the solution to the mixer. The pump's pistons are actuated by eccentric cams driven by stepper motors; a return coil springs provide for their retroaction. Leakage between the pump chamber and the drive mechanism is prevented by a piston seal. The pistons and seals are continuously lubricated by a dedicated line of 0.4% V/V acetone in water solution that flows in a closed circuit into the system.
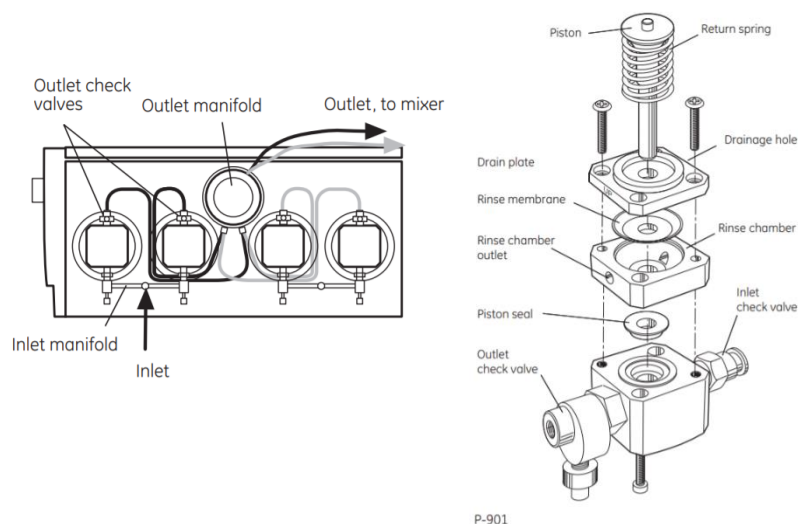
Figure 54: Pump P-900 system (left) and exploded scheme of a single P-901 pump (right) [10].

After the pumps, the flow path continues from the mixer to the injection valve, usually connected to a sample loop that allows manual injection of the sample through a syringe. Sample loops are used for low injection volumes (0-2 ml) while superloops can be used for application of large sample volumes (1-150 ml).

The injection valve can assume three different positions (Figure 55). When the valve is in Load position, the solvent that is coming from the pump is fed to the column. When the valve in is Inject position, the sample that is charged into the sample loop (connected to the ports 2-6 of the injection valve) is sent to the column through the solvent flux. Finally, if the valve is in Waste position the column is excluded from the circuit and the solvent coming from the pumps is sent directly to waste.
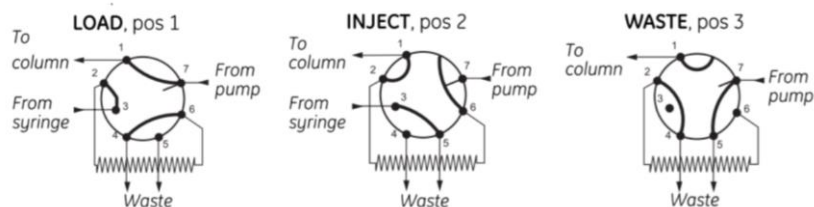
Figure 55: Injection valve positions: Load (left), Inject (center) and Waste (right) positions [10]

From the injection valve the flow is directed to the column and then to the UV flow cell, Conductivity flow cell and p-H flow cell. Finally, the flow path continues to the fraction collection lines or to the waste tank.

5.2.6.2 Chromatographic column packing with Sepharose CB-2L resin

The Econo-Column® by BioRad is used as chromatographic column. It has a volume equal to 132 ml and dimensions of 75 x 1.5 cm. The column is manually packed with Sepharose™ CL-2B resin by GE Healthcare. It is formed by cross-linked agarose beads resistant to organic solvents. The gel characteristics are reported in Table 14.

Table 14: Sepharose CL-2B specifications [11]

	Sepharose CL-2B
% Agarose	2
MW separation range	70-4000 kDa
Bead size range	60-200 µm
Recommended linear flow rate	0.4 mL/min
p-H stability (short term)	2-14
p-H stability (long term)	3-13
Chemical stability	High, also in organic solvents

Sepharose resin is supplied pre-swollen in 20% ethanol. The gel is prepared by mixing 75% of Sepharose resin and 25% of PBS 0.1M (p-H=7.4). The obtained gel slurry is degassed through mechanical stirring in a vacuum flask. Packing procedure is performed manually by pouring the gel slurry in the column in a single operation and opening the column outlet valve in such a way that the packing flowrate stays below 30 cm/h, that is the recommended flowrate for the operation. Eluent buffer is added to the top of the column when necessary to completely cover the gel slurry during sedimentation.

Once the packing procedure is concluded the column is connected to the FPLC system.
- Bed height = 69 cm
- Bed volume = 122 ml

The recommended sample volume to be injected is 2-5% of the total bed volume, therefore a 2ml sample loop is used. The lower part is connected through simple piping connections while the upper part is connected through the Econo-Column flow adaptor by BioRad that has the goal to eliminate the liquid head space above the gel bed, prevent air contact and resin disruption by upcoming the flow.

A packing efficiency test is performed injecting 2ml of a 2% (v/v) solution of acetone in filtered demi water, at the recommended flowrate of 0.4 ml/min. From resulting the chromatogram (Figure 56), obtained detecting the UV signal at 260 and 280 nm, packing performances are tested calculating the number of theoretical plates N and the asymmetry factor A_s through the following formula:

$$\frac{N}{m} = 5.54 \cdot \left(\frac{V_R}{W_h}\right)^2 \cdot \frac{1000}{L} \qquad (12)$$

$$A_s = \frac{b}{a} \qquad (13)$$

Where V_R is the retention volume, W_h is the width at half height, L is the bed height and the parameters a and b are widths calculated at a height equal to 10% of the total peak height.
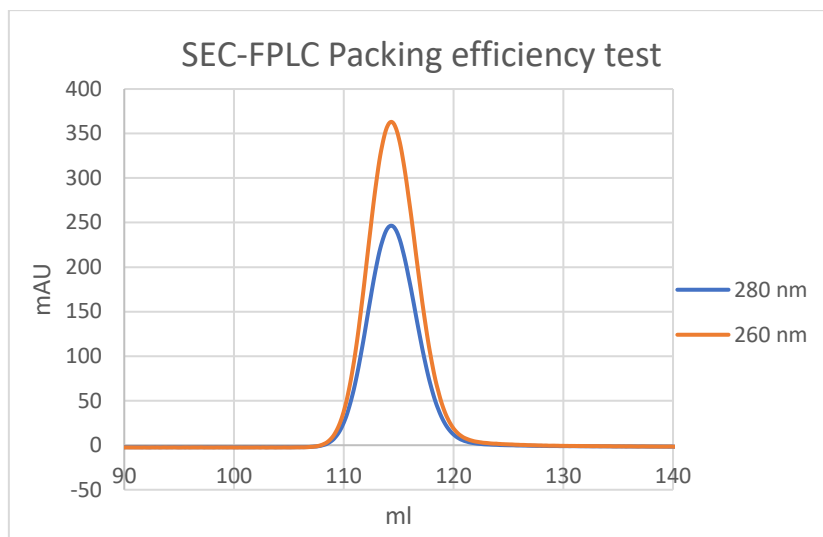
Figure 56: SEC-FPLC chromatogram of the Packing efficiency test with Acetone.

The results of the test are summarized in Table 15.

Table 15: Results of the packing efficiency test with acetone at 260 nm

Acetone test -260 nm		
L (bed height)	0,69	m
V_R (Retention volume)	114,3	ml
Peak height	363,1	mAu
Peak width	19,2	ml
W_h (width at half height)	5,1	ml
Area	1968,4	mAu*ml
a	109,95	
b	119,25	
A_s (asymmetry factor)	1,14	0,7 < 1,14 < 1,3
N/m (plate number)	4080724	>3000

The obtained theoretical plate number and asymmetry factor are in accordance with the ranges of optimal values given by the provider, so column packing appear to be efficient.

5.2.6.3 HPLC system Water separation module 2695

Gel filtration is also performed as analytical technique in a *High Pressure Liquid Chromatography* (HPLC) system as Water Alliance separation module 2695. The separation module is associated with an UV detector Waters 2487 Dual λ Absorbance (Figure 57) and the dedicated software Empower.

Figure 57: Water Alliance 2695 HPLC system [12]

It is an integrated solvent and sample management platforms. The solvent management system mix and deliver solvents from the reservoir bottles to the sample management system through a controlled flow path (Figure 58).

- The in-line vacuum degasser degasses the solvent.
- The gradient proportionating valve (GPV) blend the solvents allowing to obtain the desired input composition.
- The solvent flow through two check valves that allow optimal flow control.
- The system uses a low-pressure mixing binary pump with two pistons in series. The primary piston, in the primary piston chamber, provides the flow to fill up the accumulator piston chamber. The second piston delivers the solvent under pressure to the system pressure transducer that measures the operating pressure.
- The solvent flows from the system pressure transducer outlet to the prime/vent valve and into an in-line filter.
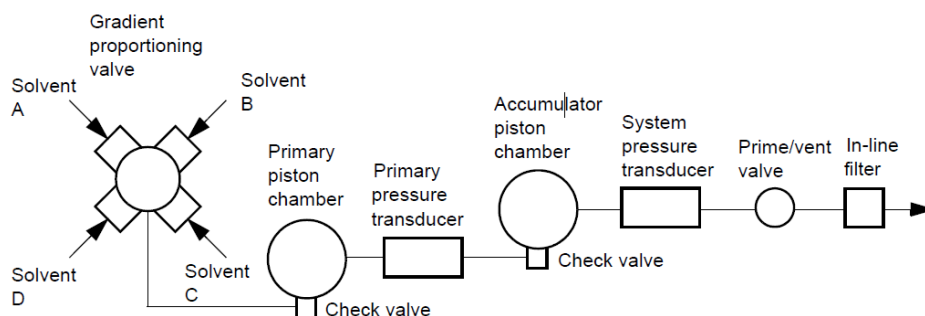
Figure 58: Flow path through the solvent management system[12]

The sample management system holds and positions the sample vials through five carousels (24 vials per carousel), inject the samples in the solvent flow through a needle. Four valves in the sample management system control the flow of solvent, sample, and needle wash solvent (V1, V2, V3, V4 in Figure 59).
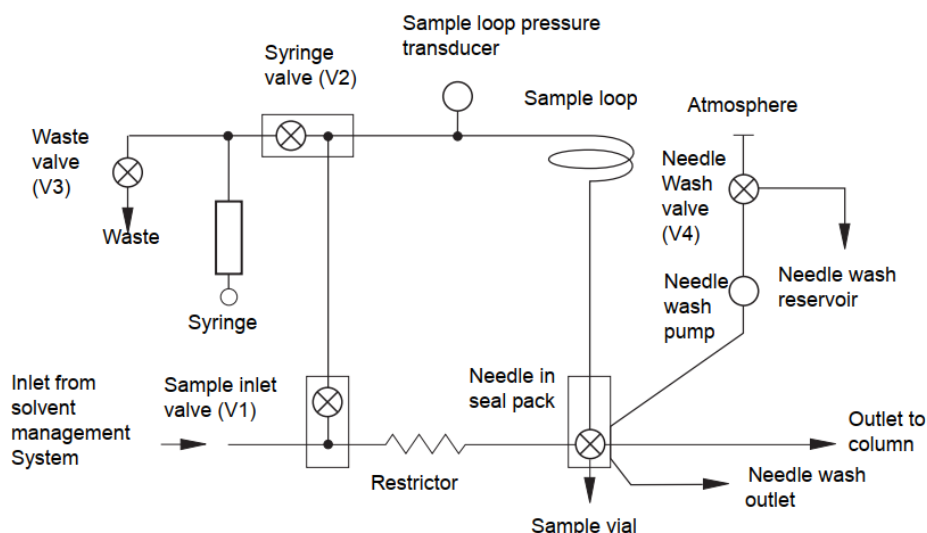
Figure 59: Flow path through the sample management system.[12]

The valve's configuration depends on the function being performed:

- In normal flow V1 is open and 95% of solvent flows through V2, the sample loop, the needle and out to the column; 5% of the solvent flows through the restrictor, the seal pack and out to the column.
- Injection is performed in three steps:
  - Isolation of the loop: V1, V2, V3 close, needle wash on, V4 opens and needle moves into the bottom seal.
  - Sample withdrawal: V3 closes, needle wash off, V4 closes, needle moves into the vial and withdraw the sample.
  - Sample injection: V3 opens, V2 closes, needle moves into the stream, V1 opens, sample is injected, syringe moves back and V3 closes.

5.2.6.4 SEC-Yarra 2000 column

HPLC system is coupled with the size exclusion column Yarra-2000 by Phenomenex®. The column has dimensions of 150 x 7.8 cm and it is pre-packed with 3 μm silica beads.

Table 16: : Yarra SEC-2000 column specifications [13]

	Yarra SEC-2000
Paricle size	3 μm
Pore size	145 Å
MW range (native)	1-300 kDa
p-H stability	2,5-7,5
Maximum backpressure	3000 psi
Maximum temperature	50°C
Maximum flowrate	1,5 ml/min
Efficiency (minimum theoretical plates)	48000

Assuming that the retention mechanism is entirely based on the Stokes radii, i.e. on the hydrodynamic size of the molecule, it is possible to relate the retention time of a compound to its molecular weight.

In particular, it has been shown that the retention time of an analyte is directly proportional to the logarithm of the molecular mass, for molecules that are neither completely excluded from the pores nor molecules that can penetrate all of them.

$$\log(MW) = mK_d + b \quad (14)$$

Where m and b are the slope and the intercept of the calibration line, and K_d is the retention factor, given by the following expression:

$$K_D = \frac{V_R - V_0}{V_{tot} - V_0} \quad (15)$$

Where:

- V_R is the retention volume of the analyte;
- V_0 is the retention volume of the column;
- V_{tot} is the total solvent volume of the column (pores volume + interstitial volume).

In SEC, the first peak to elute is that of compounds that are too large to enter any of the pores; these analytes this will be in the same retention volume V_0 as the interstitial space between beads, also called the column *exclusion limit*. Small molecules will elute at the end in a *permeation limit*, representing the total volume of solvent in both the interstitial space and the particle pores V_{tot}. Therefore, the term V_R represents the elution volume of analytes that partially interact with the resin. It allows to determine the molecular mass of unknowns through comparison of retention times of known standards, by running a calibration.

Calibration is run equilibrating the column at 1 ml/min for at least 30 minutes with PBS, chosen as mobile phase eluent. The standards used are immunoglobuline G (IgG), bovine serum albumin (BSA), horse skeletal muscle myoglobine (Myo) and tyrosine (Tyr). The analysis is carried out isocratically at 1 ml/min with a sample volume injection of 25 μm with duplicates (2 injections per sample). The resulting chromatogram is shown in Figure 61 and the standards retention times and molecular weight are reported in Table 17.
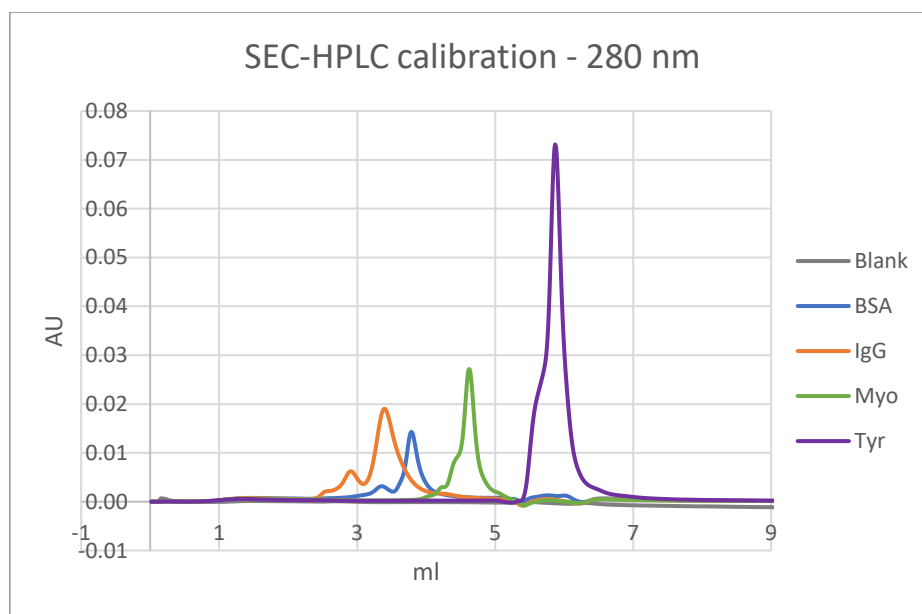

Figure 60: HPLC-SEC chromatogram obtained injecting proteins of a known MW at a certain known concentration.

Table 17: Protein standards molecular weights and retention times.

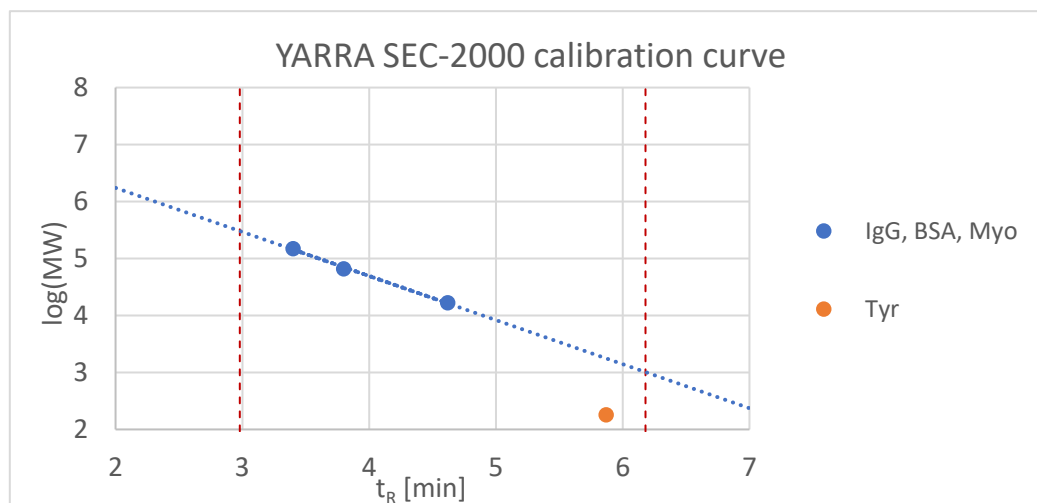|	MW	log$_{10}$(MW)	t$_R$
	Da	Da	min
IgG	150000	5.176	3.40
BSA	66000	4.819	3.80
Myo	16700	4.223	4.62
Tyr	181	2.258	5.87

Figure 61: Yarra SEC-2000 calibration curve with the column exclusion limits.

Plotting the log of the molecular weight over the protein retention time is possible to observe (Figure 62) that the points relative to IgG, BSA and Myo perfectly lie onto a straight line, whose equation is y = -0.7735x + 7.787 (R² = 0.9973) (Figure 61). The calibration curve provides an upper and lower MW limit that the column is able to separate, where a sharp deviation from linearity is observed. The phenomena is observed for Tyrosine, a very small protein (MW=1.81 kDa) shows a retention volume of 5.9 ml. The value is assumed as permeation limit for Yarra SEC-2000 column. The YARRA-SEC vendors declare a MW range for optimal separation (in native conditions) between 1 – 300 kDa. Through the equation of the calibration line, it is found that the MWs corresponds to an inclusion range between 3 ml and 6.2 ml. Due to Tyrosine behavior at 5.9 ml, the column shows a slightly narrower inclusion limit than the one declared. The phenomena may be ascribed to the potential unwanted interactions of very small analytes with the stationary phase, as well as column wear and cleaning necessities.

5.2.8 Dynamic light scattering and zeta potential measurements

Dynamic light scattering (DLS)

Dynamic Light Scattering is a technique that can be used to determine the size and size distribution profile of molecules and sub-micrometric particles in solution. DLS is based on the Brownian motion of dispersed particles. When particles are dispersed in a liquid they move randomly in all directions and are constantly colliding with solvent molecules. The Brownian motion causes laser light to be scattered at different intensities. At same viscosity and temperature, smaller particles move at higher speeds than larger particles, creating variations of the light scattering intensity. Analysis of these intensity

fluctuations yields the velocity of the Brownian motion and hence the particle size using the Stokes-Einstein relationship (equation 16).

$$\mathcal{D} = \frac{k_B T}{6\pi\eta R_H} \qquad (16)$$

Where:

- $\mathcal{D}$ particles diffusion coefficient [m^2/s], that provides the speed of the particles;
- k_B Boltzmann constant [m^{2}kg/Ks^2];
- T temperature;
- η viscosity [Pa s];
- R_H hydrodynamic radius [m];

The basic setup of a DLS instrument is shown in Figure 63.
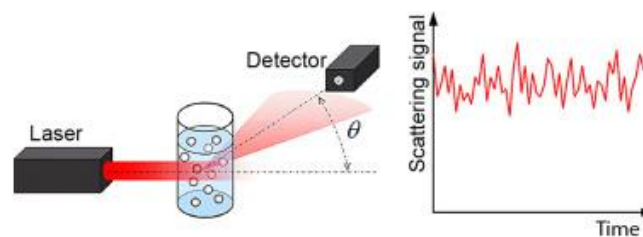
Figure 62: Schematic setup of a DLS measurement system. [14]

A single frequency laser is directed to the sample contained in a cuvette. As particles move in the sample, the incident laser light gets scattered in all directions. The scattered light is detected at a certain angle over time and this signal is used to determine the diffusion coefficient and the particle size by the Stokes-Einstein equation. It is noteworthy that DLS does not measure individual particles, and hence it is suitable for detecting monodispersed particles and is less exact in characterizing vesicles of heterogeneous size distributions.

Zeta potential

The majority of particles dispersed in buffer solutions possess a superficial charge that is different to that of the bulk solution. When a charged particle is dispersed, an external double layer (EDL) develops on its surface. The inner layer, called Stern layer, consists predominantly of ions with opposite charge to that of the particle. The external layer, called diffusive layer, is made by less firmly associated ions enclosed by the slipping plane (outer boundary of the EDL). The ZP is the potential at the slipping plane of a particle moving under an electric field. The ZP reflects the potential difference between the electric double layer of mobile particles under an electric field, and the layer of solvent ions around them at the slipping plane. Thus, it is mainly used to predict the stability of dispersion: high values of ZP values (-30eV < ZP < +30eV) mean that, due to the EDL presence, particles are far from each other and they hardly aggregate or flocculate.

By using the same principle of light scattering intensity variations, it is possible to measure the particle's zeta potential (ZP). During electrophoresis, the mobile particles scatter an incident laser. As the particles are mobile the scattered light has different frequency than the original laser and the frequency shift is proportional to the speed of the particles.

Nano Zetasizer® instrument

The instruments used is the Nano Zetasizer® Nano ZS by Malvern. It allows to perform both DLS and ZP measurements. The size range is from 0.3nm to 10µmm while the size range for ZP measurement is 3.8nm to 100µm. It is associated with an He-Ne laser (5mW, 633 nm) that lights up the EVs purified from lemon juice, introduced in a 1 cm polystyrene cuvette. The instrument is controlled by a dedicated software Zetasizer 7.12. It allows to set the desired analysis parameters and a preliminary equilibration phase, in order to monitor and keep constant temperature (25°C). In order to carry out z potential measurements, the EVs preparations are poured in gold cuvettes with gold electrodes, that allow to generate an electric field in the solution.

5.2.9 Total protein quantification

The bicinchoninic acid (BCA) assay is a colorimetric method for total protein quantification for pure protein solutions. It is a destructive method that exploit 4,4'-Dicarboxy-2,2'-biquinoline, also called bicinchoninic acid (Figure 64), that allow to reveal and quantify the total proteins present in a sample.
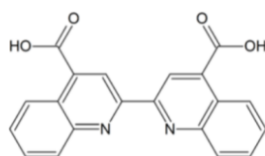
Figure 63: Bicinchoninic acid

The BCA reagent is obtained by mixing in 50:1 ratio respectively:

- Reagent A: colorless alkaline (p-H=12.5) solution containing disodic salt of BCA, sodium carbonate monohydrate, sodium tartrate, sodium hydroxide and sodium bicarbonate.
- Reagent B: light blue solution containing copper sulfate pentahydrate.

Reagent A is mixed with reagent B to allow the formation of the BCA-Cu^{2+} complex, very reactive in presence of the protein. The so-formed complex should confer to the obtained solution (BCA reagent) an apple green colour. The final mixing of the BCA reagent with the protein solution led to the formation of the final purple-coloured complex, through the following two steps reaction (Figure 65).
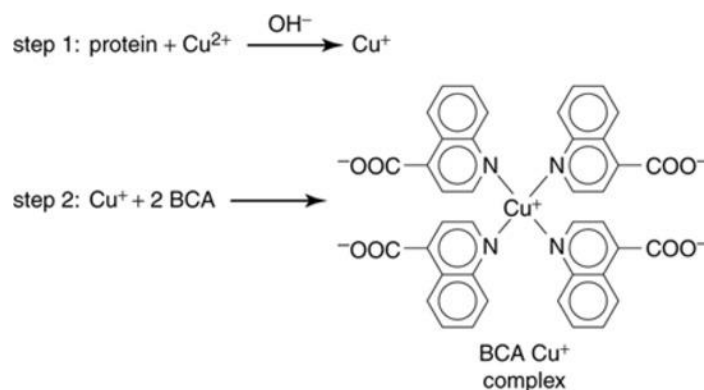

Figure 64: Scheme of the reaction of the BCA assay

It is based on the Biuret reaction which involves the chelation of the cuprous ion Cu^{2+} with the peptide backbone under alkaline conditions. The product of this reaction is a cupric ion Cu^+ that is coordinated to peptide nitrogen atoms. The BCA reagent, then reacts with these cupric ions in a 2:1 ratio, yielding a colorful blue-violet complex that absorbs light at 540 nm.

The reaction is dependent on three factors:

- *pH*: it should be equal to 11.25 to guarantee the formation of the BCA-Cu^{2+} complex, reactive to proteins.
- *Amino acids*: the types and quantities of aminoacidic residues influence the reactivity with the BCA reagent; in particular, cysteine, tryptophane and tyrosine give high values of the absorbance at 562 nm, while bi-, tri- and tetrapeptides that do not contain these residues give lower absorbance values.
- *Temperature*: the first step of the reaction is T-dependent. Greater values of absorbance are detected at 60°C but working at this high T led to a reduction of the linearity range between protein concentration and absorbance.

The standard BCA assay protocol is valid for 20-2000 µg/mL protein concentration range [15].

- 2 ml BCA reagent (40 µl B + 1,96 ml A);
- 100 µl protein solution;
- T = 37 °C for 30 minutes.

In the BCA assay protocol for low concentration samples (5-20 µg/mL) the incubation is carried out at T = 60°C for 30 minutes. After the preparation and the incubation of the BCA solution with the protein solution, spectrophotometric readings at 562 nm are performed, using water as blank solution.

Before handling the protein solution, a calibration curve is built applying the assay to solutions of known protein at a known concentration, as bovine serum albumin.

Results and discussion

The aim of the experimental work carried out in the present project is the development of an optimized membrane-based protocol for the isolation and purification of extracellular vesicles from lemon juice. To this purpose, the leading strategy is the optimization of the most relevant parameters, for both clarification and purification stages. The first part of the work is based on the individuation of the optimal *dimensional cuts* to be achieved to isolate lemon EVs through microfiltration and ultrafiltration separations. Thus, membranes having different pore size/cut offs are tested. Likewise, membranes of different materials are used, in an effort to identify the best performing material for the application. Moreover, a comparison over different lemon's sources and clarification strategies is also performed. After the optimization of the upstream conditions, the attention is focused on EVs purification through a diafiltration process. Two main approaches are evaluated: batch diafiltration in *dead-end* mode and constant volume diafiltration in *cross-flow* mode. Different runs are analyzed and compared by means of gel filtration carried out in FPLC and HPLC systems. The two key factors taken into consideration are the yield in EVs and the efficacy of the purification process in terms of removal of impurities.

An enhanced protocol for diafiltration in tangential-flow filtration (TFF) mode is proposed. It is based on the optimization of the filtration operative conditions as well as addressing of the main obstacle associated with filtration processes, being the formation of a cake/gel over the filtration surface that brings to loss of vesicles and their aggregation.

Successively, the obtained EV preparations are characterized by means of dynamic light scattering (DLS) and z-potential measurements, as well as total protein quantification through BCA assay.

Finally, preliminary passive cargo loading experiments are carried out using different EVs preparations. Curcumin is used as model hydrophobic drug for the encapsulation. The efficiency of the process is assessed through spectrophotometric readings at 425 nm using a proper blank system.

6.1 Selection of the diafiltration membrane

The membrane for the EV diafiltration process, the core purification step of the protocol, is selected testing the performance of different membranes in dead-end mode stage diafiltration in Amicon® cell. The considered alternatives are:

A. MF membrane in regenerated cellulose (RC), average pore size 0,45 µm
B. UF membrane in polyvinylidene fluoride (PVDF), MWCO = 100 kDa
C. UF membrane in polyvinylidene fluoride (PVDF), MWCO = 250 kDa
D. UF membrane in polysulfone (PES), MWCO = 100 kDa
E. UF membrane in regenerated cellulose (RC), MWCO = 300 kDa

In order to ensure uniform testing conditions, the following preliminary protocol is applied:

- Lemon juice extraction
- Centrifugation at 5000 rpm for 40 minutes;
- 1:1 dilution with PBS buffer 0.1M (p-H=7.4);
- 3 µm dead-end filtration in Amicon® stirred cell, permeate is of interest;
- Stage diafiltration in Amicon® stirred cell;
  - ○ TMP = 1,5 bar

- o Stirring at 200 rpm
- o Dilution factor = 2
- o Initial volume = 80 ml of lemon juice + 80 ml of PBS
- o 5 stages
- Centrifugation at 10,000 rpm for 10 minutes;
- Analysis of feeds, permeates and retentates through SEC-FPLC and SEC-HPLC.

The set-up of the Amicon® stirred cell in both concentration and diafiltration mode is reported in paragraph *5.2.4.3*. For each run, the values of the permeate volume over time are collected, allowing to monitor the permeate volume and flux trend over time. The permeate flux is calculated from the active filtration area that in case of the Amicon® cell is equal to 28.7 cm^2.

The permeate volume and flux trend over time, relative to 0,45 µm RC stage diafiltration (A) are reported in Figure 66 and 67.
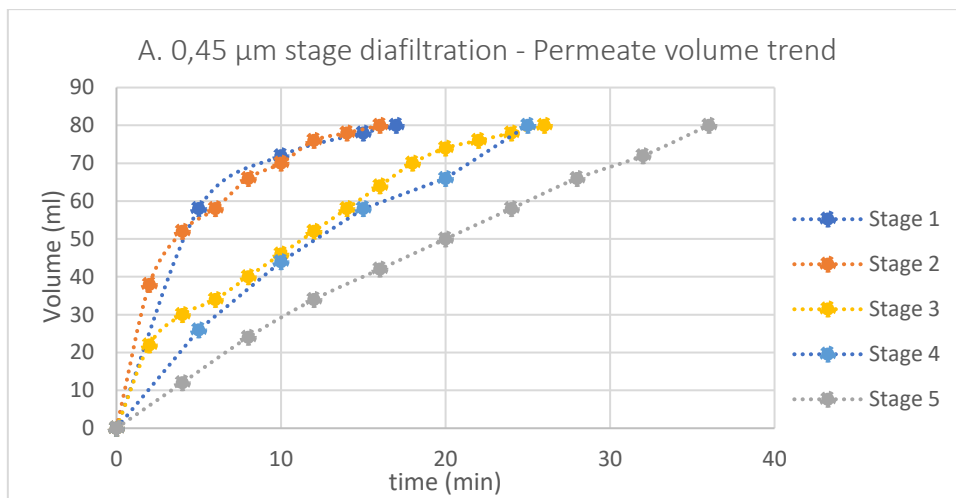
Figure 65: Volume of permeate over time for the 0,45 µm stage diafiltration process.

It is possible to see that the first two stages take approximately 17 minutes to end, while the fifth stage requires 36 minutes to be completed. The total time required to carry out the 5-stage diafiltration process with the 0,45 um membrane is 120 minutes.
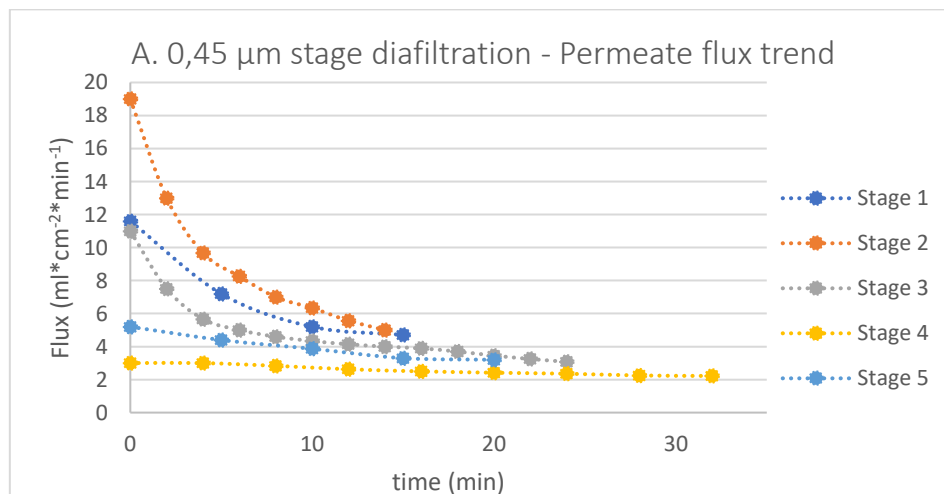
Figure 66: Permeate flux over time for the 0,45 µm stage diafiltration process.

In Figure 67 is possible to observe the permeate flux decline over filtration stages, as the membrane gets fouled and the process becomes slower.

Small amounts of retentate and permeate samples are collected at the end of each stage and analyzed by means of size-exclusion chromatography. SEC-HPLC analysis are carried out at 1 ml/min injecting 25 µm of sample to the Yarra SEC-2000 column. In Figure 68 is shown the SEC-HPLC chromatogram relative to A. 0,45 µm RC stage diafiltration. The curves relative to the retentate and permeate collected at the end of each of the five stages are shown in different colors.
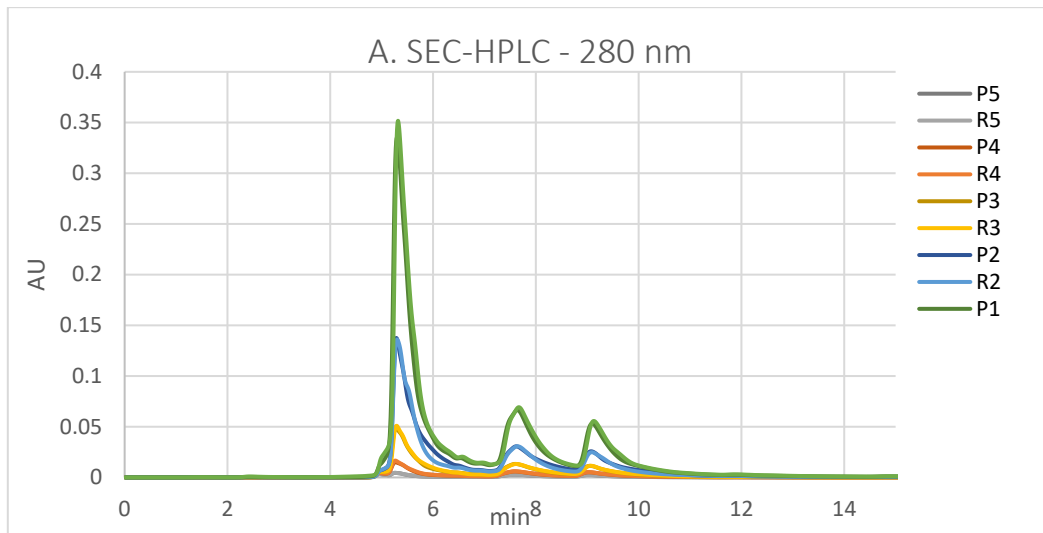
Figure 67: SEC-HPLC of permeates and retentates of stage diafiltration with 0.45 um RC membrane. UV signal detected at 260 nm.

It is possible to observe three peaks of compounds eluting after 5.4, 7.7 and 9.3 minutes, respectively. These peaks are associated to impurities present in the EVs preparations. It is possible to observe a consistent stage by stage decrease of these impurities, meaning that diafiltration process is efficient in contaminant removal. In Figure 69 the chromatogram is zoomed at short retention times.
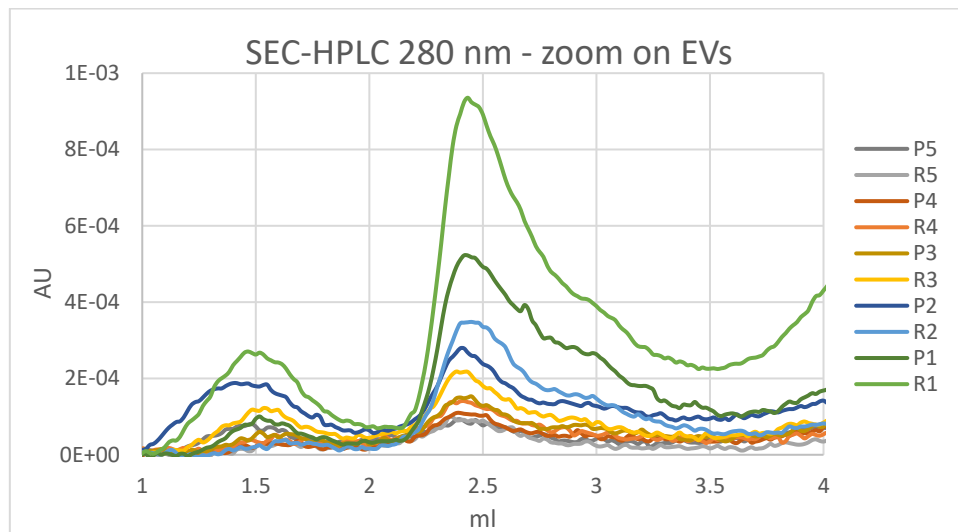

Figure 68: SEC-HPLC 0.45um RC stage diafiltration – zoom on EV peak

Two peaks are present, eluting at 1.5 and 2.4 ml. The higher peak eluting at 2.4 min is associated to EVs, while the one eluting after 1.5 min can be related to another vesicular fraction, the microvesicles.

The highest concentration of vesicles is found to be in the retentate of the first stage. As can be noted, the amount of vesicles in retentates and permeates is decreasing over stages, meaning that a consistent quantity is lost on the membrane as the cake/gel forms during filtration. Sample A is reported as model chromatogram while sample B, C and D chromatograms are reported in Appendix II.

The correspondence between the identified peak at 2.4 min and EVs was demonstrated in a previous work done on the subject [1]. By using the same chromatographic Yarra SEC-2000 column, the same peaks were identified at the same retention times and the presence of vesicles was confirmed by transmission electron microscopy (TEM). A TEM image of the EVs sample is shown in Figure 70.
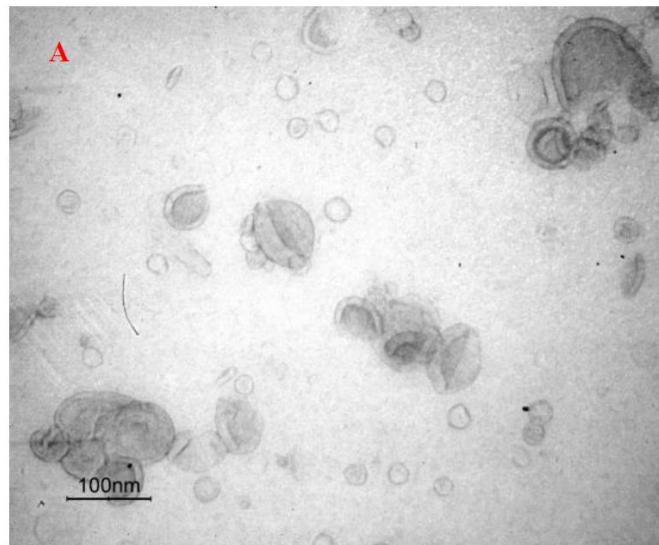
Figure 69: Lemon extracellular vesicles isolated through UF and MF processes observed with TEM microscopy. Image obtained through TEM ZEISS EM 19 with a 50,000X magnification [16].

As already discussed in paragraph *5.2.6.4,* the Yarra SEC-2000 inclusion limits ranges between 3 and 6 ml. Apparently, EV eluted at 2.4 ml are outside of the exclusion limit, the upper limit of molecular weight, beyond which molecules will elute at the same retention volume. Given that, the column seems to be able to fractionate above the range declared. For these reasons, SEC-HPLC analysis are usually supported by SEC-FPLC analysis carried out with Sepharose CL-2B resin as stationary phase.

SEC-FPLC analyses are carried out by injecting 2 ml of sample to the column with a flowrate of 0.4 ml/min. 0.1 M PBS is used as elution buffer. A model chromatogram of SEC-FPLC for the run C) stage diafiltration with 250 kDa PVDF membrane is reported in Figure 71.

For each sample, two peaks are detected by the 260 nm UV signal. The first peak is eluting between 35 and 55 ml and is associated to EVs. The second peak eluting between 100 and 140 ml is that of impurities. Through a magnification on short elution volumes EV peaks are visualized properly (Figure 71). In the chromatogram, the feed, permeate, retentate after two diafiltration stages are compared. In Figure 70 is possible to observe the relative decrease in contaminants concentration over the two stages, while in Figure 72 the fractionation of EVs in the different streams.
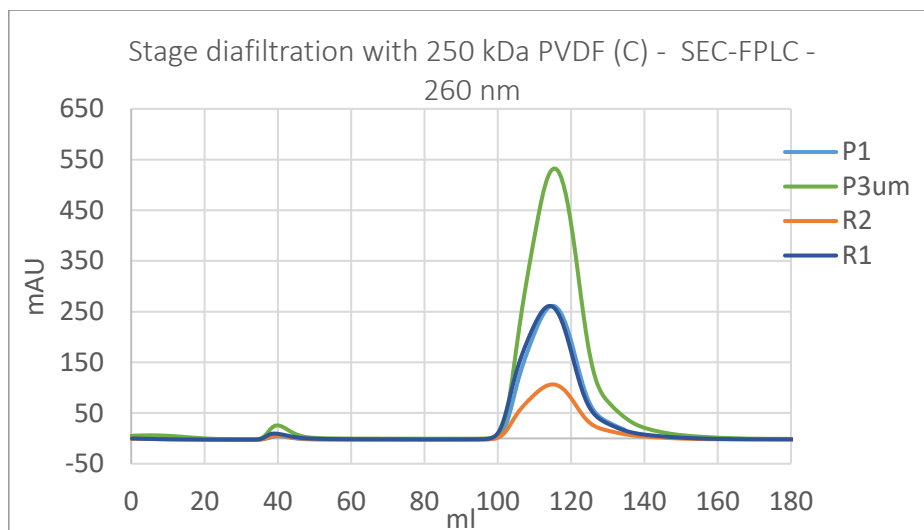
Figure 70: SEC-FPLC analysis of the feed, permeates and retentates obtained after the first diafiltration stage, using a 250kDa PVDF membrane. UV signal detected at 260 nm.
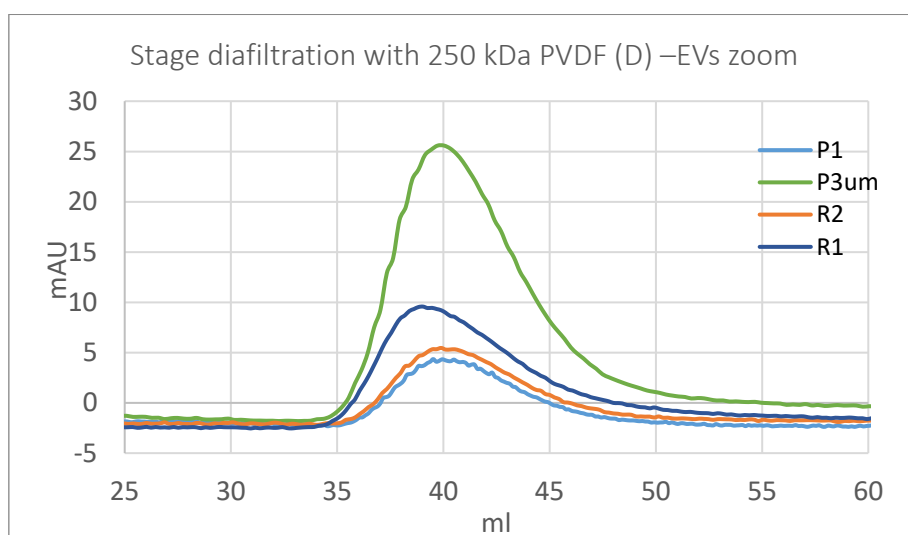

Figure 71: Zoom on EVs of SEC-FPLC analysis SEC-FPLC analysis of the feed, permeates and retentates obtained after the first diafiltration stage, using a 250kDa PVDF membrane.

The numerical integration of the peaks is performed either with FPLC Unicorn™ software or the trapezoidal rule and allows to obtain values of areas proportional to the mass of the eluted compound. The results obtained for the present chromatogram are reported in Table 18.

Table 18: Area of EV and impurities peaks obtained through numerical integration of the chromatographic curves at 260 nm.

	Area [$mAU*ml$]			
	P3µm (Feed)	R1	P1	R2
EVs	182.98	78.62	52.66	53.9
Impurities	9292.58	4575.96	4512.03	1920.41

The following quantities can be calculated:

- $\% \, Recovery = EVs \, in \, R/EVs \, in \, F$
- $\% \, Removal \, of \, impurities = Impurities \, in \, R/Impurities \, in \, F$

- $\% \, EVs \, lost \, in \, permeate = EVs \, in \, P/EVs \, in \, F$
- $\% \, EVs \, lost \, in \, cake = [EVs \, in \, F - (EVs \, in \, R + EVs \, in \, P)]/EVs \, in \, F$

Where the amount of EVs lost in the cake is obtained by simply closing the mass balance over the system. The results obtained are presented in Table 19.

Table 19: values of EVs recovery and removal of impurities over the two diafiltration stages calculated from the area of the relative peaks.

% EV recovery after 1st stage	43
% Total EV recovery after 2nd stage	29
% Removal impurities 1st stage	49
% EVs lost in permeate 1st stage	29
% EVs in the cake 1st stage	28

This procedure is repeated for each SEC-HPLC chromatogram obtained analysing samples collected after each diafiltration stage, employing different membranes. In this way is possible to make a comparison among the different runs employing different membranes, in terms of vesicles yield and impurities removal. The comparison is carried out through considering the membrane performance in the first stage of the process. Thus, the area of the peaks relative to EVs and impurities, for the feed (permeate of the 3µm filtration), retentate R1 and permeate P1 are calculated and reported in Appendix II.

The % EV recovery, EV lost in in permeate and cake and the removal of impurities are presented in Table 20 and visualized through a bar chart in Figure 73.

Table 20: % Recovery, % removal of impurities, % EVs lost in P and %EV lost in cake for A,B,C,D,E obtained from the areas of the chromatogram's peaks.

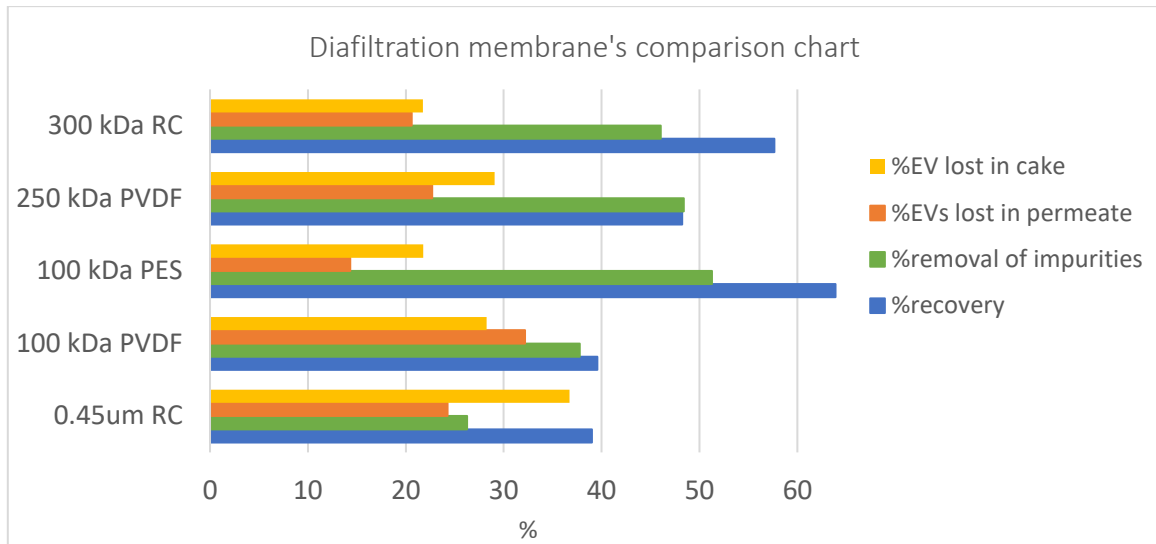| Membrane	% Recovery	% Impurities removal	%EVs lost in permeate	%EV lost in cake
A. 0.45um RC	39.0	26.3	24.3	36.7
B. 100 kDa PVDF	39.6	37.8	32.2	28.2
C. 250 kDa PVDF	48.2	48.4	22.7	29.1
D. 100 kDa PES	63.9	51.3	14.3	21.8
E. 300 kDa RC	57.6	46.0	20.6	21.8

Figure 72: Comparison of the performances of different membranes in stage diafiltration for the isolation of lemon EVs.

The 100 kDa PES is the best performing membrane. It has a % EVs recovery of almost 64% and guarantees the lowest EV losses in the permeate (14,3%). The 300 kDa RC membrane shows also a good recovery (58%) and a sufficient EVs rejection (EVs lost in permeate = 20.6%). The best performing membrane in terms of removal of impurities is the 0.45 μm membrane in RC. Both the PVDF membranes (100kDa and 250kDa) show mediocre performances in terms of % recovery (40 and 48%) and a notable loss of product (32 and 23%).

These results are confirmed by SEC-FPLC analysis of the first retentate of both C (250 kDa PVDF) and D (100 kDa PES) membranes (Figure 74 and 75).
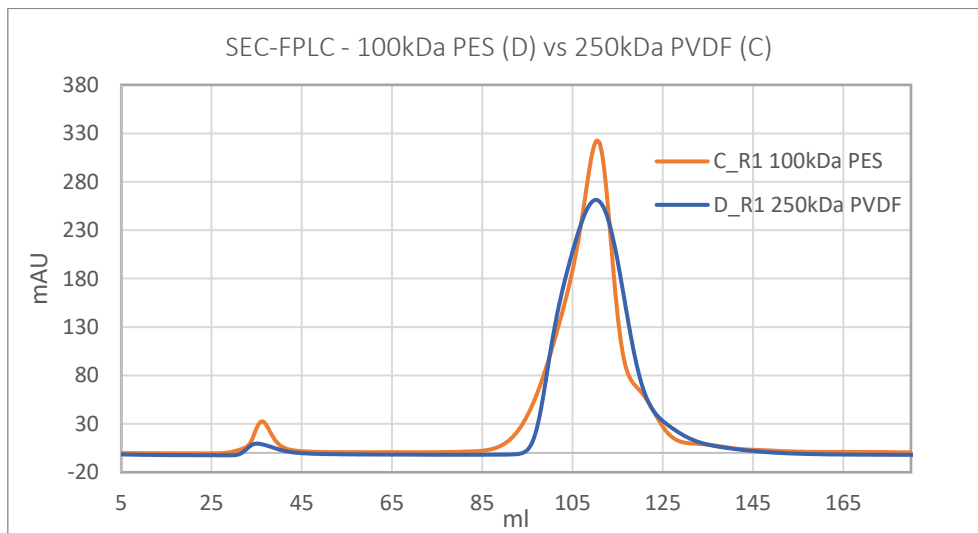
Figure 73: SEC-FPLC analyses on the first stage of the diafiltration process using both 100kDa PES (D) and 250kDa PVDF (C).
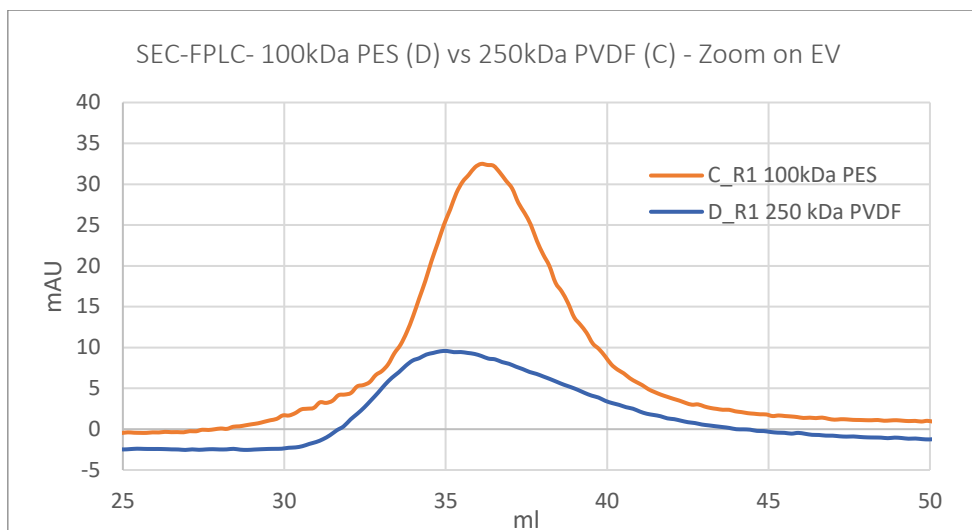
Figure 74: EV zoom of SEC-FPLC analyses on the first stage of the diafiltration process using both 100kDa PES (D) and 250kDa PVDF (C).

Table 21: Values of area obtained through numerical integration of SEC-FPLC EV and impurities peaks.

	EVs	Impurities
C) R1 100 kDa PES	191.7	4629.9
D) R1 250 kDa PES	78.62	4576

PVDF and PES polymeric membranes are both hydrophilic, and largely used in bioprocessing applications, due to their good mechanical and chemical properties, as strength and permeability (Figure 76). They are both declared as low protein binding membranes by the manufacturers.

A PES-PVDF comparative study in filtering viral suspensions by Moce and Livina [18] compared the filtration rate and volume that could be filtered before definitive fouling occurs. The authors demonstrated that PES allows for higher filtration rate and clogged more slowly. This result is confirmed in another study by Nakasone [19], where the performance of PVDF and PES membrane are compared also in terms of bacterial adhesion and migration under *Staphylococcus aureus* challenge. They confirmed that PES shows faster and more efficient filtration characteristics, although they are found to have more bacterial adherence and biofilm formation over the surface.
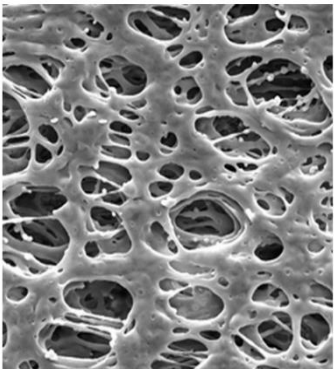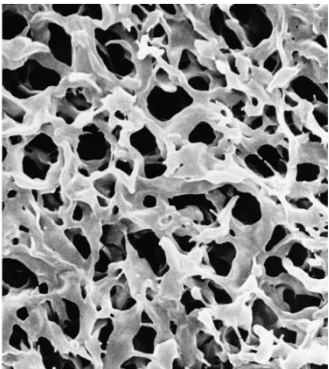
Express PLUS PES filter   Durapore PVDF filter   PVDF and PES comparison (Pearce 2007)

Parameter	PVDF	PES
Cost	Hi	Med
Ultrafiltration (UF) rating	Med	Hi
Permeability	Med	Hi
Caustic Resistance	Med	Hi
Chlorine Resistance	Hi	Med
Feed Range	Hi	Med
Fiber breaks	Nil-Lo	Med
Membrane Life	Hi	Med-Hi

It is also noteworthy that companies that invested into the development of EVs concentration methods commercialize filter units made with PES membrane (e.g. Vivaspin® centrifugal concentrators, ExoIP kit by Diagenode).

Overall, the evidences collected through the experimental work are in accordance with the studies in literature: PES membranes outperform PVDF membranes. The main parameter taken into consideration is the product lost in the permeate during diafiltration. In this respect, vesicles are found in the permeate of both PVDF and RC membrane, so they are discarded.

Concerning the membrane cut-off, typical dimensions of plant extracellular vesicles space between 50 – 200 nm. The relationship between the Stokes radius of a globular protein and its molecular weight is of the form $R_h \propto MW^{1/3}$. Consequently, is possible to estimate that:

- A globular protein of 100kDa has a minimum hydrodynamic radius of 4 nm;
- A globular protein of 500kDa has a minimum hydrodynamic radius of 7 nm;

Thus, an UF membrane having a cut-off of 500-600 kDa should guarantee total EVs rejection. These values are in agreement with values commonly used in EVs diafiltration processes. To conclude, being A, B, C, D, E the available membrane options tested, membrane (A) 100kDa PES is chosen as diafiltration membrane for the lemon EVs membrane-based isolation protocol.

6.2 Lemon's sources and feed comparison

Different feeds are compared in order to evaluate the influence of the lemon juice source and the juicing method on the clarification step. Three different sources have been tested:

- Lemons bought from different local markets (Bologna) are juiced through a juice extractor;
- Lemons bought from different local markets (Bologna) are juiced through a kitchen electrical juicer.
- Commercial lemon juice by the Italian company Achillea, made by 100% biological lemons from Sicily.

The lemon juice obtained from each source is diluted in PBS in a 1:1 ratio, centrifuged at 5000 rpm for 40 minutes and filtered through a 3 μm filter. The obtained supernatant is analyzed by means of FPLC - gel filtration. The chromatograms with the UV signal detected at 260 nm are compared in Figure 77.
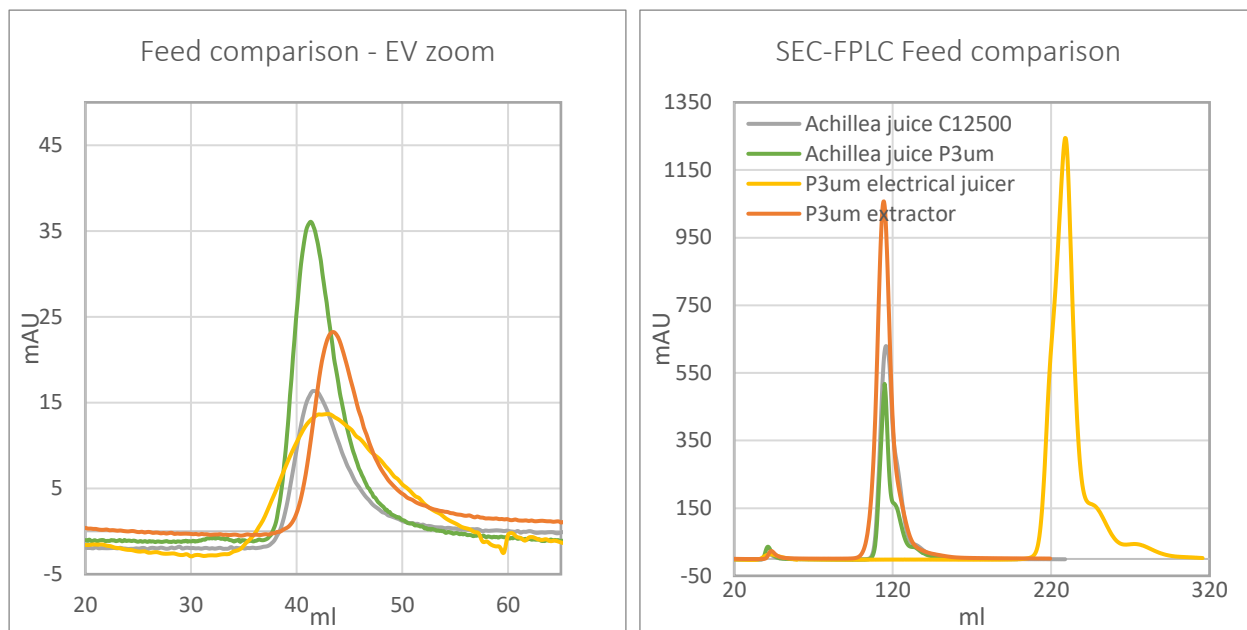
Figure 76: SEC-FPLC of different feeds used for the diafiltration process. On the left EV zoom, on the right the whole chromatogram with the impurities.

The EV peaks are integrated and the area values reported in Table 22.

Table 22: Feed comparison through SEC-FPLC analysis of the P3um obtained using different sources.

	EV Area (*ml*mAU*)
P3µm_extractor	158
P3µm_electrical juicer	450
P3µ_ Achillea juice	201
C12500_Achillea juice	127

It is possible to observe that the P3µm obtained squeezing lemons through the kitchen juicer (P3µm_electrical juicer) contains more impurities. A single impurities' peak is eluting only after 220 ml, at higher retention volumes compared to the other peaks. The electrical juicing method was tested with the idea that it could provide a more delicate squeezing method, helping to preserve vesicles integrity at this stage. Apparently, there is a repercussion on the EVs yield as the area of the peak of this sample is significantly higher than the others. The quantity of vesicles in the feed is more than doubled with respect to the sample processed with the extractor (P3µm_extractor). Since both samples are processed using the same lemons and same conditions, it is possible to conclude that the use of the extractor is detrimental on vesicles.

The P3µm obtained from Achillea juice (*P3µ_ Achillea juice)* is the purest preparation, with impurities eluting at the typical value of 120 ml present in a very low concentration with respect to the other samples. A good yield on vesicles is obtained, higher than that of *P3µm_extractor,* thus confirming the negative influence of the extractor.

It is decided to proceed with the experimental work with the use of the Achillea juice. First, because of the promising preliminary results obtained and, in second place, because it allows to have a homogeneous source of lemon juice, thus excluding from the process the variability associated with the use of different lemon batches.

After the selection of the lemon's source, another experiment is carried out aiming at understanding the influence of the preliminary *P3µm* on the process. An alternative clarification step is proposed in place of the *3µm* filtration: a centrifugation at 12,500 rpm for 30 minutes (*C12500_Achillea juice)*. The speed is the maximum achievable with the available rotor (TX-200). The FPLC-SEC chromatogram obtained by injecting the sample *C12500_Achillea* juice is also reported in Figure 76 and compared to the other curves. A modest amount of vesicles is found from the integration of the EV peak (Table 21), a value that is 36% lower than that of *P3µm_ Achillea juice*, and a comparable amount of impurities in the two samples. Based on the all the discussed considerations, *P3µm_ Achillea juice* is selected as feed for the diafiltration process.

On Achillea lemon juice
Some details on how the commercial lemon juice Achillea is processed are retrieved from the company. The Achillea company if furnished by a lemon's supplier, in Sicily. The biological lemons are washed and accurately selected in order to remove rotten or unripened fruits. Unluckily, details on how the lemons are squeezed are not provided. Right after, the juice is sent to the company and stored in insulated tanks between 0-2°C. It is then sent to the bottling unit through a tubular heat exchanger at a certain temperature. After the juice is bottled, it is successively pasteurized.

6.3 Stage diafiltration with 100kDa PES membrane

After the optimization of the upstream processing conditions and the diafiltration membrane selection, a five stage diafiltration process is carried out with the 100kDa PES membrane. The chromatograms of the retentates and permeates obtained with 5 stages diafiltration employing the chosen membrane are reported in Figure 78 and 79.
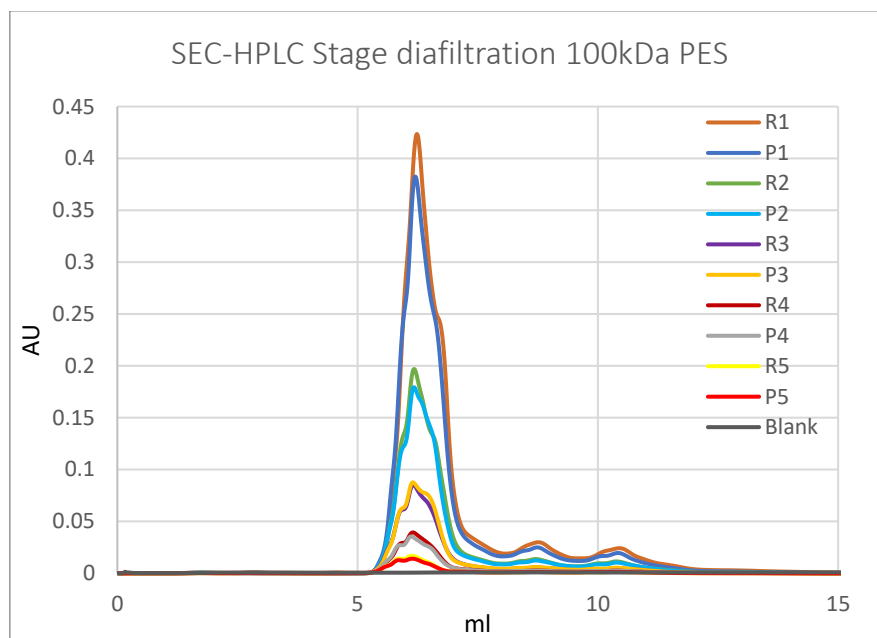

Figure 77: SEC-HPLC chromatogram of retentates and permeates of 100kDa PES stage diafiltration
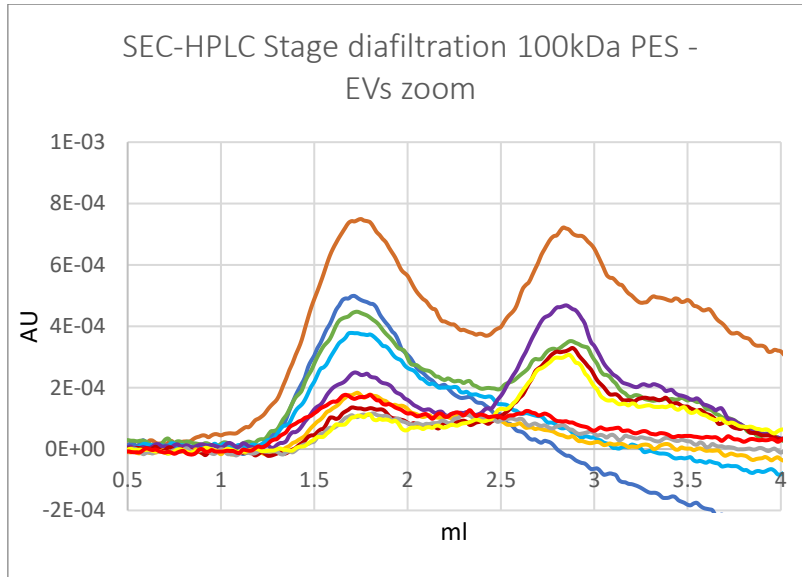
Figure 78: EV zoom of SEC-HPLC chromatogram of retentates and permeates of 100kDa PES stage diafiltration

As already discussed in Paragraph *5.2.4.1*, batch diafiltration can be modelled in the following way:

- $X = 2$ volume reduction factor
- At each stage $c = 2\,c_0$; $V = V_P = V_0/2$;
- After n=5 stages

From paragraph *5.2.4.1* equations (5) and (6)*:*

$$\frac{c}{c_0} = 2^{-5}$$

$$V_P = 5V_0 \left(1 - \frac{1}{2}\right) = 2.5V_0$$

Where a 100% permeability of impurities is assumed. To process a starting volume of $V_0 = 80\,ml$ a volume of $V_p = V_{buffer} = 200\,ml$ is necessary. From the integration of the HPLC chromatogram's peaks relative to impurities of retentates, permeates and feed, it is possible to obtain a dimensionless concentration, expressed as $c_{impurities}/c_0$, for each sample. It is compared with the values predicted by the theoretical model. The contaminant concentration normalized over the feed concentration predicted by the theoretical model and found experimentally is reported in Table 23 and plotted in a normalized graph in Figure 80.

Table 23: Theoretical and experimental removal of contaminants in stage diafiltration with 100kDa PES membrane. A 100% membrane Permeability to impurities is assumed.

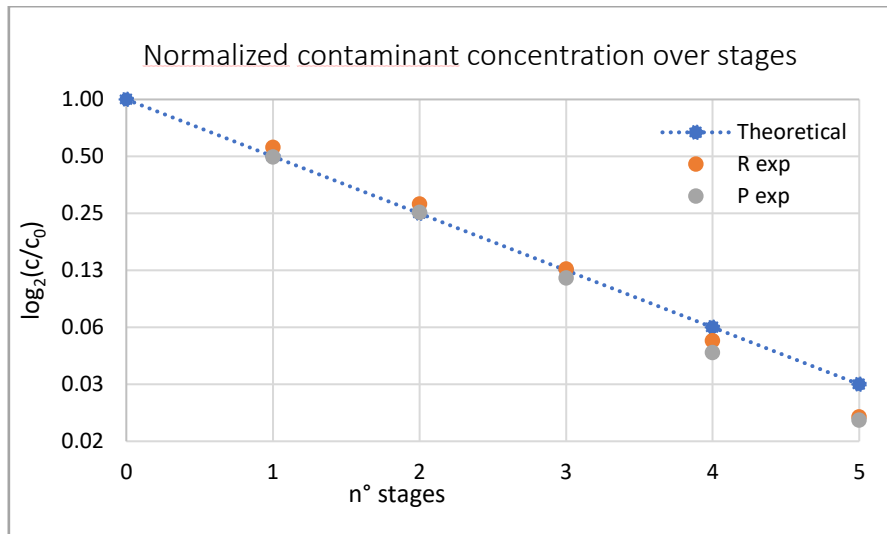| Stages	c_p/c_0 Theoretical (R=0)	c_p/c_0 Experimental	C_r/c_0 Experimental
1	50%	50%	56%
2	25%	25%	28%
3	13%	11%	13%
4	6%	5%	5%
5	3%	2%	2%

Figure 79: Normalised plot of contaminant concentration reduction over stages.

Overall, the model seems to adequately describe the phenomena. It is possible to observe that the experimental points deviate from the model from the fourth stage, with a % deviation from the theoretical model of 26% in the fourth stage, and of 35% in the fifth stage, with values lower than the theoretical ones, corresponding to better performance than those predicted by the model. Thus, the model seems to adequately describe the phenomena just for the first stages. In fact, as the process goes on, the presence of fouling led to a decrease in the membrane permeability and the assumption of 100% permeability become unrealistic.

6.4 TFF constant volume diafiltration

Constant volume diafiltration is carried out in *cross-flow* mode employing the Minitan-S UF cell and the FPLC system. The filtration system configuration set-up with the associated process flow diagram are reported in Paragraph *5.2.4.4*. Again, the membrane chosen is the 100kDa UF membrane in PES and the commercial Achillea juice is used as source. A first preliminary run is carried out through the following operative conditions:

- TMP = 1.5 bar
- Magnetic stirring at 200 rpm
- Temperature = 6°C
- PBS as dilution buffer
- Active area of filtration = 30 cm^2
- Initial volume = 200 ml of permeate of the 3μm filtration (P3μm)
- Feed concentration $c_F = 100$ (v/v % lemon juice)
- n° of diavolumes = 0.42

Buffer addition to the feed tank is carried out in a semi-continuous way. As 5 ml of permeates are collected in the permeate tank (graduated cylinder), 5 ml of fresh buffer are added to the feed tank. As already described in Paragraph *5.2.4.4,* the filtration operation is conducted at constant pressure provided by the FPLC pump (working in "Pressure controlled" mode). After an initial transient due to the start-up procedures (around 5 minutes) the pressure stabilizes to 1.5 bar. The process is stopped

after 380 minutes, when 85 ml of permeate are collected, thus 0.42 diavolumes are processed. The average feed flowrate is 4.1 ml/min.

The system is controlled through the FPLC software Unicorn™, that allows on-line monitoring of the retentate side UV, pH, conductivity signals (Figure 81).
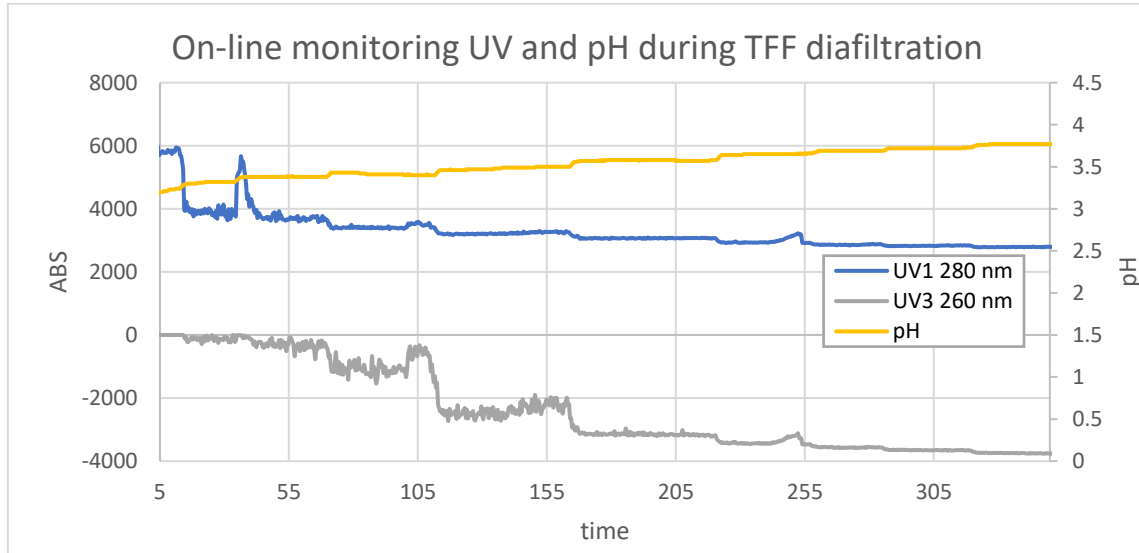

Figure 80: On-line monitoring of UV and pH signal during TFF diafiltration though FPLC detectors. Conductivity signal is detected as well even if not reported. It is possible to detect three UV signals at three different wavelenghts.

It is possible to observe that:

- The pH signal is increasing over time, due to the addition of fresh buffer and the removal of acidic lemon proteins in the permeate.
- The UV signal at both the recorder wavelength (260 and 280 nm) are decreasing over time as the diluent is added. The signals are also more "refined" over time.

The volume of permeate collected is measured over time, to obtain the permeate volume and flux time trends (Figure 82 and 83 respectively).
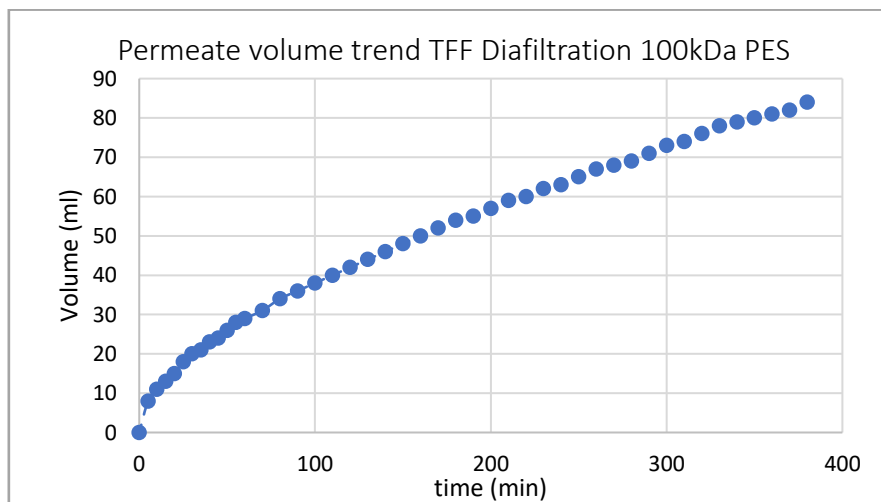

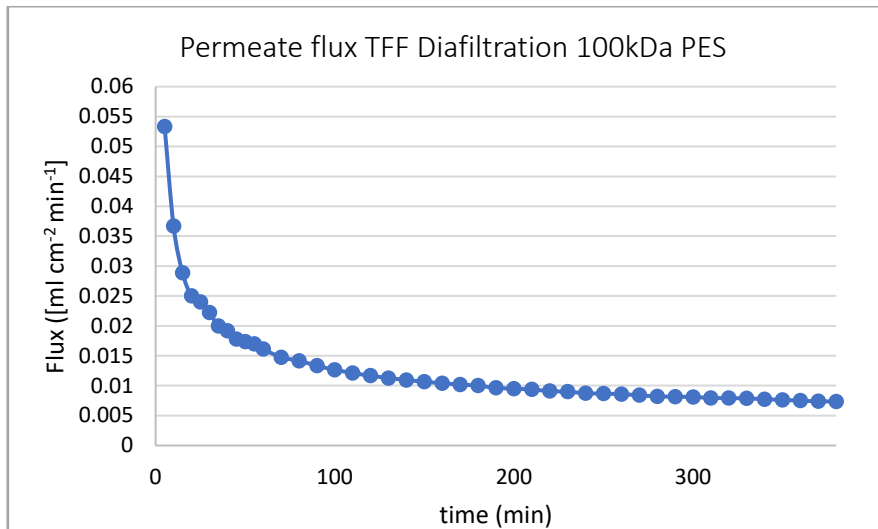*Figure 81: Pemeate volume generated over time in 100kDa PES TFF diafiltration.*

Figure 82: Permeate flux over time in 100kDa PES TFF diafiltration.

The permeate flux is calculated from the permeate volumetric flowrate and the membrane's active area that is equal to 30 cm². The flux approaches an asymptotic value of about $1*10^{-2}$ ml cm^{-2} min^{-1} after 200 minutes.

SEC-FPLC analyses of the feed (P3µm), retentate and permeate obtained after 0.4 DV are shown in Figure 84.

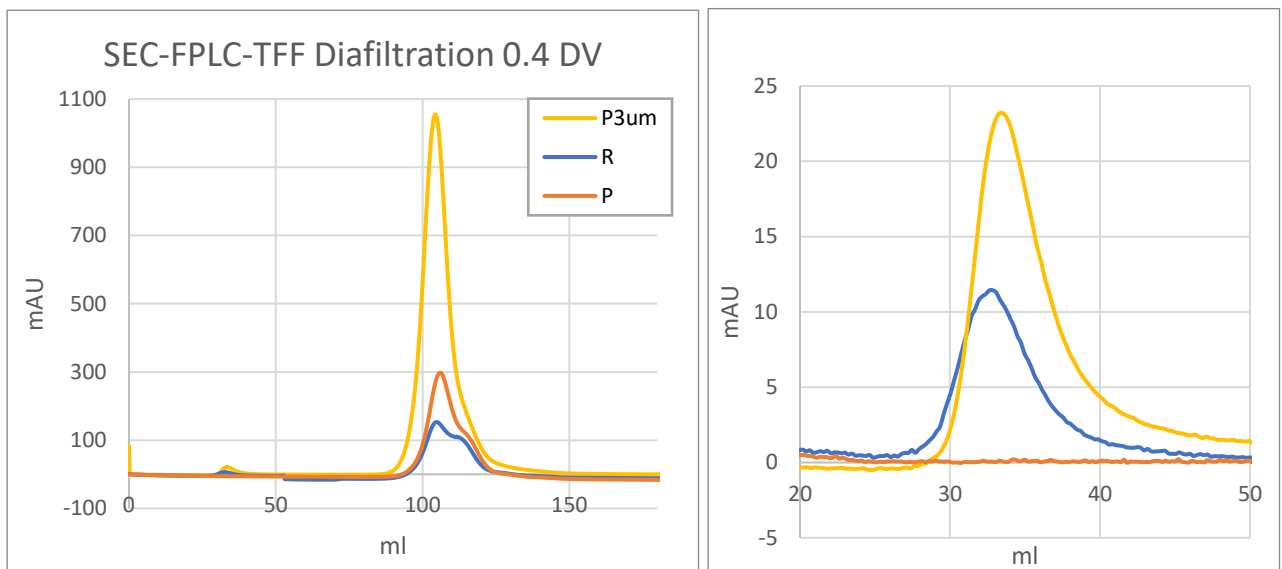*Figure 83: SEC-FPLC analyses of the feed (P3µm), retentate and permeate obtained after 0.4 DV TFF diafiltration. EV zoom shown on the right.*

From the FPLC chromatograms in Figure 84 is possible to observe that the permeate curve is completely flat at the EVs retention volume, further assessing the reliability of the PES membrane for the application. Again, EVs peaks are integrated to obtain the area values (Table 24).

Table 24: EV peaks area from SEC-FPLC analyses on the feed, retentate and permeate after 0.4 DV.

	EVs peak area (mAU*ml)
P3µm (Feed)	155.65
Retentate 0.4 DV	79.71
Permeate 0. 4 DV	0

% EVs losses in the cake	**51 %**

Through a total mass balance over the streams, it is found that 51 % of the vesicles are lost in the cake/gel. This finding is confirmed by a SEC-HPLC analysis of the cake resuspended in PBS. It is gently scraped from the membrane surface and resuspended in 10 ml of PBS through the aid of a horizontal shaker for 30 minutes. In Figure 85 is possible to observe a significant peak eluted at the same typical EVs retention volumes (2.4 ml).
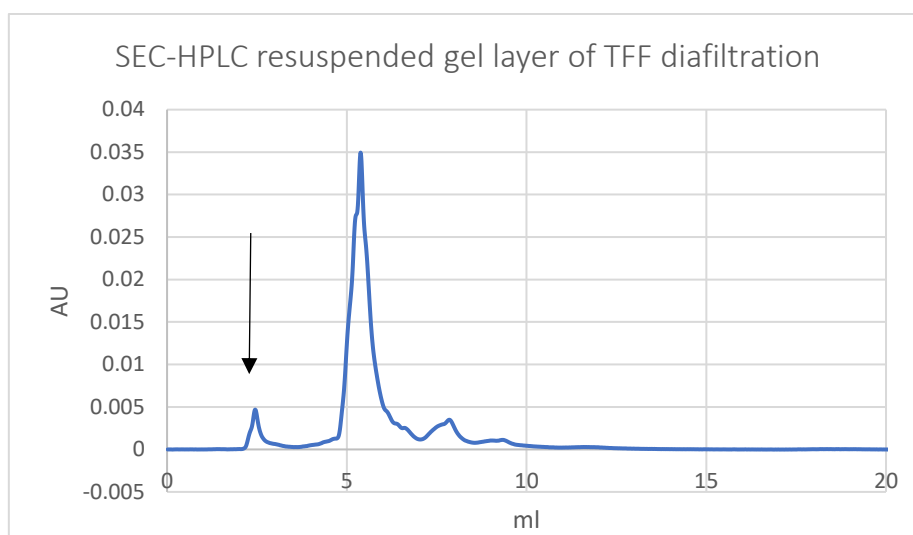

Figure 84: SEC-HPLC chromatogram of the gel layer obtained on the 100kDa PES membrane after diafiltration.

Based on this finding, efforts are taken in order to address the problem of product loss over the membrane gel layer, that now appear to be highly impacting on the EV yield of the process.

6.3.1 Characterization of the 100kDa PES membrane in TFF mode

The 100kDa PES membrane is characterized through a water permeability test and a lemon juice permeability test in TFF mode.

Water permeability test

The water permeability test is conducted flowing filtered water through the 100kDa PES membrane at different pressures equal to 0.5, 1, 1.5 and 2 bar. Once the system reaches the desired pressure value, measures of the permeate volumes are taken at short time intervals (by reading the permeate volume at two different times). The readings are repeated two times and the final flux value is averaged over the measures. The permeate fluxes obtained at the different pressures are plotted in Figure 86.
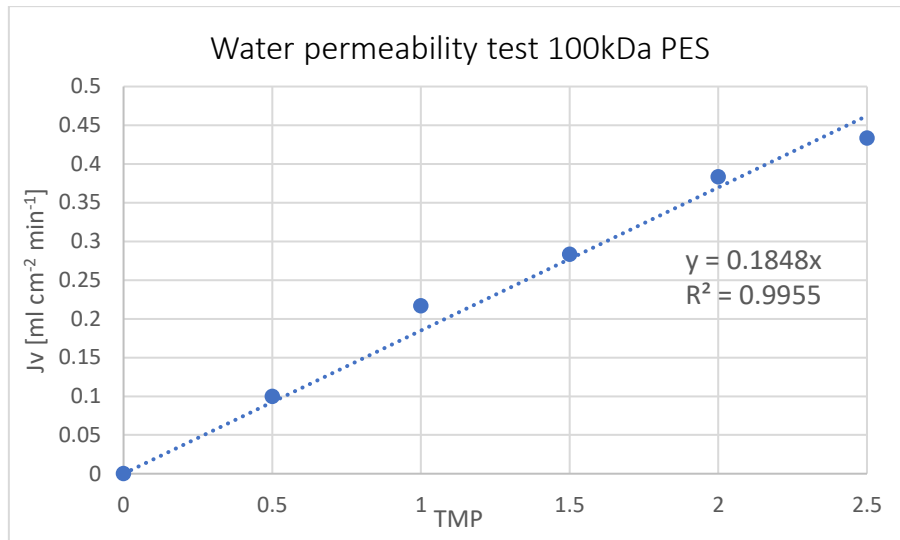
Figure 85: Water permeability test on 100kDa PES membrane in TFF mode.

As expected, the points lie on a straight line. The equation of the line is found by linear interpolation of the experimental points and it is equal to y=0.185x (R²=0.9955). The slope of the interpolating line represents the hydraulic permeability of the membrane.

$$L_{p,w} = \frac{J_{v,w}}{\Delta P} = 0.185 \frac{ml}{min \cdot cm^2 \cdot bar}$$

Lemon juice permeability test

Another membrane permeability test is performed with lemon juice, in particular with the feed of the diafiltration process, that is the permeate of the 3μm filtration. The same procedure used for the water permeability test is applied also in this case, with the feed flowing through the UF cell at 0.5, 1, 1.5 and 2 bar and collecting values of the permeate volumes over time to obtain average permeate fluxes. The results of the test are presented in Figure 86.
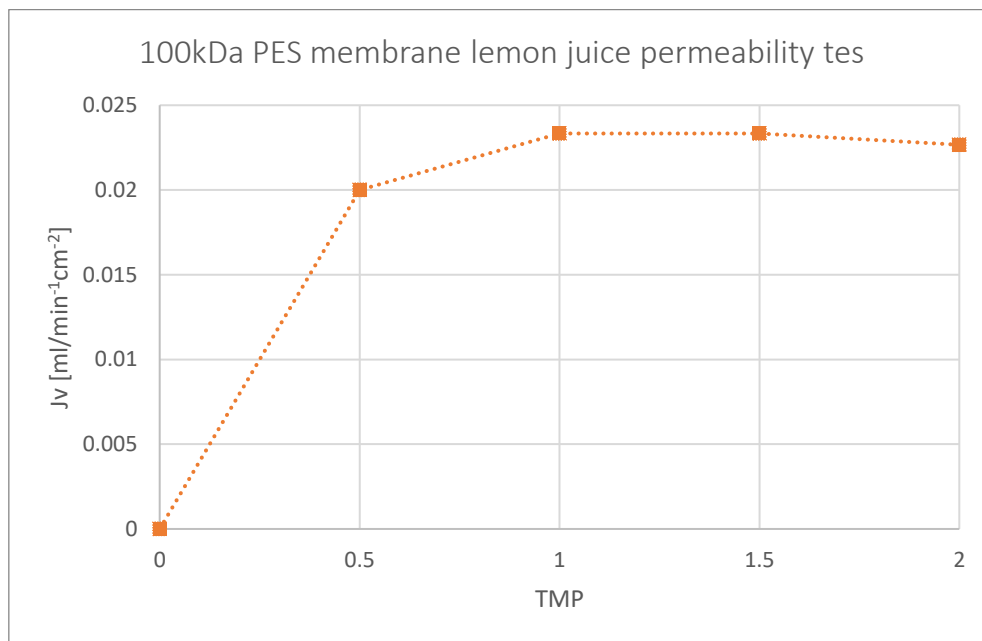

Figure 86: Membrane permeability test on lemon juice (P3um) in TFF mode.

As it can be noted In Figure 87, the flux reaches an asymptotic value at around $J_{v,g} = 2.23 \cdot 10^{-2} \frac{ml}{min \cdot cm^2}$. This value represents the flux in gel conditions, also called the *critical flux*, independent on pressure and dependent only on the mass transfer coefficient (e.g. feed flowrate) and on the bulk concentration. The optimal operative conditions are found around the *knee* of the curve J_v(TMP).

In Figure 88 the water permeability line of the membrane is compared to the lemon permeability curve.
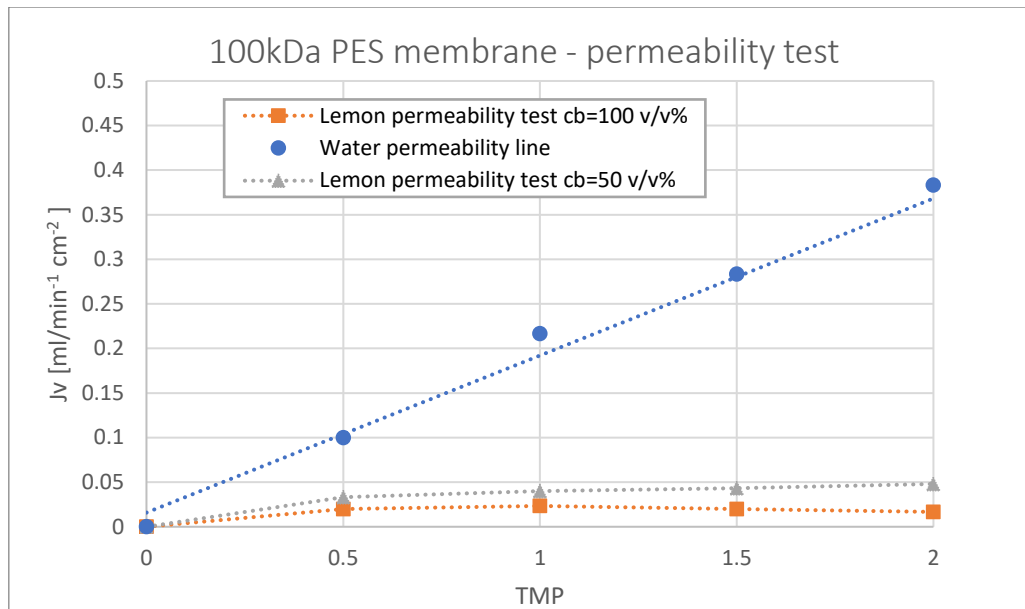

Figure 87: 100 kDa PES membrane water permeability line and lemon juice (P3um) permeability curve.

In these conditions, the critical flux is very low. As the bulk concentration decreases, the distance between the water and lemon permeability curve should decrease, leading to higher values for the critical fluxes. Thus, it appears to be clear that the use of the undiluted juice is not convenient (juice diluted in PBS afore the 3µm filtration but not preliminarily to the diafiltration process). In this framework, the subsequent diafiltration run is carried out by halving the feed concentration to the diafiltration process (c_b=50% v/v). In this case $J_{v,g}$ approaches an average value of $0.05 \cdot 10^{-2} \frac{ml}{min \cdot cm^2}$.

6.3.2 Optimized TFF diafiltration process

Based on the evidences reported in the previous paragraphs, the work progressed with the development of an optimized diafiltration protocol. The modifications introduced with respect to the previous protocol are the following:

-   *Higher feed dilution*
    The feed concentration is halved to $c_F = 50$ (v/v %), thus a 1:1 dilution ratio with PBS is used.

-   *Removal of 95% of the impurities*
    To quantify the efficacy of the purification process, a higher number of diavolumes is processed. A reduction of 95% of the impurities present in the EVs preparations is set as target goal. To this purpose, it is necessary to process approximately 3 diavolumes. From equation (9) in paragraph 5.2.4.3:

$$ln\frac{c_0}{c} = \frac{\dot{V}t}{V} \rightarrow ln\frac{100}{5} = \frac{\dot{V}t}{V} = 3\ DV$$

The equation is obtained though the solute mass balance integration over the filtration system. Starting from an initial volume of diluted solution $V = 100\ ml$ the process is concluded in *305 minutes*. The volume of dilution buffer necessary to carry out the process is three times the initial volume.

$$V(PBS) = 3V = 300\ ml$$

- *Recovery of vesicles from the cake*

    To reduce the extent of vesicles losses in the cake and recover some product a protocol for the recovery of vesicles from the cake is developed. It involved the following steps:

    o The process is stopped after each diavolume;

    o The cake is gently scraped from the membrane and resuspended in 10 ml of PBS. Resuspension is aided by 30 minutes horizontal- shaking.

    o The solution is finally added to the feed tank and the diafiltration process is started again.

    Over the three diavolumes, a total of three cakes are resuspended and processed again to the feed tank.

The process operative conditions are unchanged (TMP=1.5 bar, stirring at 200 rpm, T=6°C), as well as the TFF system set-up (paragraph *5.2.4.4*). The SEC-FPLC chromatograms of retentates and cakes obtained after 1.5 diavolumes have been processed are reported in Figure 89 and 90. These chromatograms have been used to estimate the % cake recovery in the retentate, after its reintroduction in the feed tank when 1DV is processed.
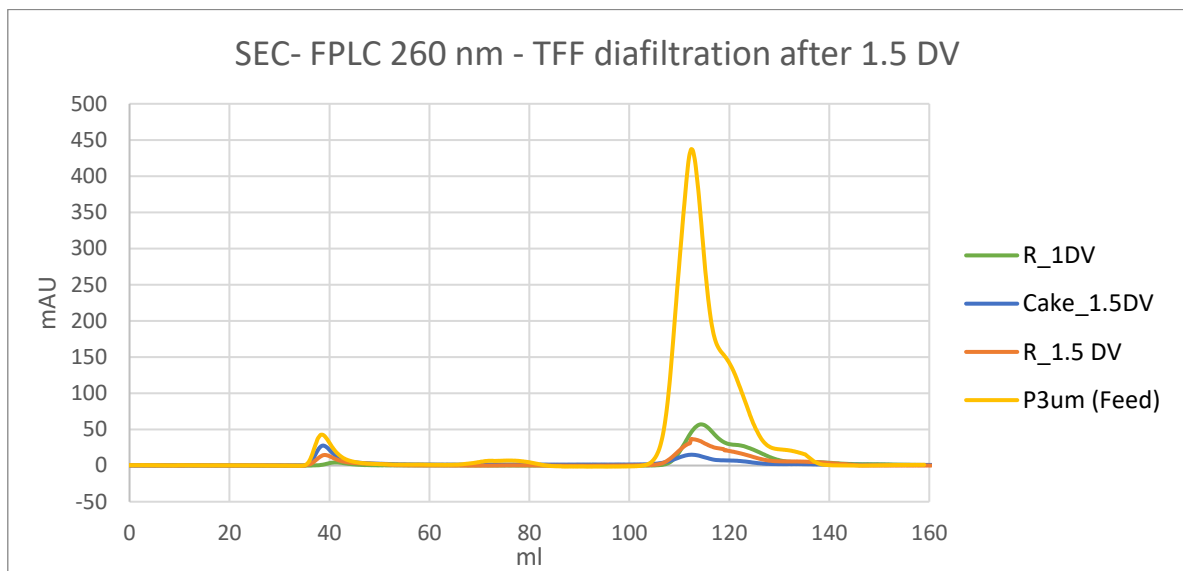

Figure 88: SEC-FPLC UV signal at 260 nm. Retentates and cakes chromatograms after 1.5 DV diafiltered.
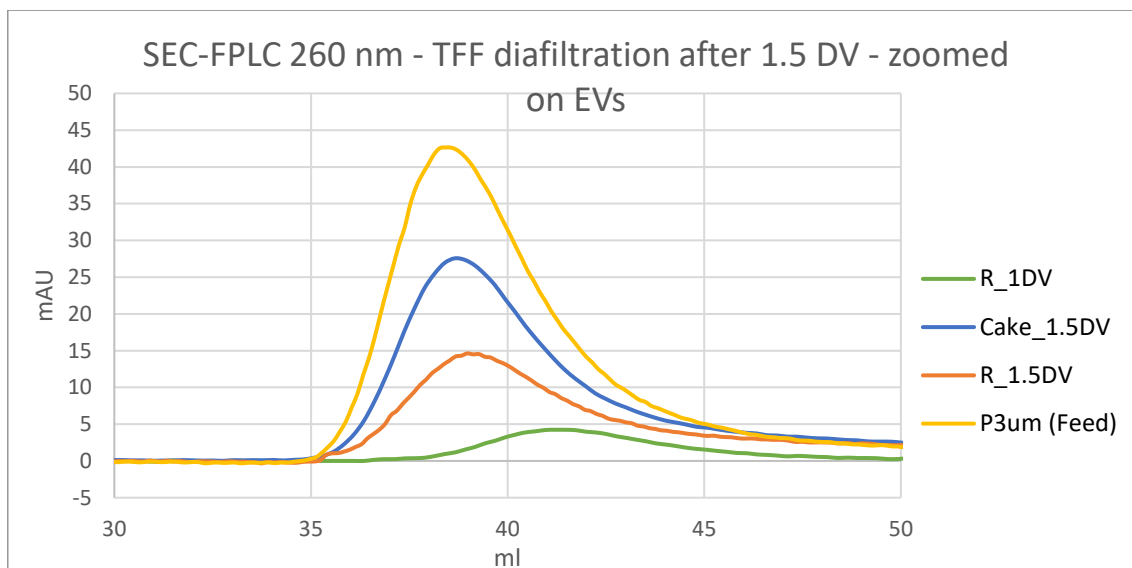
Figure 89: SEC-FPLC UV signal at 260 nm. Retentates and cakes chromatograms after 1.5 DV diafiltered. Zoom on EVs.

By visual observation of the chromatograms zoomed on EVs (Figure 90) is noted that the peak area of vesicles in the retentate rises remarkably between 1DV and 1.5DV, thus respectively before and after the addition of the cake. In order to quantify this phenomenon, the peaks relative to EVs and impurities are integrated to obtain measures of area. From the area values it has been possible to quantify the % recovery of vesicles before and after the cake recovery (Table 25).

Table 25: Area of EV peaks from SEC-FPLC chromatograms (260 nm) and cake recovery calculations.

Sample	Area EV *[mAU*ml]*
P3um (Feed)	224.0
R_1.5 DV	92.8
Cake_1.5 DV	154.3
R_1 DV	18.7
EV recovery after 1DV	8%
EV recovery after 1.5DV	41%
Increase of EV recovery after cake recovery	80%

EV recovery after cake addition rises from 8% to 41%, with a relative increase of 80% with respect to the recovery after the first diavolume. It is assumed that no vesicles are present in the permeate.
This result is confirmed by SEC-HPLC analysis, zoomed on EVs in Figure 91. In Figure 92, the whole chromatogram is reported and the removal of impurities between stages is calculated from the integration of the impurities' peaks.
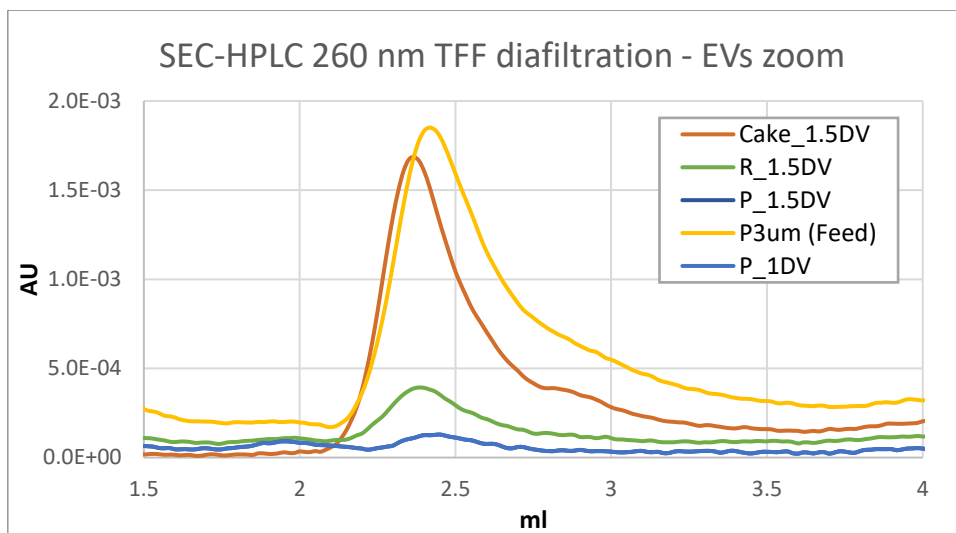
Figure 90: EVs zoom of the SEC-HPLC chromatograms of the retentates, permeates and cake of the TFF diafiltration process
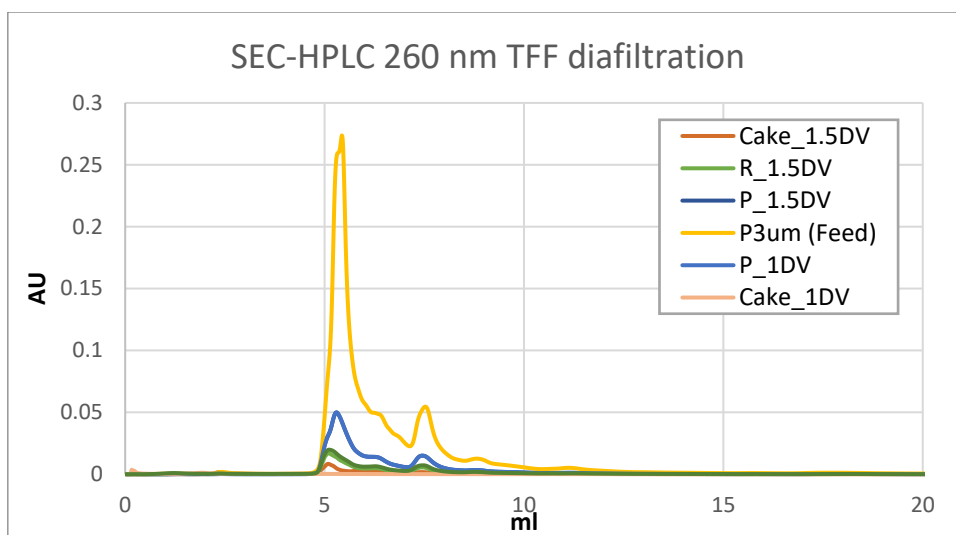

Figure 91: SEC-HPLC 260 nm of the retentates, permeates and cake of the TFF diafiltration process

In Table 26 the results of the integration of the HPLC impurities peaks are reported. Starting from these values is possible to build a curve for the removal of contaminants over time. The values are normalized by dividing them over the initial feed concentration and plotted in Figure 93 over the number of diavolumes.

Table 26: Area of the impurities peaks and normalized concentration of the retentate samples over the diavolumes

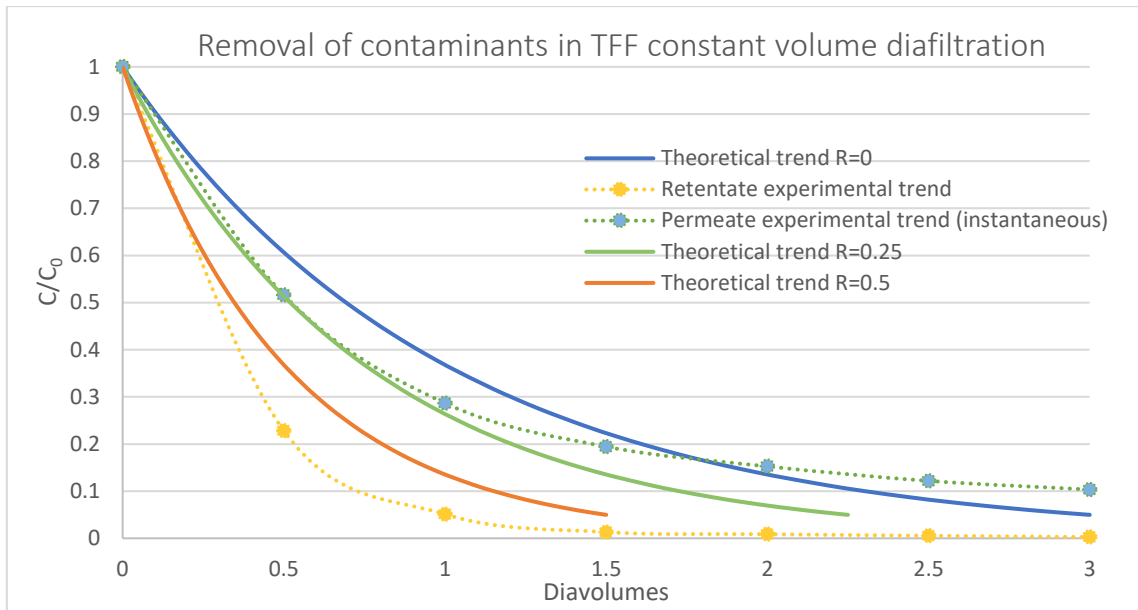| Sample	time of collection (min)	n° DV	Area of impurities (mVsec)	c/c_0
Feed	0	0	16191.3	1
R0.5	43	0.5	3696.3	0.29
R1	118	1	827.1	0.05
R1.5	155	1.5	213.2	0.013
R2	216	2	140.9	0.009
R2.5	255	2.5	89.3	0.005
R3	305	3	41.1	0.002

Figure 92: Removal of impurities in the TFF diafiltration process. Dimesionless concentration over the number of diavolumes.

As explained in paragraph *5.2.4.1* the theoretical trend is obtained through the solution of the integrated mass balance equation over the filtration system:

$$ln\left(\frac{c}{c_0}\right) = -\frac{\dot{V}(t)}{V}(1 - R) \qquad (10)$$

Where R is the membrane rejection coefficient to the impurities. The assumption that R=0 seems to be most adequate. In fact, the experimental reduction of contaminants in the retentate stream outperforms that predicted by the theoretical model. Thus, the reduction of contaminants appears to be misrepresented and this superior purification effect is just apparent. As the gel layer forms, impurities get trapped in it and are not efficiently filtered. By assuming an impurities rejection coefficient equal to R=0.5. the theoretical trend better represents the experimental data. In fact, the desired level of purification is reached just after 1.5DV.

The final level of purification is better assessed through a final SEC-FPLC analysis on the feed, final retentate and final permeate after 3DV. The comparative chromatogram is reported in Figure 94.
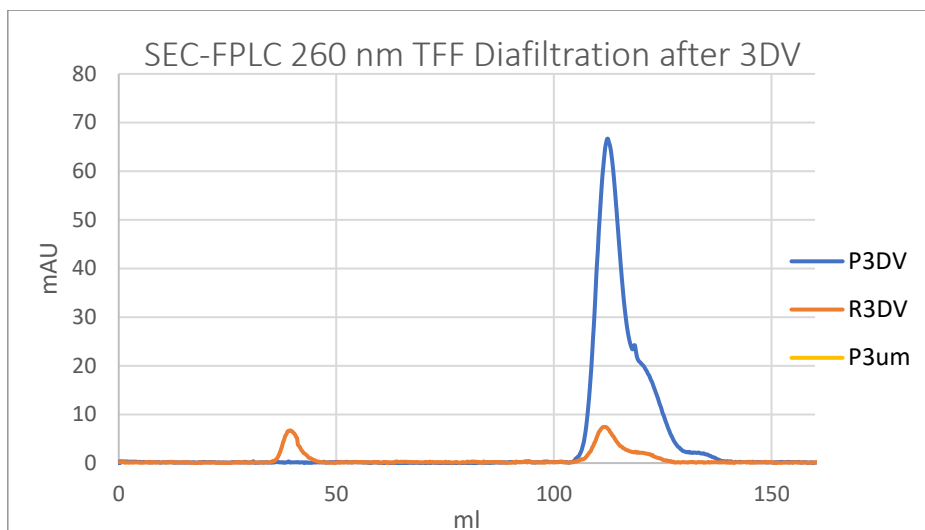
Figure 93: SEC-FPLC on the feed, permeate and retentates of the 3DV diafiltration to close the mass balance.

By integrating the impurities and EVs peaks of the chromatogram, it is finally possible to confirm the results obtained with SEC-HPLC and close the total mass balance of the process (Table 27).

Table 27: Area from the integrated peak of SEC-FPLC chromatograms.

	Area EVs (*mAU*ml*)	Area impurities (*mAU*ml*)
R3DV	34.66	62.8
P3DV	0	615.4
P3um (Feed)	223.9	4079.5
Total removal of impurities after 3DV	98.5 %	
Total recovery of EVs after 3DV and cake resuspended 3 times	15.5 %	

The removal of impurities after 3DV is 98.5%, thus assessing that the diafiltration process is effective in the purification of lemon EVs. Nonetheless, the EV losses on the cake's membrane are undoubtedly the major pitfall of the process. Even if the membrane cake is recovered and reintroduced three times in the retentate, after 3 diavolumes the *total recovery of vesicles is only 15.5 %.*

6.3.3 TFF diafiltration: yield on EVs

In order to retrieve a value of the yield in extracellular vesicles over the whole process, a calibration curve is built by injecting samples of known concentration to the Yarra 2000 SEC-HPLC column. The aim is to correlate the height of the SEC-HPLC peaks to known values of concentration. BSA (Bovine serum albumin) standard solutions are obtained from a stock solution of 0.56 mg/ml BSA in PBS, through serial dilutions in the range 5-100 µg/ml. The standard solutions are injected to the column at 1 ml/min. From the resulting chromatograms the height values, relative to the eluted BSA proteins, are collected and plotted over their concentration. The calibration line y=0.0128x is obtained through linear interpolation of the experimental points (Figure 95).
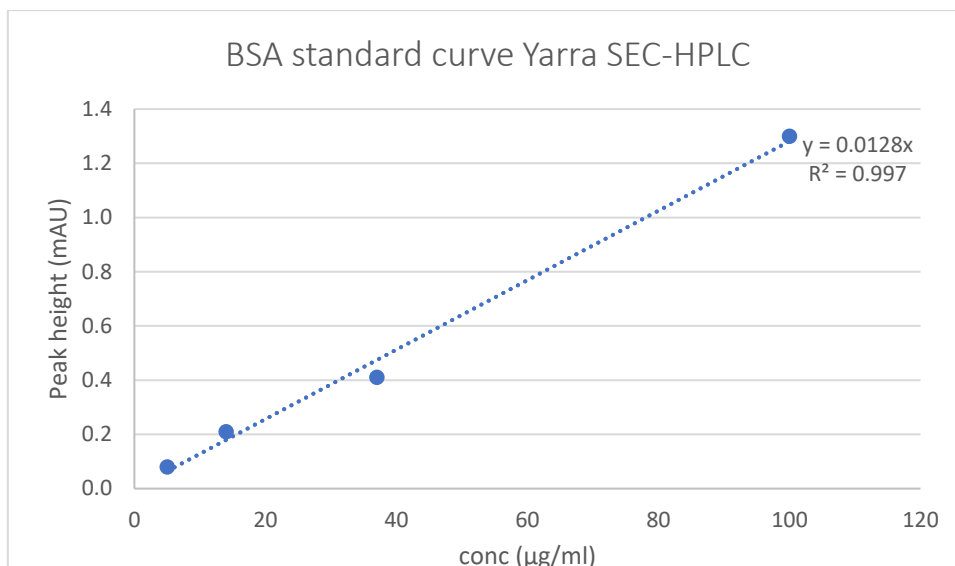
Figure 94: BSA calibration curve built correlating the SEC-HPLC peak heights of eluted BCA protein solutions at known concentrations

The values of EV concentration after 3DV TFF diafiltration are obtained fitting the EV peak's height with the BSA calibration curve (Table 28). Consistency is guaranteed by the use of the same dilution buffer (PBS) and same SEC-HPLC analytic conditions (same injection volume, same flowrate = 1 ml/min).

Table 28: Concentrations of EV obtained after stage and TFF diafiltration with a 100kDa PES membrane, obtained fitting the EV peak heights with the BSA calibration curve.

		Sample	Peak height (mAU)	EV concentration (µg/ml)
100 kDa PES membrane	*TFF diafiltration (3 diavolumes)*	P3um	1.8	140.6
		R 3 DV	1.07	83.6
	Stage diafiltration (5 stages)	R1	0.72	56.2
		R5	0.31	24.2

The value obtained for the feed (P3um) falls outside of the calibration range, thus it cannot be considered reliable. The other values, all fall within the concentration range provided by the BSA curve. After 3 diavolumes in TFF mode, the final retentate contains around *83.6 µg of veiscles per ml of PBS.* It is then possible to make a final comparison between TFF diafiltration and stage diafiltration, considering 3 diavolumes and 5 stages realized respectively, with the use of the same source, dilution ratio, membrane, TMP and same dilution buffer. In stage diafiltration, there is a 43 % decrease in the product yield from stage 1 to stage 5. The EV yield obtained with TFF diafiltration *is 3.5 times higher* than that of stage diafiltration.

Finally, considering that:

- On average 30 ml of lemon juice are squeezed from one middle-sized lemon;
- With the preliminary centrifugation run around 5 ml of juice are lost as pellet.
- In the current protocol lemon juice is diluted two times with PBS in a 1:1 ratio, before the preliminary 3 µm filtration to the feed of the diafiltration process.

Upon these considerations, with the current protocol is possible to obtain *4.2 mg of extracellular vesicles starting from one single lemon*, or equivalently *0.14 mg per ml of lemon juice*.

6.3.4 Gel layer under microscopy

The 100kDa PES membrane with the gel layer formed after diafiltering 0.5 diavolumes is shown in Figure 96.

Figure 95: 100kDa PES membrane with the gel formed after 0.5 diavolumes.

The gel deposited over the membrane is analyzed through the Axiolab 5 lab microscope by Zeiss. The images in Figure 96 and 97 are taken at two different magnifications (50 and 20 micron scales).

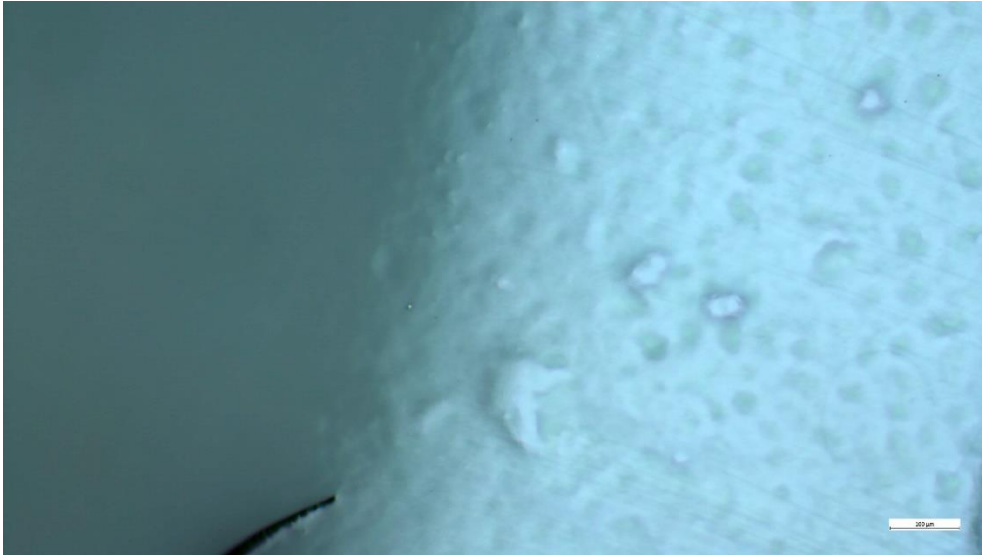*Figure 96: Membrane's gel layer at 50 µm scale.*

Figure 97: Membrane's gel layer at 100 μm scale.

In Figure 98 is possible to observe the border between the membrane's surface and the gel layer, at a 100 μm scale.

6.4 Differential ultracentrifugation method

Differential ultracentrifugation method is carried out with the aim to compare its performances with the membrane-based isolation protocol. The dUC protocol is adapted from the ones proposed by Pocsfalvi et al. [20] and Thery et al. [21] It comprises preliminary centrifugation steps (400 x g, 1000 x g, 15000 x g) and the ultracentrifugation run where vesicles are pelletized. Two protocols have been developed, schematized in Figure 99, which differ only in the final UC runs.
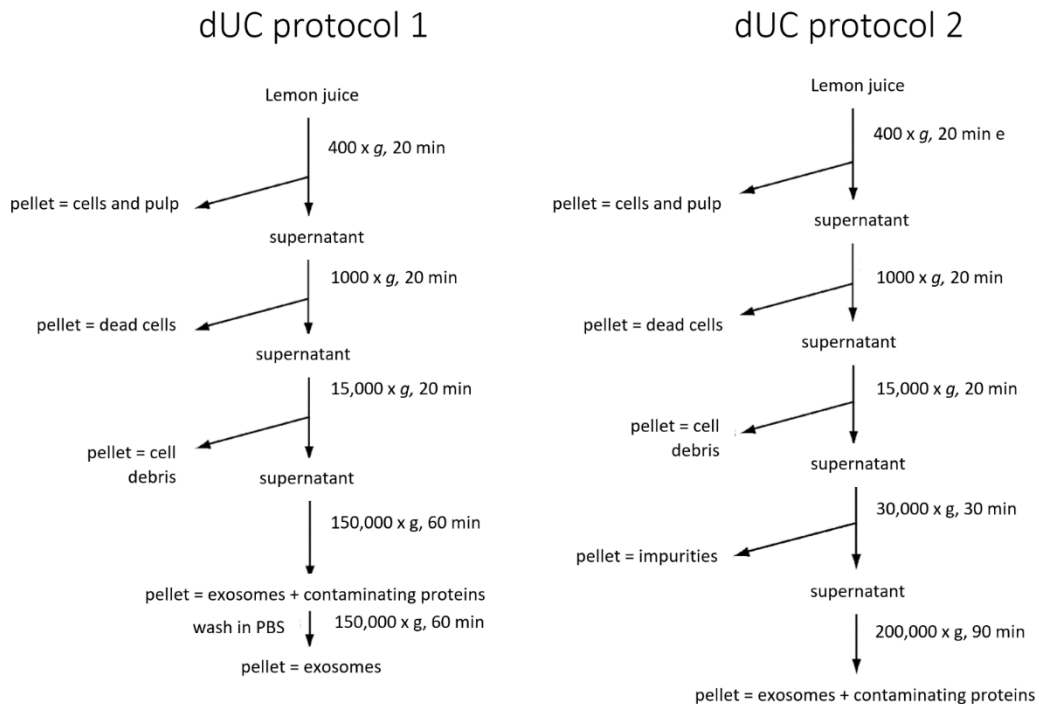

Figure 98: Differential UC protocol used for the isolation of lemon extracellular vesicles.

The first protocol involves the ultracentrifugation of the supernatant obtained from the preliminary stages at 150,000 x g for one hour. The new supernatant is discarded and the EV pellet is resuspended in PBS through pipetting and with the aid of a potter (lab homogenizer). The resuspended pellet is subjected to another UC run at the same conditions to remove the contaminating proteins and newly pelletize EVs. The final pellet is resuspended again in fresh PBS. The second protocol instead, included an additional purification step at 30,000 x g for 30 minutes and a prolonged UC run at 200,000 x g for 2 hours.

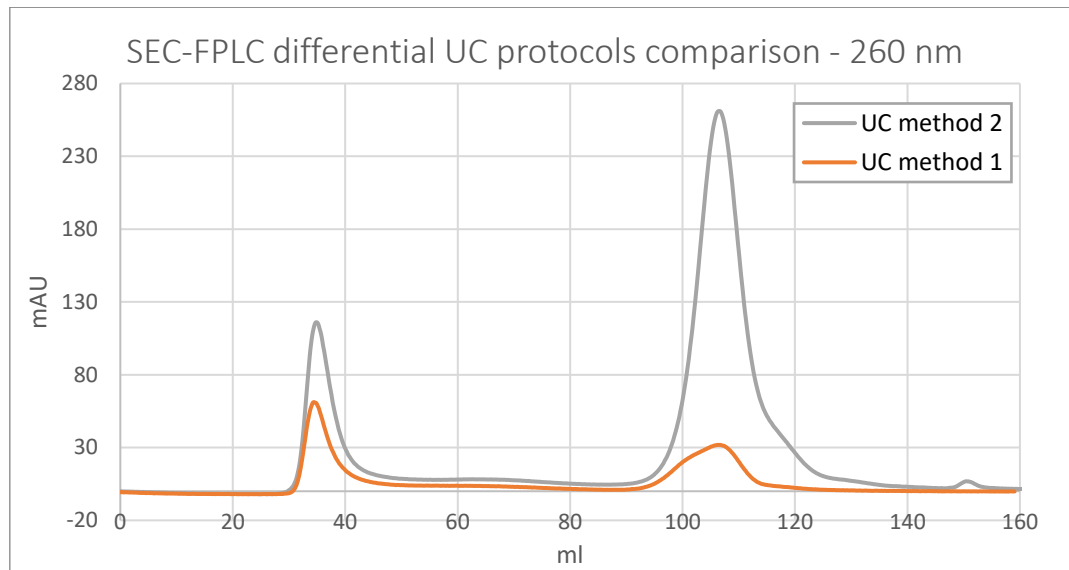The so-obtained EVs preparations are analyzed though SEC-FPLC and the chromatograms are shown in Figure 100.

Figure 99: SEC-FPLC chromatogram of the EVs preparations obtained through dUC protocol 1 and 2.

Method 1 is more effective in breaking down impurities, but it has a lower yield in EVs. Method 2 allows to pellet a higher amount of vesicles due to the prolonged and higher speed UC run, but it leads to co-pelletize a high amount of impurities. The best solution could be the use of method 2 coupled with the final EV-pellet wash in PBS, that was employed in method 1.

By comparing the SEC-FPLC chromatograms of sample UC_1 and UC_2 (Figure 99) and sample R3DV (Figure 93) is possible to calculate that EV peaks area obtained through ultracentrifugation are 90% bigger than those of EVs obtained through the present membrane-based process.

Unluckily, the comparison is unreliable and it is not possible to quantify the yield difference between the two methods by the FPLC chromatographic analysis shown, since they use different starting volumes.

- The UC vesicles are isolated starting from about 40 ml of juice, undiluted over the whole process.
- The EV purified through TFF diafiltration are diluted two times, and the juice starting volume for the conducted run was 25 ml.

Thus, a comparison between the two methods can be only provided by data from literature. Raimondo et al. isolated lemon EVs through a dUC-based protocol and obtained a yield of 2.5 mg/ml of lemon juice [22]. This result is comparable to the yield obtained with the developed membrane-based isolation protocol that is 0.14 mg/ml of lemon juice.

6.5 BCA assay

Total protein quantification is carried out through the bicinchoninic acid (BCA) colorimetric assay. Different EVs preparations are tested, to quantify the total proteomic content of different EVs preparations. These are:

- Permeate of the preliminary 3μm filtration (P3um);
- Retentate, permeate and cake of TFF diafiltration with 100kDa PES membrane after 0.8DV (R_0.8DV, P_0.8DV and Cake_0.8DV);
- Retentate, permeate and cake of TFF diafiltration with 100kDa PES membrane after 1.5DV (R_1.5DV, P_1.5DV and Cake_0.8DV);
- Retentate and permeate of TFF diafiltration with 100kDa PES membrane after 3DV (R_3DV and P_3DV);

The BCA *standard protocol* is carried out, valid for a 5-2000 μg/mL protein concentration range. Through a preliminary test, it is verified that the EV sample concentration is within the range of the reference curve. F BCA working reagent is prepared by mixing reagent A and B in a 50:1 ratio. Both reagents are provided by the Pierce™ BCA Protein Assay kit (Thermo Fisher) and 100 μl of sample are pipetted to 2 ml of BCA working reagent, for each EVs preparation.

First, a calibration line is built using Bovine Serum Albumin (BSA) as protein standard. Solutions of BSA at different concentrations are obtained through serial dilutions with PBS, in the range 5-2000 μg/ml, starting from a BSA stock solution of 2 mg/ml. After the addition of the BCA working reagent to the sample, the resulting solution is incubated at T = 37 °C for 30 minutes.

Subsequently, spectrophotometric readings at 562 nm are performed, using water as blank solution. All the absorbance values are corrected by subtracting the value of absorbance at 562 nm relative to PBS. Two replica for each sample are performed, and the final absorbance value is averaged consequently. The corrected values of the absorbance of the BSA standard solutions at different known concentrations are plotted over the concentration. Through linear interpolation the calibration line y=1.095x is obtained, as shown in Figure 101.
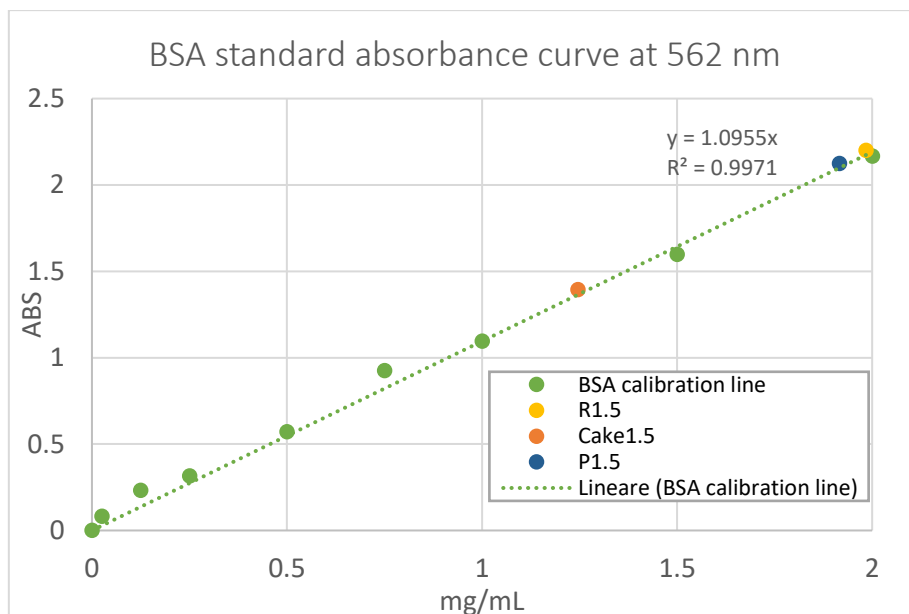
Figure 100: BSA calibration curve at 562 nm. The values of the average absorbance at 562 nm of the EVs preparations are fitted with the calibration line.

The values of the total protein concentration for each sample are obtained by fitting the average absorbance values with the calibration line (Table 29).

Table 29: Total protein concentration of the EVs preparation, obtained fitting the calibration line.

Sample	Average absorbance at 562 nm [ABS]	Average protein's concentration [mg/ml]
P3μm	2.54	2.29
R_3DV	0.60	0.50
P_3DV	2.41	2.17
Cake_0.8DV	1.61	1.44
R_0.8DV	2.42	2.18
P_0.8DV	2.40	2.18
Cake_1.5DV	1.40	1.24
R_1.5DV	2.20	1.98
P_1.5DV	2.12	1.91

It can be observed that the values of protein concentration in the retentates and permeates are comparable. This observation reflects the fact that since BCA measures the total protein content, also protein impurities are accounted for when performing BCA colorimetric assays. Thus, EVs protein quantification in the retentates can result in overestimation due to co-isolated protein contaminants. To conclude, protein measurements though BCA assay are inadequate to quantify EVs, except for exceptionally pure preparations. As a consequence, only the values relative to the permeate and retentate collected after 3 diavolumes, that are 0.5 mg/ml and 2.17 mg/ml respectively, can be used to have a very rough estimate about EV protein yield. In fact, they are the purest preparations among the others.

6.6 Size distribution and zeta-potential measurements

Size distribution and zeta potential of different EVs preparations are measured through the Nano Zetasizer® instrument by Malvern. The analyzed samples are:

- Permeate of 3μm filtration (feed of diafiltration);
- Retentate of 100kDa PES TFF diafiltration after 0.8DV, 1.5DV, 3DV;
- Cake of 100kDa PES TFF diafiltration after 0.8DV;

The input parameters are given to the software in order to optimize the run conditions. These are temperature (25°C), diluent type (0.1 M PBS), diluent and nanoparticles refractive indexes, viscosity and measurement cell. A summary Table of the input parameters used to configure the DLS and ZP measurement runs is reported in Appendix II. After the initial set-up and a temperature equilibration phase, the system performs a preliminary investigation over the sample to set the attenuator index and the measurement position. These are automatically adjusted by the software to find an optimal count rate for each sample.

- Attenuator index (AI) is set to calibrate the laser power to find the optimal count rate for each sample. High scattering samples requires large attenuation, with AI=0 denoting full attenuation and total laser block. Typical AI values falling between 6-8 are set by the system for the EVs preparation.
- The measurement position of the system is automatically moved depending on the nanoparticles' concentration within the sample, to allow the detection of a large amount of sample. If the preparations are too diluted, the measurement position gets closer to the cuvette wall. For the EVs preparations the measurement position is adjusted to 4.65 mm for each sample. This is the default position, meaning that our EVs preparations are in a proper concentration range to perform DLS measurements.

Each measurement is repeated five times for each sample. In each measurement the system detects the scattering intensity though different readings with a duration given by the count rate. The size distribution by intensity of sample R0.8 for each of the five measurements is shown in Figure 102.
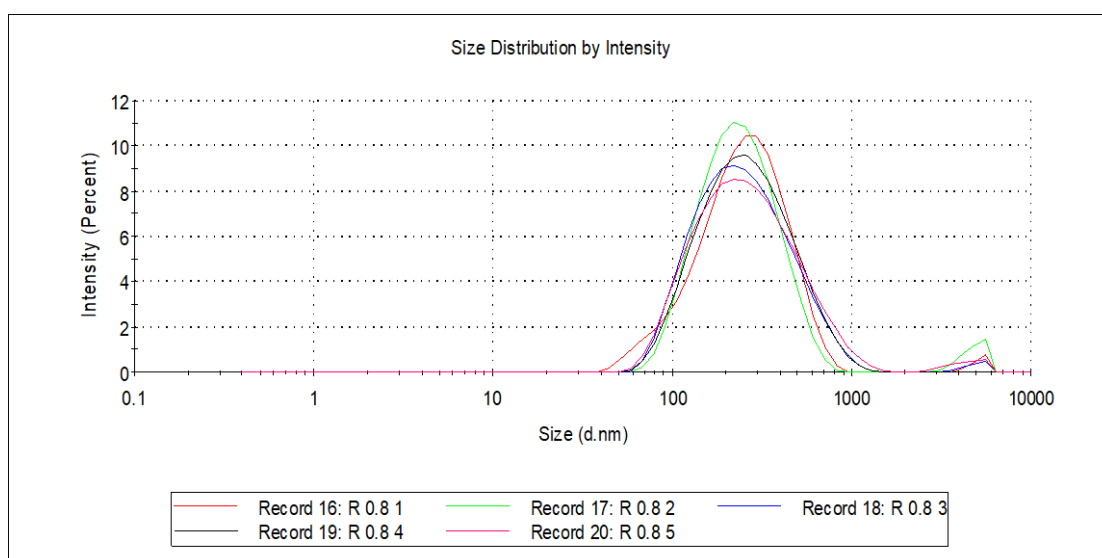

Figure 101: Size distribution by intensity for sample R0.8. Each color corresponds to a different measurement.

The size distribution by intensity obtained by different measurements on the same sample overlaps in a remarkable way. Thus, a good reproducibility within the different measurements is ensured. This result can be used to have a preliminary estimation on the stability of the EVs preparations. During the whole analysis duration the EVs preparations have a constant size distribution, i.e. they are scattering light in the same way over time without degrading and/or aggregating. In this sample, two different populations are found: the first is centered around 274,4 nm average particle diameter with an intensity of 98,7% and the second is detected with an intensity of 1.3% centered at 5165 nm average particle diameter. It may be assumed that the first population is that of EVs, while the second is that of residual impurities in the preparations. This hypothesis, however, need to be confirmed through TEM microscopy. The size distribution by number relative to one measurement on sample R0.8 is shown in Figure 103.
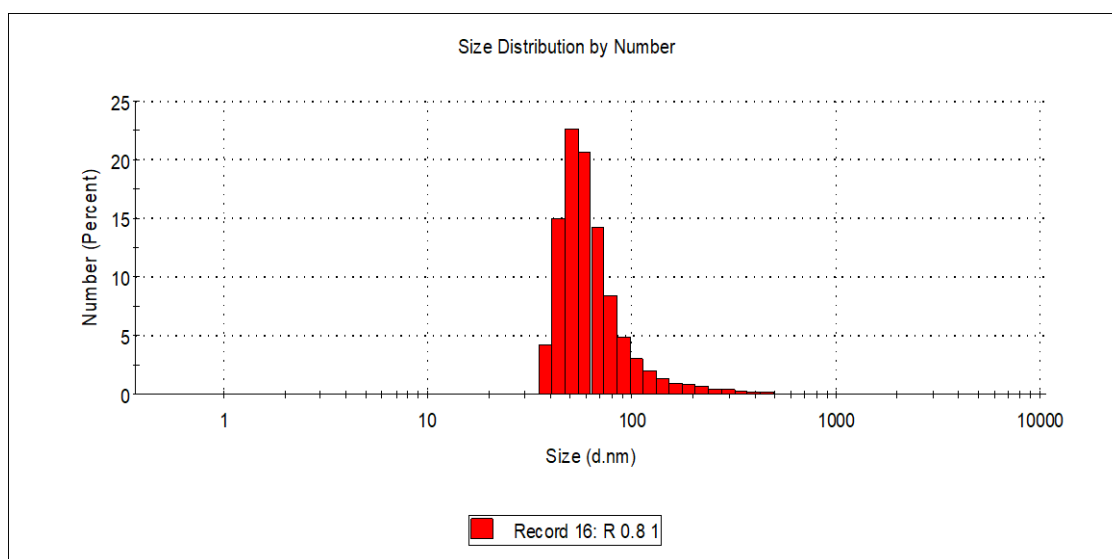

Figure 102: Size distribution by number of sample R0.8 throughout one measurement.

According to the data, more than 20% of the particles in solution have dimensions between 50 and 100 nm. The size distribution by intensity and the size distribution by number of each analyzed sample are reported in Appendix II. In Table 29 are reported the most relevant results obtained for each sample in terms of average Z-value and average polydispersity index.

The Z-value expresses the mean size through an intensity-weighted mean diameter. The polydispersity index is a dimensionless measure of the width of the size distribution. It ranges from 0 to 1 and values close to 1 indicate a very high sample polydispersity. In Table 30 reports also the zeta potential for each sample, obtained through a dedicated run. For zeta potential detection, only one measurement per sample is performed. ZP analysis may be invasive, due to the electric field applied through the gold electrodes present in the cuvettes, thus measurements following the first may be inaccurate due to possible damages to the nanovesicles.

Table 30: Average Z-value, polydispersity index and Z-potential of the EVs samples obtained through DLS and ZP measurements.

Sample	Avg Z-value d,nm	Avg Polydispersity index (PI)	Zeta potential mV
P3um	228,8	0,227	-3,75

R1.5	217,5	0,263	-10,3
Cake0.8	210,4	0,372	-9,21
R0.8	218,0	0,266	-6,26
R0.5	253,0	0,521	-3,83
R3	298,0	0,482	-9,40
Average value	237.6	0.355	-7,13
Std Dev	53,14	0,117	2,92

The mean size diameter, obtained through z-average, spaces between 217,5 nm (R1.5) and 298 nm (R3). The most polydisperse sample is R0.5 while the most size-uniform samples are P3um (0,23) and R0.8 (0,26). Concerning zeta potential measures, as expected all samples display a negative superficial charge ranging from -3.75 mV for P3um and -10,3 mV for R1.5. High values of the zeta potential (absolute values) indicate a good stability of the preparations, thus a low tendency to aggregate/flocculate. In this context, R1.5 (-10.3 mV) and R3 (-9.4) show the most promising results.

Finally, a comparison of the different sample size distribution is shown in Figure 104. Since all the samples showed a good reproducibility between the different measures, the comparison relative to one measurement can be considered reliable.
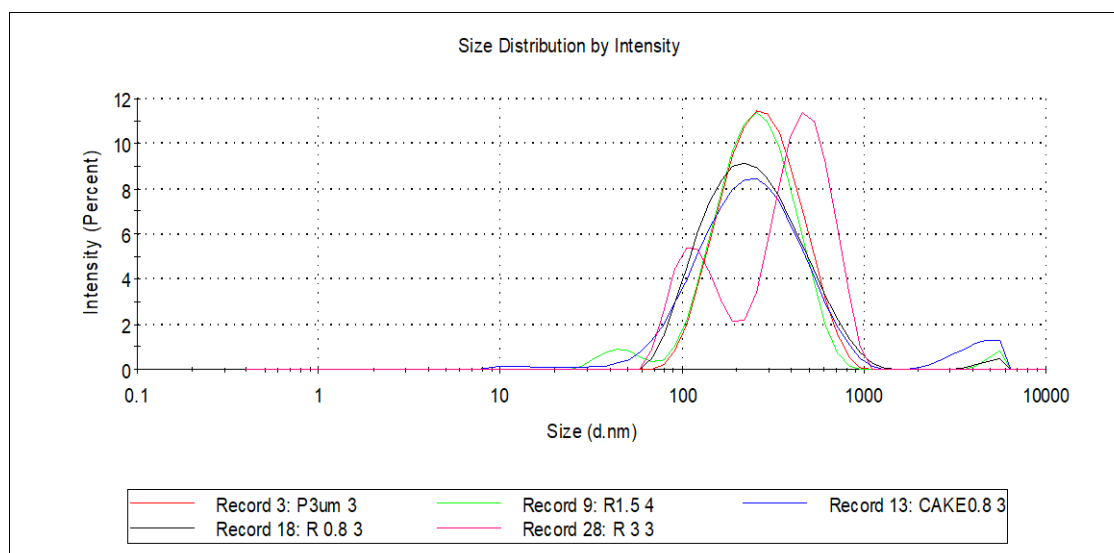

Figure 103: Comparison on the sample's size distribution by intensity.

Overall, all samples contain particles with diameters ranging from 100 to 1000 nm. One population centered around 237 nm is detected in each sample with the highest intensity. Interestingly, sample R3 is the only one displaying two different populations centered around 100 nm and 600 nm. The identified populations having diameters bigger than 1000 nm are present in almost all samples, with the exception of R3 that is the purest preparation.

6.7 Curcumin encapsulation

Loading of curcumin into lemon extracellular vesicles is attempted through passive cargo loading techniques. By using a series of blank sampling, encapsulation is monitored through spectrophotometric readings. An UV-visible spectrophotometer allows the detection of the amount of curcumin uptaken, as difference in absorbance. Spectrophotometric readings are performed at 425 nm, maximum peak of the curcumin UV-Vis absorption spectra.

To begin, a 150 µg/ml stock solution of curcumin in methanol is prepared. Methanol increases curcumin solubility and as the curcumin-methanol solutions come in contact with PBS or water, curcumin hydrophobic behavior is restored, thus favoring the compound encapsulation into the lipid-enclosed vesicles.

Curcumin calibration curve

Curcumin standard solutions are prepared by serial dilution of the stock solution in 0.1M PBS (pH 7.4). The chosen concentration range is 5–100 µg/ml. Absorbance is measured at 420 nm and a standard calibration curve is obtained by plotting the absorbance at 425 nm over the concentration of standard curcumin solutions and interpolating the experimental points. The spectrophotometer is blanked with PBS. In order to correlate the absorbance to curcumin concentration, the ABS signal of the standard solution is corrected by subtracting the absorbance of methanol. The calibration line obtained by linear interpolation is y=0.0365x+0.004 (Figure 105).
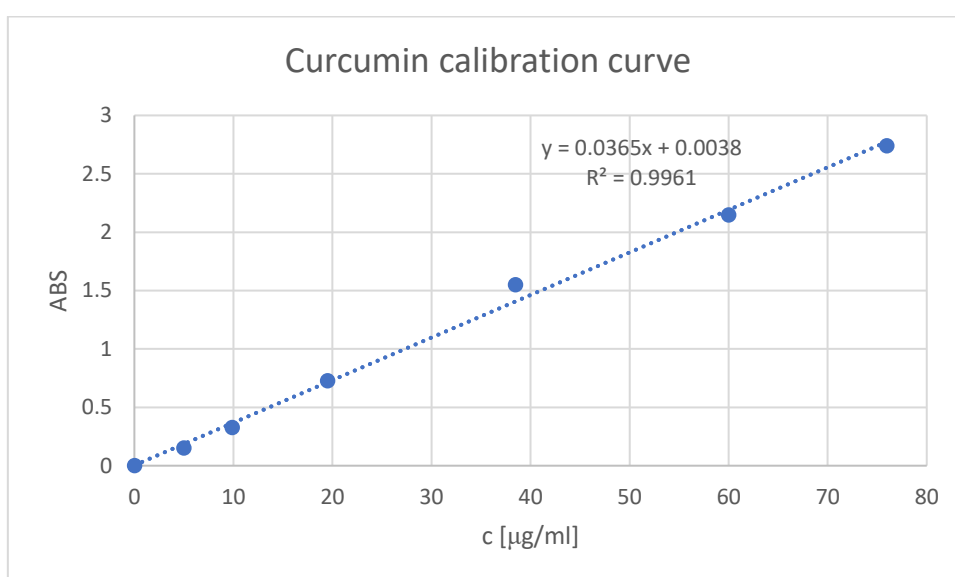

Figure 104: Curcumin calibration curve

Loading of curcumin is performed by adding 100 µl of curcumin stock solution to 1 ml of different EVs preparations.

A) EVs preparations obtained from 100kDa PES TFF diafiltration. Retentate obtained after 3 diavolumes is used.
B) EVs isolated by differential ultracentrifugation method (protocol 1)
C) EVs isolated by SEC-FPLC through the injection of 2 ml of the permeate of the 3µm filtration at 0.4 ml/min. EVs peak eluting between 36 and 50 ml is collected.

Curcumin degradation over time

Degradation of curcumin over time is tested to have an initial estimation on the stability of the preparations and to compare the stability of free curcumin over curcumin in EVs samples. A protocol is adapted from the one developed by Vashish et al. [23]. Samples with an identical concentration of curcumin are prepared in different tubes:

- A solution of 1 ml of PBS + 0.1 ml of curcumin stock solution is prepared to test free curcumin stability;
- 0.1 ml of Stock solution are added to 1 ml of each of the EVs samples A, B and C;

The amount of curcumin added to each sample is equal to 15 µg, with a final concentration of 13.6 µg/ml. The tubes are incubated in the dark at 37 °C in a water bath. After 0, 30, 60, 90 and 130 minutes samples are collected and their absorbance is measured at a wavelength of 425 nm. Each reading is repeated twice and the final ABS value is averaged. In the normalized plot in Figure 106 is possible to see the relative variation of the curcumin concentration over time with respect to the initial concentration.
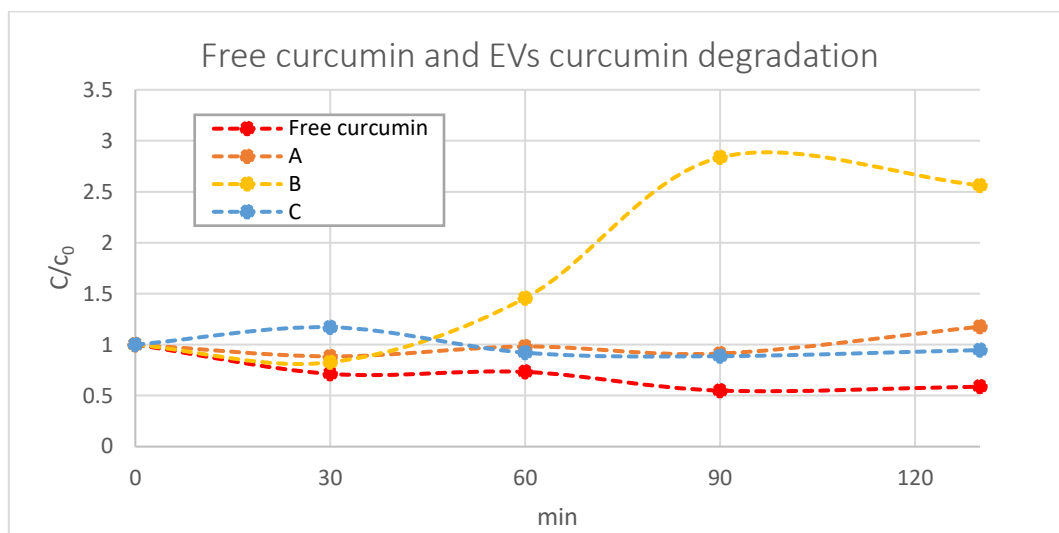

Figure 105: Degradation of curcumin over time in different EVs preparations.

The free curcumin (red curve) is degrading over time and in 130 minutes its concentration is halved. Concerning samples A and C, they show a smaller relative degradation with respect to free curcumin and after 90 minutes there is a small increase in curcumin concentration. Sample B displays a very strange behavior as curcumin concentration rises over time. This phenomena is unexplained. The corrected absorbance values of all samples seem to increase after 90 minutes. It can be speculated that as the samples are incubated at 37°C, after some time vesicles are damaged by the high temperature, thus they release their content as free curcumin is solution that is detected by the instrument.

Passive curcumin loading on EVs

After the addition of 0.1 ml of curcumin stock solution to 1ml of each sample A, B and C, the resulting preparations are centrifuged at 10,000 x g for 20 minutes to favor encapsulation and pellet unbound curcumin. Subsequently the supernatant is stored in a light resistant container at °4C and incubated overnight.

The day after, after an additional centrifugation run to pellet unbound curcumin residuals, the absorbance values of each sample are read at 425 nm. Each measurement is repeated twice, and the final absorbance value is averaged. The spectrophotometer is blanked with PBS. The readings of the samples and the blanking system adopted are summarized in Table 31.

Table 31: Spectrophotometric readings at 425 nm for the different EVs samples encapsulated curcumin and the relative blanking system.

Sample	Composition	Avg ABS 425 nm	Concentration [µg/ml]	% Loading efficiency
A - blank	1 ml EVs preparation + 0,1 ml MeOH	0.081		
B - blank	1 ml EVs preparation + 0,1 ml MeOH	0.470		
C - blank	1 ml EVs preparation + 0,1 ml MeOH	0.021		
Curcumin	1 ml PBS + 0,1 ml Stock	0.900	24.6	
A	1 ml EVs preparation + 0,1 ml stock	0.268	5.1	21%
B	1 ml EVs preparation + 0,1 ml stock	0.9135	12.1	49%
C	1 ml EVs preparation + 0,1 ml stock	0.0715	1.4	6%

The average absorbance values are corrected by the subtraction of the relative blank, and the curcumin concentration is retrieved by fitting through the calibration curve. A % loading efficiency is finally estimated by performing a mass balance over the curcumin in the system:

$$Curcumin\ added = Free\ curcumin + Encapsulated\ curcumin$$

$$Loading\ efficiency\ \% = \left(\frac{Amount\ of\ encapsulated\ curcumin}{Total\ amount\ of\ curcumin\ added}\right) * 100 \qquad (11)$$

The obtained Loading efficiencies are reported in Table 30. Sample B has the highest loading efficiency (49%), followed by sample A (21%) and sample C (6%). These results are to be intended as very preliminary estimations on the encapsulation ability of lemon-derived extracellular vesicles.

Chapters 5 and 6 references

[1]   I. Manual, "Thermofisher Tx-400 rotor user manual," no. October, 2009.

[2]   I. Manual, "Thermofisher Microliter 30x2 rotor user manual," no. October, 2010.

[3]   I. Beckman-Coulter, "Beckman-Coulter ultracentrifuge and rotor user manual," *Ultracentrifuge*, pp. 1–100, 2000, [Online]. Available: papers3://publication/uuid/1D6A64F1-39DD-4177-BB08-1D668C741FA3.

[4]   R. G. Harrison, P. W. Todd, S. R. Rudge, and D. P. Petrides, *Bioseparations Science and Engineering*. 2015.

[5]   L. Schwartz, "Diafiltration: A Fast, Efficient Method for Desalting or Buffer Exchange of Biological Samples," *Pall Sci. Tech. Rep.*, p. 6, 2003, [Online]. Available: http://www4.pall.com/pdf/02.0629_Buffer_Exchange_STR.pdf.

[6]   Millipore Corporation, "Stirred Ultrafiltration Cells Models 8003, 8010, 8050, 8200, 8400 User Guide," *User Guid.*, pp. 1–35, 2008, [Online]. Available: http://www.millipore.com/userguides.nsf/a73664f9f981af8c852569b9005b4eee/e7e01888fa ba2f89852574dc00818382/$FILE/99228.pdf.

[7]   Millipore Corporation, "Millipore Minitan User Guide 1995.pdf." 1995.

[8]   D. Yang *et al.*, "Progress, opportunity, and perspective on exosome isolation - Efforts for efficient exosome-based theranostics," *Theranostics*, vol. 10, no. 8. 2020, doi: 10.7150/thno.41580.

[9]   GE Healthcare, "GE Handbook - Size Exclusion Chromatography," *GE Healthc.*, 2018.

[10]   Äkta, "FPLC System Akta purifier user manual."

[11]   GE Healthcare, "Sepharose and sepharose CL," *GE Healthc.*, pp. 1–11, 2015, [Online]. Available: https://us.vwr.com/assetsvc/asset/en_US/id/16839294/contents.

[12]   W. Corporation, "Waters Alliance e2695 Separations Module user manual," 2013.

[13]   Phenomenex, "Yarra SEC-2000 Columns Tips for Care and Use," pp. 9–11, 2008.

[14]   F. Babick, "Dynamic light scattering (DLS)," in *Characterization of Nanoparticles: Measurement Processes for Nanoparticles*, 2019.

[15]   A. S. Ampules, "Pierce BCA Protein Assay Kit," vol. 0747, no. 23225, pp. 0–3, 2000.

[16]   Gaia Gravili, "Purificazione e caratterizzazione di vescicole extracellulari dal succo di limone" thesis

[17]   Pearce, G. (2007). "Introduction to membranes: Membrane selection." Filtration + Separation 44(3): 35-37.

[18]   Moce-Llivina, L., et al. (2003). "Comparison of polyvinylidene fluoride and polyether sulfone membranes in filtering viral suspensions." Journal of Virological Methods 109: 99-101.

[19]   Sandra Nakasone, "Characterization of Polyethersulfone (PES) and Polyvinylidene Difluoride (PVDF) Resistive Membranes under In Vitro Staphylococcus aureus Challenge", thesis

[20]   Pocsfalvi, Gabriella, et al. "Protein biocargo of citrus fruit-derived vesicles reveals heterogeneous transport and extracellular vesicle populations." Journal of plant physiology 229 (2018): 111-121.

[21]   Théry, Clotilde, et al. "Isolation and characterization of exosomes from cell culture supernatants and biological fluids." Current protocols in cell biology 30.1 (2006): 3-22.

[22]   Raimondo, Stefania, et al. "Citrus limon-derived nanovesicles inhibit cancer cell proliferation and suppress CML xenograft growth by inducing TRAIL-mediated cell death." Oncotarget 6.23 (2015): 19514.

[23]   Vashisht, Monika, et al. "Curcumin encapsulated in milk exosomes resists human digestion and possesses enhanced intestinal permeability in vitro." Applied biochemistry and biotechnology 183.3 (2017): 993-1007.

Conclusions

Extracellular vesicles are membrane-enclosed nanometric particles, naturally released by cells. They are key players in cells signalling functions, in both interspecies and intraspecies communication. They act as natural molecules and genes transporters, displaying a therapeutic action that can be exploited in many applications in nanomedicine as diagnostic biomarkers, as drug delivery systems and in tissue regeneration.

Besides mammalian cells, also plants do release vesicles and are proven to contribute to plant physiology in cell proliferation, differentiation, response to environmental stress and defense against pathogens. We continuously ingest plant and animal vesicles as we eat, thus their role on regulating our genes and, consequently, the whole body homeostasis, has been widely studied.

Vegetal nanovesicles have structures and compositions similar to that of mammalian EVs, rich in bioactive molecules as lipids, proteins and nucleic acids.

Due to the vast interest in the field of extracellular vesicles, many efforts are undertaken by researchers to identify the most advantageous methods to isolate and purify EVs, in terms of yield, purity, reproducibility, clinical translation potential and cost effectiveness.

It is not possible to identify a unique method suitable for all the application, as the EVs features are strictly dependent on that of the parent's cell phenotype.

A special focus is placed upon the use of plant vesicles as drug nanocarriers, as they possess innate advantages over synthetic nanoparticles as liposomes. They can naturally perform cell-specific drug release, while being intrinsically biocompatible, safe and a-toxic.

Vegetal EVs allow their purification from large fluid volumes and, being a very cheap source of materials, their industrial application is regarded as extremely feasible.

In this context, the experimental work carried out is aimed at the development of a scalable method for the isolation of extracellular vesicles from *citrus limon* juice.

The golden standard method in the field of EV isolation is differential ultracentrifugation. However, it has many limitations and no potential for scalability. Filtration techniques are very promising as they are already industrially exploited in the field of liposome production, where tangential flow filtration (TFF) is considered as the standard purification method. The flexibility, together with the short processing times, the scalability, and the adaptability to continuous operations of filtration processes make them the most suitable candidates as unit operations for the large-scale production of EVs.

The main core of the experimental work is the development of a protocol for lemon EVs purification through a diafiltration process. First, different membranes have been compared, in terms of materials and cut off. Their performances have been tested in stage *dead-end* diafiltration mode and assessed through gel filtration carried out in FPLC and HPLC systems.

The 100 kDa PES is found to be the best performing membrane. Compared to PVDF and RC membranes, it showed the highest recovery of vesicles and the lowest EV losses in the permeate stream. Conversely, PVDF membranes showed mediocre performances in terms of product recovery and a notable loss of EVs.

The PES membrane performances are then also tested in TFF constant-volume diafiltration mode through the set-up of a semi-continuous lab filtration system. It exploited the use of the FPLC system and a TFF UF filtration cell and allowed on-line monitoring of different retentate-side parameters.

The membrane, operating in TFF mode, is then characterized through permeability tests, aimed at the identification of the optimal operative conditions. Through simple mass balances obtained from the

integration of the chromatographic peaks, it is found that 51 % of vesicles are lost in the cake after that 0,4 diavolumes have been processed.

Therefore, an optimized diafiltration protocol is proposed. It involved the recovery of the gel layer formed over the membrane surface after each diavolume, and its resuspension and reintroduction to the feed tank. After the cake reintroduction an 80% EV recovery increase is found, with respect to the recovery before the cake reintroduction.

The removal of impurities after 3 diavolumes is 98.5%, thus assessing that the diafiltration process is effective in the purification of lemon EVs. Nonetheless, the EV losses on the membrane cake are undoubtedly the major pitfall of the process. Even if the membrane cake is recovered and reintroduced three times in the retentate, after 3 diavolumes the total recovery of vesicles is only 15.5 %.

It is then possible to make a final comparison between TFF diafiltration and stage diafiltration, considering 3 diavolumes and 5 stages realized, respectively, with the use of the same source, dilution ratio, membrane, TMP and same dilution buffer. In stage diafiltration, there is a 43 % decrease in the product yield from stage 1 to stage 5. The EV yield obtained with TFF diafiltration is *3.5 times* higher than that of stage diafiltration.

The yield of the whole TFF process is then estimated by means of SEC-HPLC chromatograms and a BSA calibration curve. It is calculated that with the current protocol is possible to obtain *4.2 mg of extracellular vesicles starting from one single lemon*, or equivalently *0.14 mg per ml of lemon juice*.

Raimondo et al. isolated lemon EVs through a dUC-based protocol and obtained a yield of 2.5 mg/ml of lemon juice. The results are thus comparable.

The EVs preparation obtained with the TFF process have been finally characterized by means of different physical and biochemical techniques. Total protein quantification assay resulted in a protein yield of 0.5 mg/ml. The same sample displayed an average Z-potential of – 9.4 mV. DLS measurements revealed a particle size distribution between 100 and 1000 nm, with an average particle diameter of 237 nm.

Finally, passive curcumin loading into lemon EVs is attempted. After the centrifugation and overnight sample incubation, the uptake capability of the EV-enriched fraction is verified through spectrophotometric readings. Through a mass balance on curcumin, a loading efficiency equal to 21% is found for the product of the process.

Overall, the results obtained are very promising, both in terms of the purification efficacy of the whole process and the final EV yield. Nonetheless, product losses on the membrane gel layer are the major hindrance to the process. The problem has been just partially addressed with the cake resuspension strategy. Thus, further studies should be aimed towards a further optimization of the purification protocol, in terms of process operative conditions, as well as the identification of more reproducible and reliable strategies to recover vesicles from the membrane gel layer.

Acknowledgments

Foremost, I would like to express my deep and sincere gratitude to my supervisor, Prof. Cristiana Boi, for giving me the opportunity to carry out this project and providing invaluable guidance and encouragement throughout the research. Her competence and commitment to the work has been truly inspiring.

Further, I would like to thank prof. Serena Bandini. Her expertise on membrane processes contribute to the development of the strategies and the methodologies adopted.

Additionally, I am thankful to Prof. Francesco Francia and Dr. Stefano Cerini for allowing us to perform analyses in their laboratories, and for their kind explanations and the time dedicated.

My sincere thanks go to Dr. Riccardo Onesti, whose insights and support has been fundamental since the very beginning. Day by day, he patiently helped us to set up experiments and enhance our hands-on lab skills.

A special thank goes also to Thomas Fabiani, who introduced us to the work and his initial help has been truly precious to set on track the experiments.

Last but not least, an immense thank goes to my fellow lemon lab companion, Zubin K. Mahin. I don't have enough words to express the pleasure I had working with him. Without our incredible team work and mutual support, any of the results achieved would have been possible. Thank you for bearing me when I was anxious. I am very proud of ourselves!

Appendix I

Literature review of the obtained plant-derived nanovesicles (NVs) and microvesicles (MVs), reporting the isolation method, physical and biological properties, yield and number of particles (where reported).

Source	Part	Isolation method	Diameter [nm]	Yield	Particle Number	Cell uptake	Stability	Ref.
Ginger	rhizome	dUC/gUC	102 – 998 (mean ~386 and ~294)	n.r.	n.r.	Uptaken by primary hepatocyes	Very stable in stomach-like and small intestine-like solutions	Zhuang et al.[31]
Ginger	rhizome	PEG precipitation	100-900 (mean ~400)	2-3.8 g/kg	n.r.	Uptaken by the murine macrophages; protects cells from H_2O_2 induced oxidative stress.	/	Kalarikkal et al.[41]
Grape	fruit	dUC/gUC	50-300 (mean 380.5 ± 37.47)	n.r.	n.r.	Uptaken by mouse intestinal stem cells	/	Ju et al.[25]
Grapefruit	fruit	dUC/gUC	105-390 (mean 210.8 ± 48.62)	n.r.	n.r.	Uptaken by mouse intestinal macrophages	Very stable at 37 °C	Wang et al.[24]
Grapefruit	fruit	dUC/gUC	180-200	2.21±0.044 g kg^{-1}	n.r.	Uptaken by splenic and liver cancer cells lines in mouse models	Very stable at 4 °C for more than one month and loaded with curcumin	Wang et al.[42]
Tomatoes	fruit	dUC/gUC/SEC	50–500	MVs 35.6 ± 8.6 mg/kg (protein) NVs 25.8 ± 11.4 mg/kg (protein) for NVs.	MVs 2.7 x 10^{16} particles/kg NVs 3.8 x 10^{16} particles/kg			Bokka et al.[43]
Broccoli	flower	dUC/gUC	~18 and 118.	n.r.	n.r.		Broccoli NVs administration in mice protects from intestinal inflammation and prevent colitis	Deng et al.[32]
Apple	fruit	dUC	100-400	n.r.	1.6 x 10^{13} particles/L	Uptaken by Caco.2 cells (intestinal epithelium)	NVs disappear when boiled or sonicated	Fujita et al.[44]

|							
Coconut	fruit	dUC/MF	10-100 (Mean coconut water 59.72, milk 100)	n.r.	n.r.			Zhao et al.[45]
Citrus clementina	fruit	dUC/gUC	75–345 (mean populations at 75, 120, 155)	1.67 x 10^{-3} g/L (protein)	1.16 x 10^{12} particles/L juice		Significant presence of membrane transporters protein	Stanly et al.[46]
***Citrus sinensis* (sweet orange)**	fruit	dUC	950, 480 (avg sizes)	0.178 g/L (protein)	n.r.			Pocsfalvi et al.[23]
***Citrus paradisis* (grapefruit)**	fruit	dUC	255, 350 (avg sizes)	0.134 g/L (protein)	n.r.			Pocsfalvi et al.[23]
***Citrus aurantium* (bitter orange)**	fruit	dUC	5500, 700 (avg sizes)	0.161 g/L (protein)	n.r.			Pocsfalvi et al.[23]
Citrus limon	fruit	dUC	820, 460 (avg sizes)	0.409 g/L (protein)	n.r.			Pocsfalvi et al.[23]
Citrus limon	fruit	dUC/MF/gUC	50-70	2.5 x 10^{-3} g/L	n.r.	Uptaken by human lung carcinoma cell line and myeloid leukemia cell line	***Citrus* NVs inhibit the growth of tumor cell lines** inducing TRAIL-mediated cell death.	Raimondo et al.[22]
Carrot	root	dUC/gUC	100-1000	n.r.	n.r.	Targeting properties to intestinal macrophages and stem cells	Data suggest that the vesicle size can be altered in a pH-dependent manner	Mu et al.[36]
Blueberry	fruit	dUC/MF	100-900	n.r.	n.r.		* miRNA profiling of PDEVs of 11 different fruits and vegetables.	Xiao et al.[33]
Hami melon	fruit	dUC/MF	100-800	n.r.	n.r.		*	Xiao et al.[33]
Pea	seed	dUC/MF	100-800	n.r.	n.r.		*	Xiao et al.[33]
Pear	fruit	dUC/MF	100-800	n.r.	n.r.		*	Xiao et al.[33]
Soybean	seed	dUC/MF	100-700	n.r.	n.r.		*	Xiao et al.[33]
Orange	fruit	dUC/MF	100-700	n.r.	n.r.		*	Xiao et al.[33]
Kiwifruit	fruit	dUC/MF	10- 700	n.r.	n.r.		*	Xiao et al.[33]
Sunflower	seed	MF/ dUC	50-200 nm	n.r.	n.r.			Reagente et al.[18]

Appendix II

II.I Comparison between the different diafiltration membranes employed in EVs stage diafiltration. SEC-HPLC comparative chromatograms between the different streams.
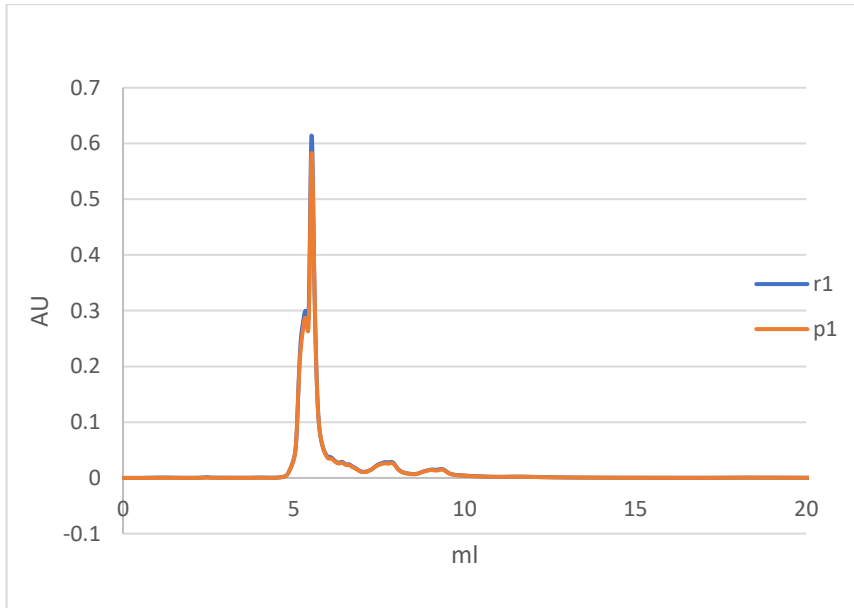
II.I.B   100 kDa PVDF
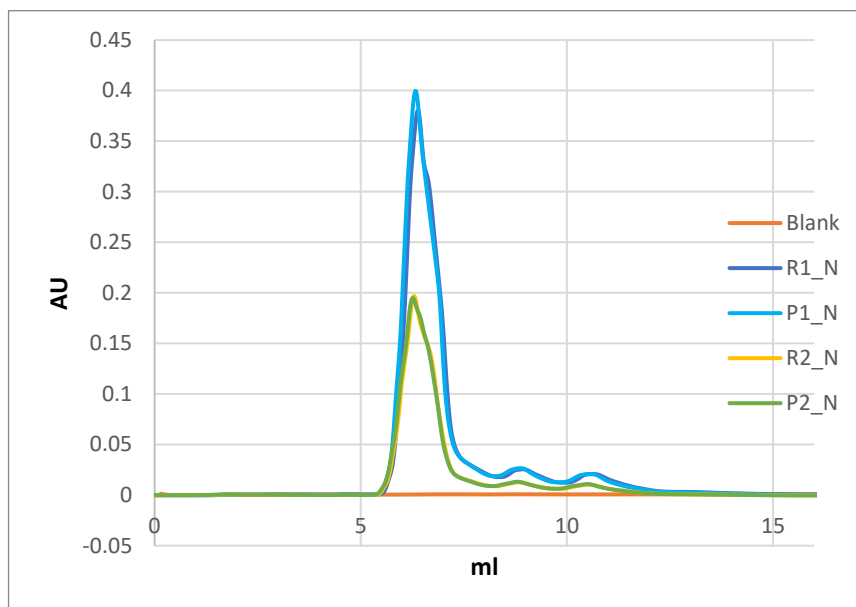
II.I.C   250 kDa PVDF
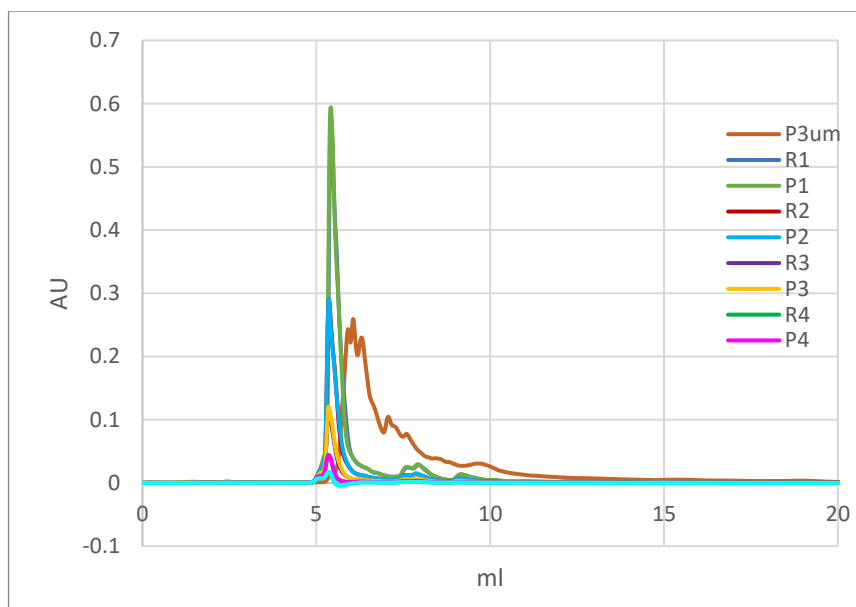
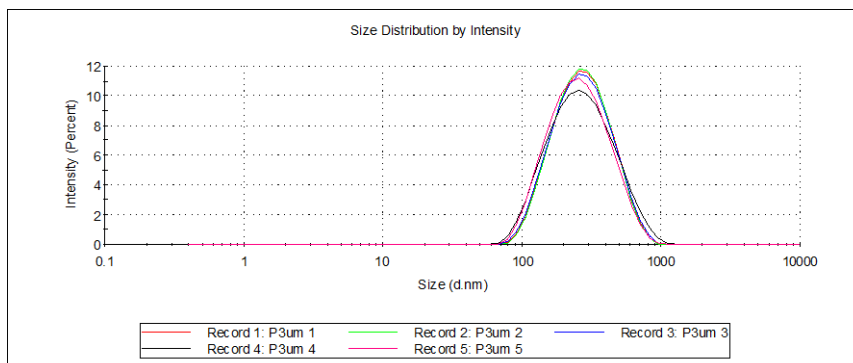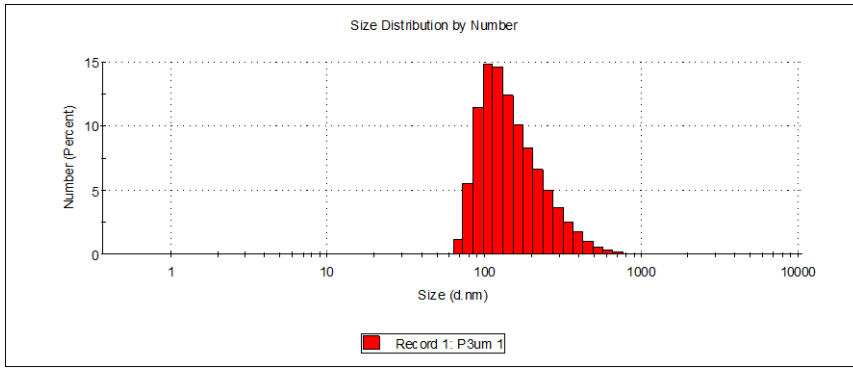

II.I.E   300 kDa RC

II.II Area of the peaks of the SEC-HPLC chromatograms obtained by collecting R, P, F of stage diafiltration with different membranes. Values are calculated through numerical integration of the SEC-HPLC chromatographic peaks of EVs and impurities.

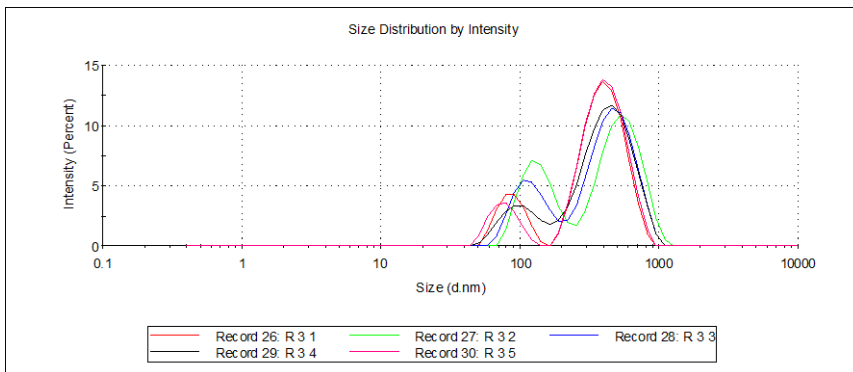| Membrane	Area [mVsec]					
	Feed (F)		Retentate (R1)		Permeate (P1)	
	EVs	Impurities	EVs	Impurities	EVs	Impurities
A. 0.45um RC	61.9	30333.4	24.1	14440.7	15.0	7970.5
B. 100 kDa PVDF	13.0	33349.5	5.1	24282.4	4.2	12595.6
C. 250 kDa PVDF	61.9	30333.4	29.8	14404.6	14.0	14676.7
D. 100 kDa PES	13.4	33003.9	8.5	16721.8	1.9	16922.5
E. 300 kDa RC	23.6	34896.2	13.6	16152.5	4.9	16064.1

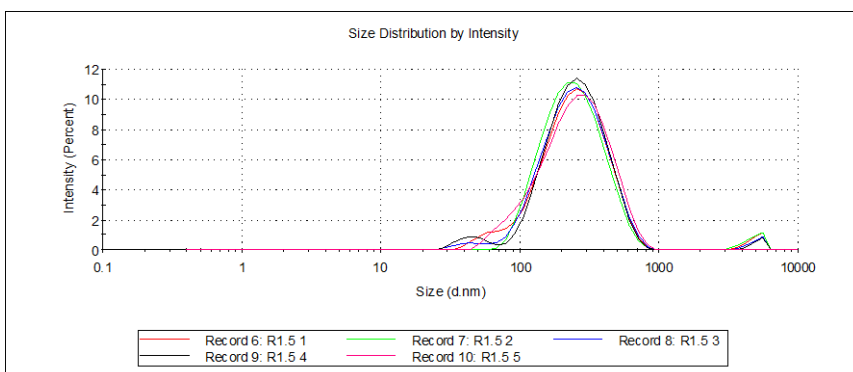**II.III Size distribution by intensity and by number of different EV samples obtained through DLS measurements**

P3um

R3DV

R1.5 DV

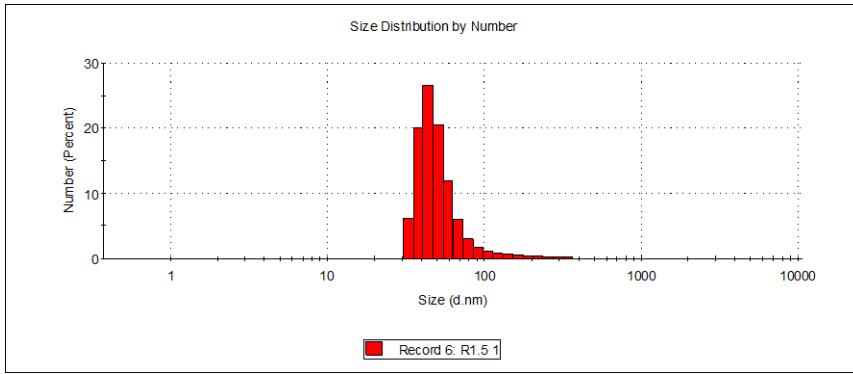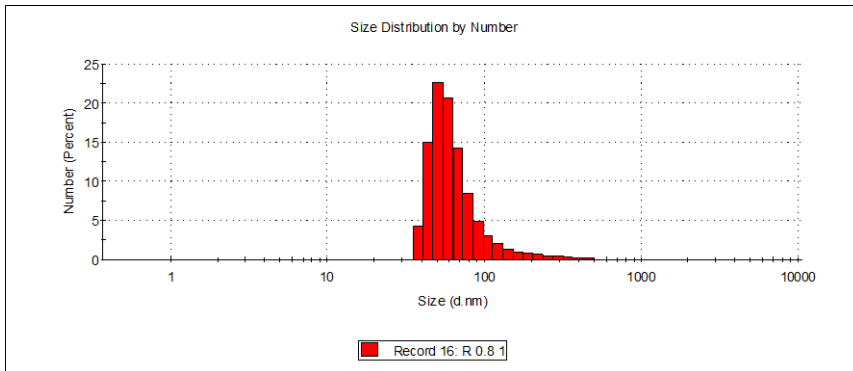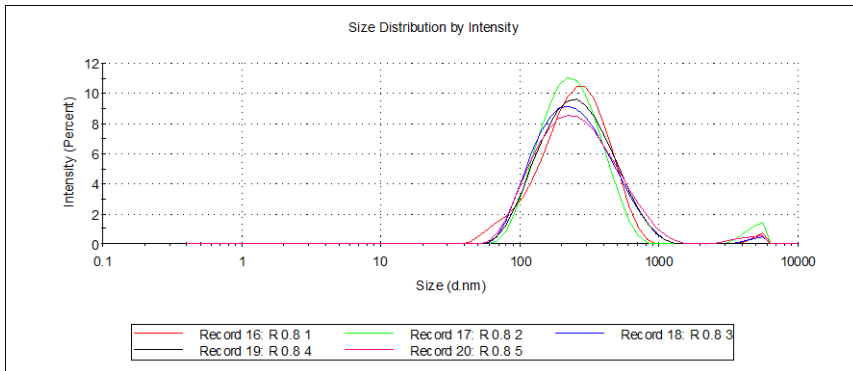## R 0.8DV

CAKE 0.8DV

Size Distribution by Number